Open Research Online

On impact and volcanism across the Cretaceous-Paleogene boundary

Journal Item

Constraining the Role of Impact and Volcanism in Marine Extinctions across the Cretaceous-Paleogene Boundary

Pincelli M. Hull[1*♦], André Bornemann[2*♦], Donald Penman[1♦], Michael J. Henehan[1,3♦], Richard D. Norris[4♦], Paul A. Wilson[5♦], Peter Blum[6♦], Laia Alegret[7], Sietske Batenburg[8], Paul Bown[9], Timothy J. Bralower[10], Cecile Cournede[11,12], Alexander Deutsch[13], Barbara Donner[14], Oliver Friedrich[15], Sofie Jehle[16], Hojung Kim[9], Dominik Loroch[13], Peter Lippert[17], C. Brenhin Keller[18], Dick Kroon[19], Iris Moebius[15,20], Kazuyoshi Moriya[21], Daniel J. Peppe[22], Gregory E. Ravizza[23], Ursula Röhl[14], Philip Sexton[24], Julio Sepúlveda[25], Jonathan D. Schueth[26], Elizabeth Sibert[4,27,28], Kasia K. Sliwinska[29], Roger E. Summons[30], Ellen Thomas[1,31], Thomas Westerhold[14], Jessica Whiteside[5], Tatsuhiko Yamaguchi[32], James C. Zachos[33]

[1] Department of Geology and Geophysics, Yale University, 210 Whitney Ave, New Haven, CT 06511, USA
[2] Bundesanstalt für Geowissenschaften und Rohstoffe, Stilleweg 2, 30655 Hannover, Germany
[3] GFZ German Research Centre for Geosciences, Telegrafenberg, 14473 Potsdam, Germany
[4] Scripps Institution of Oceanography, University of California San Diego, 9500 Gilman Drive, La Jolla, CA 92093-0244, USA
[5] National Oceanography Centre Southampton, University of Southampton, Waterfront Campus, European Way, Southampton SO14 3ZH, UK
[6] International Ocean Discovery Program, Texas A&M University, 1000 Discovery Drive, College Station, TX 77845, USA
[7] Departamento de Ciencias de la Tierra & Instituto Universitario de Ciencias Ambientales, Universidad Zaragoza, 50009 Zaragoza, Spain
[8] Géosciences, Université de Rennes 1, Campus de Beaulieu, 35042 Rennes, France
[9] Department of Earth Sciences, University College London, Gower Street, London WC1E 6BT, UK
[10] Department of Geosciences, Pennsylvania State University, University Park, PA, USA
[11] CEREGE, Université Aix-Marseille, Europole de l'Arbois BP 80 1, 13545 Aix en Provence, France
[12] Institute for Rock Magnetism, University of Minnesota, John T. Tale Hall, 116 Church St. SE, Minneapolis, MN 55455, USA
[13] Institut für Planetologie, Universität Münster, Wihelm-Klemm-St. 10, 48149 Münster, Germany
[14] MARUM – Center for Marine Environmental Sciences, University of Bremen, Leobener Strasse 8, 28359 Bremen, Germany
[15] Institute of Earth Sciences, Heidelberg University, Im Neuenheimer Feld 234-236, 69120 Heidelberg, Germany
[16] Institut für Geophysik und Geologie, Universität Leipzig, Talstr. 35, 04103 Leipzig, Germany
[17] Department of Geology & Geophysics, The University of Utah, 115 S 1460 E, Salt Lake City, UT 84112-0102, USA
[18] Department of Earth Sciences, Dartmouth College, Hanover NH 03755
[19] School of Geosciences, University of Edinburgh, Edinburgh EH8 9XP, United Kingdom
[20] Department of Biogeochemical Systems, Max Planck Institute for Biogeochemistry, Hans-Knöll St. 10, 07745 Jena, Germany
[21] School of Natural Sciences and Technology, Kanazawa University, Kakuma-machi, Kanazawa, Ishikawa 920-1192, Japan
[22] Department of Geology, Baylor University, One Bear Place #97354, Waco Texas 76798-7354, USA
[23] Department of Geology & Geophysics, University of Hawai'I at Manoa, Honolulu, HI 96822, USA
[24] School of Environment, Earth & Ecosystem Sciences, The Open University, Walton Hall, Milton Keynes MK7 6AA, UK
[25] Department of Geological Sciences and Institute of Arctic and Alpine Research, University of Colorado Boulder, UCB 450, Boulder CO 830309-0450, USA
[26] ConocoPhillips Company, 925 N Eldridge Pkwy, Houston, TX 77079, USA
[27] Harvard Society of Fellows, Harvard University, 78 Mount Auburn Street, Cambridge, MA 02138, USA
[28] Department of Earth and Planetary Sciences, Harvard University, 20 Oxford Street, Cambridge, MA 02138, USA
[29] Department of Stratigraphy, Geological Survey of Denmark and Greenland (GEUS), Øster Voldgade 10, DK-1350 Copenhagen K, Denmark
[30] Department of Earth, Atmospheric and Planetary Science, Massachusetts Institute of Technology, Cambridge, MA 02139, USA
[31] Department of Earth and Environmental Sciences, Wesleyan University, Middletown CT 06459, USA
[32] Center for Advanced Marine Core Research, Kochi University, Monobe B200, Nankoku, Hochi, 783-8502, Japan
[33] Department of Earth and Planetary Sciences, University of California Santa Cruz, CA 95064, USA

* Co-first authors (pincelli.hull@yale.edu and andre.bornemann@bgr.de)
♦ First seven authors in order of contribution, all others alphabetical

1   *Abstract*

2   The cause of the end-Cretaceous mass extinction is vigorously debated due to the presence of

3   two smoking guns near the boundary: a very large bolide impact and flood basalt volcanism.

4   Disentangling their relative importance is complicated by uncertainty regarding kill mechanisms

5   and the timing of volcanogenic outgassing relative to impact and extinction. Here we constrain

6   the timing of volcanogenic outgassing through model-data comparisons using carbon cycle

7   modeling and paleotemperature records. We find support for major outgassing beginning and

8   ending distinctly prior to the impact, with only the impact coinciding with mass extinction and

9   biologically amplified carbon cycle change. A second major outgassing event following the

10 impact is also possible because extinction-related changes in the carbon cycle can mask the Earth

11 system effects of post-impact volcanism.

12

13 *Introduction*

14 Sixty-six million years ago two planetary-scale disturbances occurred within a geologically brief,

15 less than one million-year-long, interval. At the boundary between the Cretaceous and the

16 Paleogene (~66 Ma), an asteroid of more than 10 km in diameter collided with the Yucatan

17 Peninsula producing the ~200 km wide Chicxulub impact crater (*1-3*). Impact markers in

18 hundreds of sites globally co-occur with the deposition of the Cretaceous-Paleogene (K/Pg)

19 boundary clay/impact ejecta and include elevated abundances of siderophilic elements such as

20 iridium, osmium, and nickel, and tektites and shocked quartz (*1, 4, 5*). During the K/Pg

21 boundary-spanning magnetochron C29r (65.688-66.398 Ma (*6*), although see (*7*)), an estimated

22 123,000 km^3 of lava flooded across much of India and into the deep sea in a large igneous

23 province (LIP) known as the Deccan Traps (*8, 9*). Deccan volcanism was, like most flood basalts

24 (*8, 10*), highly episodic with flows deposited in pulses throughout the ~710,000 years of

25 magnetochron C29r (*11, 12*). That both planetary-scale events occurred, and did so within

26 several hundred thousand years of the K/Pg boundary, is now beyond reasonable doubt (*4, 11,*

27 *12*). What remains fiercely debated, however, is the relative timing and magnitude of volcanic

28 effects on the biosphere (*12, 13*), the relationship between impact and volcanism (*12, 14*), and

29 whether impact or volcanism act as the sole, primary, or joint drivers (*4, 8, 15*).

30

31   The case for the Chicxulub impact as a driver of K/Pg mass extinction includes processes

32   hypothesized to operate during the days to decades following the collision. The bolide impact

33   injected an estimated >50,000 km^3 of ejecta (*16*), and ~ 325 Gt of sulfur and ~425 Gt CO_2 and

34   other volatiles (*17*) into the atmosphere from the marine carbonate and anhydrite target rock of

35   the Yucatan Peninsula (*4*). The combined effects of an expanding impact fireball and the re-entry

36   of molten ejecta from the skies (*18*) may have raised temperatures to the point of spontaneous

37   combustion near the impactor and caused severe heat stress and even death many thousands of

38   km away from the impact site in the minutes to days after impact (*19*). In the day to years that

39   followed, nitrogen and sulfur vapors reacted to form nitric and sulfuric acids and, with CO_2

40   gases, may have acidified the oceans (*20, 21*). Finally, models and empirical evidence suggest

41   that the combination of dust and aerosols precipitated a severe impact winter in the decades post-

42   impact (*22-25*).

43

44   Significant though these environmental effects may be, some experts question whether the

45   Chicxulub impactor acted as the sole (or even main) driver of the K/Pg mass extinction for three

46   primary reasons. First, no single kill mechanism appears to explain the extinction patterns:

47   acidification (*26*) and primary productivity decline (*27*) (due to darkness and cold (*24*)) are

48   favored in the marine realm, whereas heat exposure and/loss of productivity (due to darkness and

49   cold (*24*)) are favored in the terrestrial realm (*28, 29*). Second, asteroid and comet impacts occur

50   throughout the history of life, but no other major mass extinction is unambiguously linked to

51   such a collision (*30*). In contrast, flood basalt volcanism can be deadly – the third objection to an

52   impact-only driver. Flood basalt volcanism is strongly implicated as the driver of two of the

53   greatest mass extinctions in the last half billion years (the Permian-Triassic [P/T] and Triassic-

54   Jurassic [T/J]), leading many to favor a similar role for Deccan volcanism in the K/Pg (e.g., *31*).

55   However, most episodes of flood basalt volcanism after the T/J produced no discernable increase

56   in extinction rates (*27*). This is possibly attributable to important earth system changes that

57   dampened the effects of flood basalts post-P/T: increased oxygen levels (*32*) and potentially

58   some combination of the breakup of Pangea (*33*) and changes in the biological pump (*34, 35*)

59   may have reduce the risk of marine anoxia, and, after the T/J, pelagic calcifiers rose to

60   dominance, changing the carbon cycle's response to exogenous perturbations (*36-38*).

61

62   For the K/Pg mass extinction, the role of Deccan volcanism is questionable because of a lack of

63   solid evidence for a volcanogenic driver. In spite of considerable advances in chronology, the

64   timing of the most voluminous Deccan eruptions relative to the K/Pg boundary remains unclear

65   because of uncertainties in estimating flow volumes from partially eroded and obscured terrains.

66   Many have argued that most of the Deccan flood basalts (>85%) were emplaced in a relatively

67   short interval (~140,000 years) before the K/Pg starting around the C29r/C30n boundary (~66.39

68   Ma) and ending well *before* the K/Pg impact (*10, 11*). In contrast, using updated numerical ages

69   and volumetric estimates, Renne et al. (2015) proposed that the vast majority of Deccan basalts

70   were emplaced *after* the impact (*12, 39*), and Schoene et al. (2019) proposed major pulses of

71   emplacement just *before* and just *after* the impact (*40*). Pre- and post-impact scenarios are

72   debated in part because they are tied to different environmental disruption scenarios. Pre-event

73   volcanism may have acted in concert with the impact to drive K/Pg extinctions (*8*), whereas post-

74   event volcanism suggests a role for volcanism in the delayed recovery of biodiversity (*12*). For

75   the environment and life, however, the main environmental effects of LIPS are attributed to

76   volatile release (*41-43*), not lava emplacement, and the magnitude of volcanic outgassing is not

77   necessarily linked directly to the volume of erupted lava. In the case of flood basalt volcanism,

78   early eruptive phases typically have higher volatile concentrations (*41*), so it is possible that most

79   volatiles could be released before the impact even if most of the lava was emplaced after (*39*).

80

81   Here we provide a new constraint on Deccan Trap outgassing by comparing new, exceptionally

82   resolved and temporally expanded ocean drilling records, and global temperature records, with

83   four modeled end-member scenarios for timing, magnitude, and composition of outgassing (*44*).

84   These comparisons allow for a detailed consideration of the relative effect of Deccan Trap

85   outgassing and bolide impact on the marine carbon cycle and biological change.

86

87   ***Marine environmental record of outgassing***

88   Deccan Trap degassing released a mix of volatiles including sulfur dioxide (SO_2), chlorine (Cl),

89   and carbon dioxide (CO_2), with sulfur having perhaps the greatest direct effect on ecosystems

90   through environmental acidification and pronounced global cooling (>4.5°C) (*42*). The

91   environmental effects of sulfur dioxide, however, would have been relatively short-lived (years

92   to centuries at most) -time scales that are difficult, or even impossible, to detect in most slowly

93 accumulating deep-sea sediments. Instead, the influence of CO_2 emissions should be detectable

94 in marine sediments as a global warming event paired with a carbon isotope anomaly (*38*). We

95 use this fingerprint of CO_2 emissions as a proxy for the timing of potentially disruptive

96 outgassing of sulfur (and other noxious gasses).

97

98 We investigate the timing of Deccan Trap outgassing by modeling the effects of CO_2 and sulfur

99 emissions on long-term global temperatures using the geochemical box model LOSCAR (Long-

100 term Ocean Sediment CArbon Reservoir v. 2.0.4) (*45*). All volcanic outgassing scenarios assume

101 the same (i) initial climatic and oceanographic conditions: 600 ppm *p*CO_2 and climate sensitivity

102 of 2-4°C per CO_2 doubling (*38*), LOSCAR Paleocene continental configuration, and marine

103 [Mg^{2+}] of 42 mmol/kg and [Ca^{2+}] of 21 mmol/kg; (ii) K/Pg impact-related volatile release (325

104 Gt S; 425 Gt CO_2)(*17*); (iii) upper and lower end-estimates for total volcanic outgassing volumes

105 (4091-9545 Gt C and 3200-8500 Gt S (*8, 11*)) (*44*); and iv) extinction related changes in the

106 marine carbon cycle (*38, 46*) (here estimated as 50% reduction in organic carbon export, 42.5%

107 reduction in carbonate export, 22% increase in shallow water remineralization, Table 1) that

108 taper back to pre-event values over 1.77 Myr following the extinction (*47*). Guided by competing

109 hypotheses in the literature, we tested four major Deccan Trap emissions scenarios. These differ

110 in the timing of volatile release: (i) Case 1: Leading, majority (87%) of degassing pre-K/Pg

111 boundary (ii) Case 2: 50/50, half of degassing prior to and half following the K/Pg boundary;

112 (iii) Case 3: Lagging, majority (87%) of degassing post-K/Pg boundary; and (iv) Case 4:

113 Spanning, emissions released throughout magnetochron C29r (Table 1).

114

115 Two features of the global temperature compilation are used to consider the likelihood of

116 different volcanic emissions scenarios (Fig. 1) (*44*). First, a late Maastrichtian warming event

117 occurs in marine and terrestrial records (Figs. S1-S16), and is similar in magnitude and timing to

118 other well-documented records of the event (*48, 49*). Late Maastrichtian warming of ~2°C on

119 average is constrained to the Cretaceous portion of C29r (over ~250 kyrs) and shows cooling to

120 pre-event temperatures about 50 kyrs prior to the K/Pg boundary clay (Fig. 1). Second, the

121 earliest Danian has comparable temperatures to the late Maastrichtian prior to the warming

122 event. The earliest Danian is ~0.5°C warmer than the latest Maastrichtian on average for the first

123 ~500,000, with distinct differences between the relative temperatures recorded in terrestrial

124 (cooler) and marine (warmer) archives (Figs. S13-S14). By ~600,000 years after the impact, a

125 gradual warming trend led to temperatures to be, on average, >1°C warmer than the latest

126 Maastrichtian (Fig. 1). Benthic foraminifera typically track changes in global mean temperatures

127 and these archives show both temperature features (Fig. 1, 2, S13a), as do most other archives

128 (Figs. S1-S16). Two exceptions, bulk carbonate records and fish teeth phosphate records from El

129 Kef (Fig. S10c, S11, S12), likely do not track global temperature for extinction-related reasons

130 (*44*) and were excluded from the calculation of global mean temperatures in Fig. 1.

131

132 Two of the modeled scenarios differ distinctly in the predicted pattern of temperature change,

133 and are considered unlikely to represent the true outgassing history. Case 3 (Lagging) fails to

134 reproduce the late Maastrichtian warming and Case 4 (Spanning) creates a muted warming that

135 continues to increase up to the K/Pg boundary, unlike the empirical record (Fig. 1). Only two

136 outgassing scenarios produce modeled temperatures like the proxy records: Cases 1 (Leading)

137 and 2 (50:50), thus they are considered most likely to represent Deccan Trap outgassing.

138

139 In Case 1 (Leading), the majority of CO_2 and sulfur dioxide degassing occurs in the latest

140 Maastrichtian and leads to global warming and subsequent cooling prior to the K/Pg, followed

141 by relatively consistent early Paleocene temperatures with a gradual warming over the 600kyrs

142 following the impact. A volcanic CO_2 driver for late Maastrichtian warming (*48*) is supported by

143 new and existing high-resolution records from the open ocean (Figs. 2, S17-S18). Our new

144 multiproxy, astronomically tuned record from the North Atlantic J-Anomaly Ridge Site (*50*),

145 with an exceptionally complete Maastrichtian sequence and an intact mm-thick tektite layer at

146 the K-Pg boundary (Figs. 3, S17-S19), documents eruption-driven warming in the latest

147 Maastrichtian as an excursion to lower values in both $\delta^{18}O$ and $\delta^{13}C$ recorded in bulk sediments,

148 coincident with a decline in osmium isotopes (Fig. 3). Similar patterns occur in records from

149 sites at South Atlantic Walvis Ridge and North Pacific Shatsky Rise (Figs. 2, S18) (*48, 51*).

150 Volcanogenic warming evidenced by $\delta^{18}O$ and $\delta^{13}C$ recovers to pre-warming event like values in

151 the very latest Maastrichtian.

152

153 Case 2 (50/50) also presents a good match to the empirical temperature data (Fig. 1). Although

154 the Late Cretaceous warming differs between Case 2 and Case 1 due to reduced volcanic

155 outgassing in the Late Cretaceous in Case 2, uncertainty regarding climate sensitivity (*52*) and

156 total Deccan Trap emissions (*8, 11*) has a greater effect on modeled temperatures than the

157 difference in outgassing volume between Case 1 & 2 (Fig. 1).

158

159 Remarkably, the climatic effects of a major pulse (50%) of Deccan outgassing immediately

160 following the impact, as in Case 2, is readily masked by extinction-related changes to the carbon

161 cycle, primarily attributable to the reduction in $CaCO_3$ export to the seafloor. Marine $CaCO_3$

162 export indirectly affects atmospheric CO_2 by changing the distribution of carbon and alkalinity

163 between the surface and deep-ocean, and the removal of CO_2 from the system via $CaCO_3$ burial.

164 The difference between Case 1 and 2 is almost imperceptible—Case 2 has slightly warmer

165 (~0.25°C) early Danian temperatures than Case 1.

166

167 Our results inform several important boundary debates. First, the ~50 kyr lag between the onset

168 of late Maastrichtian warming in the empirical records and our models (Fig. 1) suggests that this

169 major phase of outgassing more likely began ~300 kyr rather than 358 kyr prior to impact.

170 Second, if the timing of volcanic emplacement proposed by Schoene et al. (2019) is correct, with

171 a large pulse of emplacement just 20-60 kyrs prior to the impact (*40*), then most CO_2 *outgassing*

172 (and associated environmental impacts) must have preceded this pulse of lava emplacement by

173 several hundred thousand years – prior to eruption of the most voluminous stages of Deccan

174 volcanism (i.e., pre-Wai subgroup) as modeled for Case 1 and 2 (Fig. 1). We were unable to find

175 an emission and weathering scenario allowing for synchronous proportional outgassing and

176 emplacement with the timing of the Schoene et al. (2019) scenario (Figs. S36-37), given the

177 volume of total outgassing hypothesized, the shape of the $\delta^{13}C$ curve just prior to impact, and the

178 coincidence of the Ir and Os isotope anomalies (expanded discussion in (*44*)). Third, while

179 roughly equal pre- and post-impact volcanic degassing is possible (i.e., Case 2, Fig. 1), our

180 results are not consistent with the majority (>75%) of volcanogenic degassing post-impact (i.e.,

181 outgassing more similar to eruptive volumes in refs. *12, 39*), because modeled warming is too

182 muted in the Cretaceous and too pronounced in the early Paleocene (i.e., Case 3) as compared to

183 empirical records (Fig. 1). Fourth, boundary impact-related volatile release has a negligible

184 climatic effect (Fig. S29), so is unlikely to account for the dramatic warming indicated by fish

185 teeth $\delta^{18}O$ in the first 100 kyr (*53*). Instead, the fish tooth $\delta^{18}O$ record likely predominately

186 reflects changes in fish biology rather than environmental temperatures. Fifth, biotic recovery

187 can account for the apparent gradual early Danian warming as observed in marine records if it

188 begins at or shortly after impact and occurs over >1.5 myr. This biotic recovery scenario

189 reproduces the general pattern of change in $\delta^{13}C$ gradients (Fig. 2, S35), carbonate saturation

190 state (Fig. 2c, S35) and temperature, but is distinct from existing biological recovery hypotheses

191 that posit a delay in the onset of biological recovery for ~ 500kyr or more (e.g., 44, 54; Fig. S35).

192

193 **No marine evidence for joint cause, but joint delay is possible**

194 The fossil record indicates no lasting, outsized, or cascading affects of the late Maastrichtian

195 warming event on marine ecosystems of the sort that might predispose them to mass extinction

196 by impact. First, there is no evidence for elevated extinction rates in the latest Cretaceous in

197 marine taxa (Table S1). Indeed, in the Cretaceous portion of magnetochron C29r, the notable

198 scarcity of biostratigraphic datums signifies a conspicuous lack of extinction in widespread

199 species from clades including planktonic foraminifera, nannoplankton, radiolarian, and

200 ammonites (6). Second, late Cretaceous outgassing does not have a lasting effect on the

201 community structure of well-fossilized taxa. Although range and community shifts coincide with

202 warming, there is a shift back to pre-warming event like communities *prior* to impact (see Table

203 S1). Third, marine carbon cycle indicators ($\delta^{13}C$ and carbonate deposition) show that there was

204 no discernable effect of late Maastrichtian outgassing and warming on a major ecosystem

205 function: the export and cycling of carbon. The $\delta^{13}C$ anomaly size is consistent with a

206 volcanogenic driver (Fig. 2: ~0.5‰ in both pelagic and benthic carbonates, Figs. S30, S32: ~0.2-

207 0.8 ‰ in simulated excursions depending on outgassing volume and climate sensitivity) given

208 the magnitude of warming, without biological amplification.

209

210 There is, in contrast, major and enduring change to ecosystems coincident with the K/Pg impact

211 and boundary clay deposition. In deep-sea records, impact markers coincide with the abrupt mass

212 extinction of >90% planktonic foraminifera and 93% of nannoplankton species (Fig. 2). In some

213 groups without evidence of elevated extinction, such as small fishes, there is a permanent change

214 in community structure (55). Planktonic foraminifers and nannoplankton also exhibit rapid

215 turnover and high dominance in community composition for the first 500 kyrs of the Paleocene

216 (56, 57), an interval where bulk carbonate $\delta^{18}O$ likely reflects community composition rather

217 than surface ocean temperatures (Figs. 3, 4, S20). At the same time, tracers of the marine carbon

218 cycle indicate a profound change in marine ecosystem function. The $\delta^{13}C$ composition of

219 surface-dwelling planktonic foraminifera and nannoplankton falls to or below that of benthic

220 foraminifera with the deposition of the iridium anomaly (Figs. 2-4)(*47, 49*). The loss or inversion

221 of the $\delta^{13}C$ gradient typically maintained by the biological pump is unmatched in the fossil

222 record of pelagic calcifiers (~150 million years), and indicates that the K/Pg boundary impact

223 had an outsized impact on the marine carbon cycle.

224

225 After the impact, an already altered marine carbon cycle is needed to counteract the CO_2 emitted

226 by a major post-impact pulse of outgassing as in Case 2 (Fig. 1) to avoid a warming event of the

227 same magnitude as the Late Cretaceous warming event. This suggests that the major ecological

228 change of the KPg mass extinction must have occurred prior to any major post-impact

229 volcanism. Intriguingly though, our modeling does support a scenario in which Deccan

230 volcanism could have contributed to the aftermath of the impact and mass extinction as in (*12*), if

231 environmentally destructive gases like SO_2 or sulfate aerosols contributed to (or drove) the

232 persistence of unusual marine communities for the first ~500 kyrs of the Paleocene. To date, no

233 study has documented acidification coupled to extreme cold snaps in the earliest Paleocene as

234 predicted by this hypothesis, and no study has provided an explanation for why SO_2 would have

235 greater biotic effects in the very well-buffered early Danian oceans than in the latest

236 Maastrichtian oceans (Fig. S1-S32), but few have tried.

237

238 By combining climatic, biotic, and carbon cycle records with modeled impact and outgassing

239 scenarios, we find support for a bolide impact as the primary driver of the end-Cretaceous mass

240 extinction. In doing so, we provide evidence for a pronounced decoupling between CO_2

241 outgassing and lava flow emplacement given new age estimates for the Deccan Traps (*39, 40*).

242 The Late Cretaceous warming event attributed to Deccan degassing is of a comparable size to

243 small warming events in the Paleocene and early Eocene that are not associated with elevated

244 extinction or turnover (*49, 58*), similar to what we find here. We thus argue that impact and

245 extinction created the initial opportunity for the rise of Cenozoic species and communities, but

246 Deccan volcanism might have contributed to shaping them during the extinction aftermath.

247

268

References

1. L. W. Alvarez, W. Alvarez, F. Asaro, H. V. Michel, Extraterrestrial cause for the Cretaceous-Tertiary extinction - experimental results and theoretical interpretation. *Science* **208**, 1095-1108 (1980).

2. A. R. Hildebrand *et al.*, Chicxulub crater - a possible Cretaceous Tertiary Boundary impact crater on the Yucatan Peninsula, Mexico. *Geology* **19**, 867-871 (1991).

3. B. Collen *et al.*, Clarifying misconceptions of extinction risk assessment with the IUCN Red List. *Biology Letters* **12**, (2016).

4. P. Schulte *et al.*, The Chicxulub Asteroid Impact and Mass Extinction at the Cretaceous-Paleogene Boundary. *Science* **327**, 1214-1218 (2010).

5. G. Ravizza, D. VonderHaar, A geochemical clock in earliest Paleogene pelagic carbonates based on the impact-induced Os isotope excursion at the Cretaceous-Paleogene boundary. *Paleoceanography* **27**, PA3219 (2012).

6. F. M. Gradstein, J. G. Ogg, M. D. Schmitz, G. M. Ogg, *The Geologic Time Scale 2012*. (Elsevier B.V., Amsterdam, 2012).

7. C. J. Sprain, P. R. Renne, W. A. Clemens, G. P. Wilson, Calibration of chron C29r: New high-precision geochronologic and paleomagnetic constraints from the Hell Creek region, Montana. *Geological Society of America Bulletin* **130**, 1615-1644 (2018).

8. A. L. Chenet *et al.*, Determination of rapid Deccan eruptions across the Cretaceous-Tertiary boundary using paleomagnetic secular variation: 2. Constraints from analysis of eight new sections and synthesis for a 3500-m-thick composite section. *Journal of Geophysical Research-Solid Earth* **114**, B06103 (2009).

9. A. E. Jay, M. Widdowson, Stratigraphy, structure and volcanology of the SE Deccan continental flood basalt province: implications for eruptive extent and volumes. *Journal of the Geological Society* **165**, 177-188 (2008).

10. A. L. Chenet, X. Quidelleur, F. Fluteau, V. Courtillot, S. Bajpai, K-40-Ar-40 dating of the Main Deccan large igneous province: Further evidence of KTB age and short duration. *Earth and Planetary Science Letters* **263**, 1-15 (2007).

11. B. Schoene *et al.*, U-Pb geochronology of the Deccan Traps and relation to the end-Cretaceous mass extinction. *Science* **347**, 182-184 (2015).

12. P. R. Renne *et al.*, State shift in Deccan volcanism at the Cretaceous-Paleogene boundary, possibly induced by impact. *Science* **350**, 76-78 (2015).

13. P. R. Renne *et al.*, Time Scales of Critical Events Around the Cretaceous-Paleogene Boundary. *Science* **339**, 684-687 (2013).

14. M. A. Richards *et al.*, Triggering of the largest Deccan eruptions by the Chicxulub impact. *Geological Society of America Bulletin* **127**, 1507-1520 (2015).

15. E. Font *et al.*, Deccan volcanism induced high-stress environment during the Cretaceous-Paleogene transition at Zumaia, Spain: Evidence from magnetic, mineralogical and biostratigraphic records. *Earth and Planetary Science Letters* **484**, 53-66 (2018).

16. J. Morgan *et al.*, Size and morphology of the Chicxulub impact crater. *Nature* **390**, 472-476 (1997).

17. N. Artemieva, J. Morgan, E. S. Party, Quantifying the Release of Climate-Active Gases by Large Meteorite Impacts With a Case Study of Chicxulub. *Geophysical Research Letters* **44**, 10180-10188 (2017).

313   18.   D. A. Kring, D. D. Durda, Trajectories and distribution of material ejected from the
314   Chicxulub impact crater: implications for postimpact wildfires. *Journal of Geophysical*
315   *Research-Planets* **107**, (2002).
316   19.   J. Morgan, N. Artemieva, T. Goldin, Revisiting wildfires at the K-Pg boundary. *J*
317   *Geophys Res-Biogeo* **118**, 1508-1520 (2013).
318   20.   S. Ohno *et al.*, Production of sulphate-rich vapour during the Chicxulub impact and
319   implications for ocean acidification. *Nature Geoscience* **7**, 279-282 (2014).
320   21.   T. Tyrrell, A. Merico, D. I. A. McKay, Severity of ocean acidification following the end-
321   Cretaceous asteroid impact. *Proceedings of the National Academy of Sciences of the*
322   *United States of America*, 6556-6561 (2015).
323   22.   J. Vellekoop *et al.*, Rapid short-term cooling following the Chicxulub impact at the
324   Cretaceous-Paleogene boundary. *Proceedings of the National Academy of Sciences of the*
325   *United States of America* **111**, 7537-7541 (2014).
326   23.   K. Kaiho *et al.*, Global climate change driven by soot at the K-Pg boundary as the cause
327   of the mass extinction. *Sci Rep-Uk* **6**, (2016).
328   24.   J. Brugger, G. Feulner, S. Petri, Baby, it's cold outside: Climate model simulations of the
329   effects of the asteroid impact at the end of the Cretaceous. *Geophysical Research Letters*
330   **44**, 419-427 (2017).
331   25.   C. G. Bardeen, R. R. Garcia, O. B. Toon, A. J. Conley, On transient climate change at the
332   Cretaceous-Paleogene boundary due to atmospheric soot injections. *Proceedings of the*
333   *National Academy of Sciences of the United States of America* **114**, E7415-E7424 (2017).
334   26.   L. Alegret, E. Thomas, K. C. Lohmann, End-Cretaceous marine mass extinction not
335   caused by productivity collapse. *Proceedings of the National Academy of Sciences of the*
336   *United States of America* **109**, 728-732 (2012).
337   27.   M. Aberhan, S. Weidemeyer, W. Kiessling, R. A. Scasso, F. A. Medina, Faunal evidence
338   for reduced productivity and uncoordinated recovery in Southern Hemisphere
339   Cretaceous-Paleogene boundary sections. *Geology* **35**, 227-230 (2007).
340   28.   P. M. Sheehan, T. A. Hansen, Detritus Feeding as a Buffer to Extinction at the End of the
341   Cretaceous. *Geology* **14**, 868-870 (1986).
342   29.   D. S. Robertson, M. C. McKenna, O. B. Toon, S. Hope, J. A. Lillegraven, Survival in the
343   first hours of the Cenozoic. *Geological Society of America Bulletin* **116**, 760-768 (2004).
344   30.   J. D. Archibald *et al.*, Cretaceous Extinctions: Multiple Causes. *Science* **328**, 973-973
345   (2010).
346   31.   G. Keller, J. Punekar, P. Mateo, Upheavals during the Late Maastrichtian: Volcanism,
347   climate and faunal events preceding the end-Cretaceous mass extinction.
348   *Palaeogeography Palaeoclimatology Palaeoecology* **441**, 137-151 (2016).
349   32.   W. Y. Lu *et al.*, Late inception of a resiliently oxygenated upper ocean. *Science* **361**, 174-
350   177 (2018).
351   33.   P. B. Wignall, *The worst of times: how life on earth survived eighty million years of*
352   *extinctions*. (Princeton University Press, 2015).
353   34.   K. M. Meyer, A. Ridgwell, J. L. Payne, The influence of the biological pump on ocean
354   chemistry: implications for long-term trends in marine redox chemistry, the global carbon
355   cycle, and marine animal ecosystem. *Geobiology* **14**, 207-219 (2016).
356   35.   A. H. Knoll, M. J. Follows, A bottom-up perspective on ecosystem change in the
357   Mesozoic oceans. *Proceedings of the Royal Society B-Biological Sciences* **283**, 20161755
358   (2016).

359 36. R. E. Zeebe, P. Westbroek, A simple model for the CaCO3 saturation state of the ocean:
360   The "Strangelove", the "Neritan", and the "Cretan" Ocean. *Geochemistry Geophysics*
361   *Geosystems* **4**, 1104 (2003).
362 37. A. Ridgwell, A Mid Mesozoic Revolution in the regulation of ocean chemistry. *Marine*
363   *Geology* **217**, 339-357 (2005).
364 38. M. J. Henehan, P. M. Hull, D. E. Penman, J. W. B. Rae, D. N. Schmidt, Biogeochemical
365   significance of pelagic ecosystem function: an end-Cretaceous case study. *Philosophical*
366   *Transactions of the Royal Society B-Biological Sciences* **371**, 20150510 (2016).
367 39. C. J. Sprain *et al.*, The eruptive tempo of Deccan volcanism in relation to the Cretaceous-
368   Paleogene boundary. *Science* **363**, 866-+ (2019).
369 40. B. Schoene *et al.*, U-Pb constraints on pulsed eruption of the Deccan Traps across the
370   end-Cretaceous mass extinction. *Science* **363**, 862-866 (2019).
371 41. M. T. Jones, D. A. Jerram, H. H. Svensen, C. Grove, The effects of large igneous
372   provinces on the global carbon and sulphur cycles. *Palaeogeography Palaeoclimatology*
373   *Palaeoecology* **441**, 4-21 (2016).
374 42. A. Schmidt *et al.*, Selective environmental stress from sulphur emitted by continental
375   flood basalt eruptions. *Nature Geoscience* **9**, 77-82 (2016).
376 43. S. Self, S. Blake, K. Sharma, M. Widdowson, S. Sephton, Sulfur and chlorine in Late
377   Cretaceous Deccan magmas and eruptive gas release. *Science* **319**, 1654-1657 (2008).
378 44. Materials and methods are available as supplementary materials at the Science website.
379 45. R. E. Zeebe, LOSCAR: Long-term Ocean-atmosphere-Sediment CArbon cycle Reservoir
380   Model v2.0.4. *Geoscientific Model Development* **5**, 149-166 (2012).
381 46. J. C. Zachos, M. A. Arthur, W. E. Dean, Geochemical evidence for suppression of
382   pelagic marine productivity at the Cretaceous/Tertiary boundary. *Nature* **337**, 61-64
383   (1989).
384 47. H. S. Birch, H. K. Coxall , P. N. Pearson, D. Kroon, D. N. Schmidt, Partial collapse of
385   the marine carbon pump after the Cretaceous-Paleogene boundary. *Geology*, (2016).
386 48. J. S. K. Barnet *et al.*, A new high-resolution chronology for the late Maastrichtian
387   warming event: Establishing robust temporal links with the onset of Deccan volcanism.
388   *Geology* **46**, 147-150 (2018).
389 49. J. S. K. Barnet *et al.*, A high-fidelity benthic stable isotope record of Late Cretaceous-
390   Early Eocene climate change and carbon-cycling. *Paleoceanography and*
391   *Paleoclimatology* **34**, 672-691 (2019).
392 50. R. D. Norris, P. A. Wilson, P. Blum, a. t. E. Scientists, in *Proc. IODP, 342,* R. D. Norris,
393   Wilson, P.A., Blum, P., and the Expedition 342 Scientists, Ed. (Integrated Ocean Drilling
394   Program, College Station, TX, 2014).
395 51. N. Robinson, G. Ravizza, R. Coccioni, B. Peucker-Ehrenbrink, R. Norris, A high-
396   resolution marine Os-187/Os-188 record for the late Maastrichtian: distinguishing the
397   chemical fingerprints of Deccan volcanism and the KP impact event. *Earth and*
398   *Planetary Science Letters* **281**, 159-168 (2009).
399 52. E. J. Rohling *et al.*, Comparing Climate Sensitivity, Past and Present. *Annual Review of*
400   *Marine Science, Vol 10* **10**, 261-+ (2018).
401 53. K. G. MacLeod, P. C. Quinton, J. Sepulveda, M. H. Negra, Postimpact earliest Paleogene
402   warming shown by fish debris oxygen isotopes (El Kef, Tunisia). *Science* **360**, 1467-+
403   (2018).

404   54.   S. D'Hondt, P. Donaghay, J. C. Zachos, D. Luttenberg, M. Lindinger, Organic carbon
405   fluxes and ecological recovery from the Cretaceous-Tertiary mass extinction. *Science*
406   **282**, 276-279 (1998).
407   55.   E. C. Sibert, M. Friedman, P. M. Hull, G. Hunt, R. D. Norris, Two pulses of origination
408   in Pacific pelagic fish following the Cretaceous-Paleogene Mass Extinction. *Proceedings*
409   *of the Royal Society B-Biological Sciences*, 20181194 (2018).
410   56.   P. M. Hull, R. D. Norris, T. J. Bralower, J. D. Schueth, A role for chance in marine
411   recovery from the end-Cretaceous extinction. *Nature Geoscience*, (2011).
412   57.   J. J. Pospichal, in *The Cretaceous-Tertiary event and other catastrophes in Earth history:*
413   *Geological Society of America Special Paper 307,* G. Ryder, D. Fastovsky, S. Gartner,
414   Eds. (1996), pp. 335-360.
415   58.   P. F. Sexton *et al.*, Eocene global warming events driven by ventilation of oceanic
416   dissolved organic carbon. *Nature* **471**, 349-352 (2011).
417   59.   R. D. Norris, in *Palaeobiology II,* D. E. G. Briggs, P. G. Crowther, Eds. (Blackwell
418   Science Ltd., Oxford, 2001), pp. 229-231.
419   60.   T. Westerhold, U. Röhl, B. Donner, H. K. McCarren, J. C. Zachos, A complete high-
420   resolution Paleocene benthic stable isotope record for the central Pacific (ODP Site
421   1209). *Paleoceanography*, (2011).
422
423
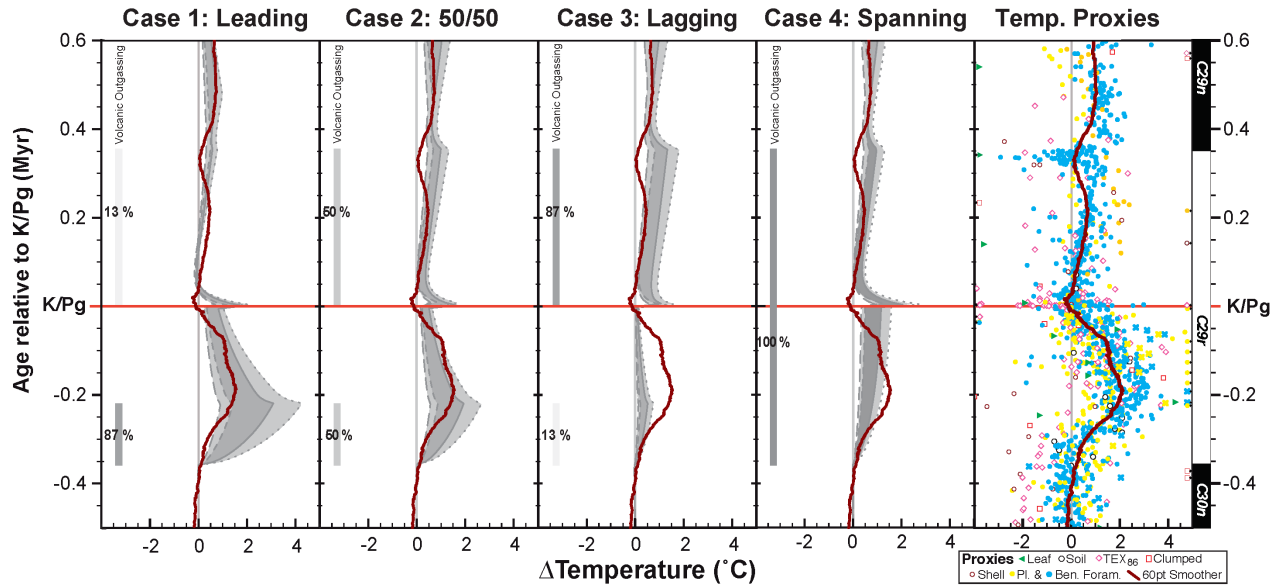
Figure 1. Global temperature change across the Cretaceous-Paleogene boundary as compared to four scenarios for Deccan Trap outgassing. Four Deccan Trap outgassing scenarios include (a) Case 1 (Leading): most outgassing prior to impact, (b) Case 2 (50/50): 50% outgassing prior to and 50% post impact, (c) Case 3 (Lagging): most outgassing post impact, and (d) Case 4 (Spanning): outgassing throughout magnetochron C29r (Table 1). Each model scenario is represented by four lines (bounding a shaded region) delineating different combinations of climate sensitivity and volcanic outgassing: high degassing (9545 GtC and 8500 GtS) & 3°C/doubling (solid line); high degassing & 4°C/doubling (dotted line), low degassing (4090 GtC and 3200 GtS) & 3°C/doubling (short dashed line), and low degassing & 2°C/doubling (long dashed line), and compared to a 60pt fast Fourier transform smoother of global temperature change (red line) from the records shown in (e). New and existing empirical temperature records from marine sediments ($\delta^{18}O$ of foraminifera, TEX_{86}), shallow marine carbonates (clumped isotopes of mollusk carbonate), and terrestrial proxies (leaf margin analysis, biomarkers, clumped isotopes of mollusk carbonate) in (e) were aligned to common age model (Table S2 and S3) and normalized to Late Cretaceous temperature within each record. Data are provided in Table S4-S12 and a detailed proxy symbol legend in Fig. S16.
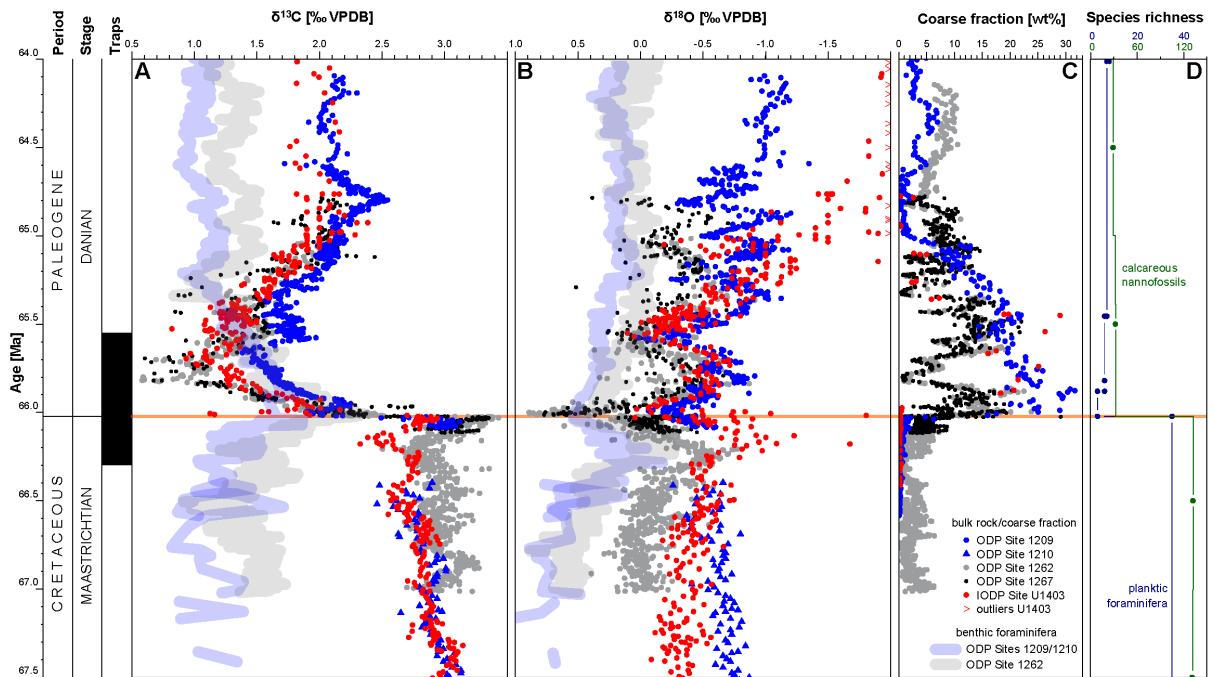
15

Figure 2. K/Pg boundary dynamics at the best-resolved deep-sea sites globally: Shatsky Rise, Walvis Ridge, and J-Anomaly Ridge. High resolution carbon (a) and oxygen (b) isotope dynamics in benthic foraminifera (transparent lines) and bulk carbonate (discrete points), and sediment composition (c, weight % coarse fraction), at Shatsky Rise (blue), Walvis Ridge (grey), and J-Anomaly Ridge (red), compared to (d) global records of nannofossil (grey) and foraminifera (blue, from (*59*)) species richness. Deccan Trap emplacement interval indicated at left by the black bar. Data is from new and published records as described in ref. 44.

16
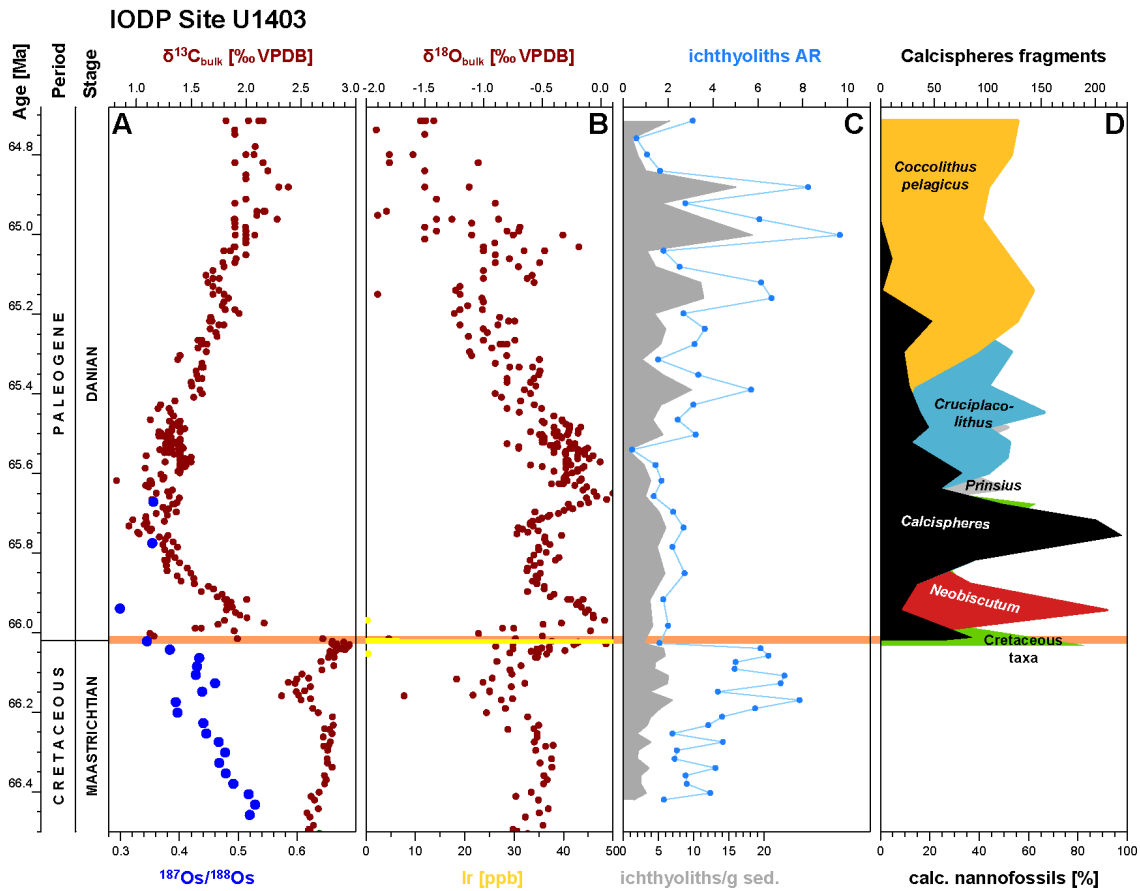
Figure 3. Late Cretaceous warming and early Paleocene record of environmental and biotic change at IODP Site U1403, J-Anomaly Ridge, Newfoundland. A negative carbon isotope anomaly (a) coincides with late Cretaceous warming in $\delta^{18}O$ (b), and osmium isotope evidence for volcanism (a) at IODP Site U1403. The collapse in surface ocean $\delta^{13}C$ values (a) coincides with iridium anomaly (b), and step change in fish tooth accumulation (c). Earliest Paleocene $\delta^{18}O$ values of bulk carbonate appear to be strongly influenced by vital effects driven by rapid turnover in the dominant calcareous nannofossil taxa (d). Data in Tables S12, S16, S17, S29.
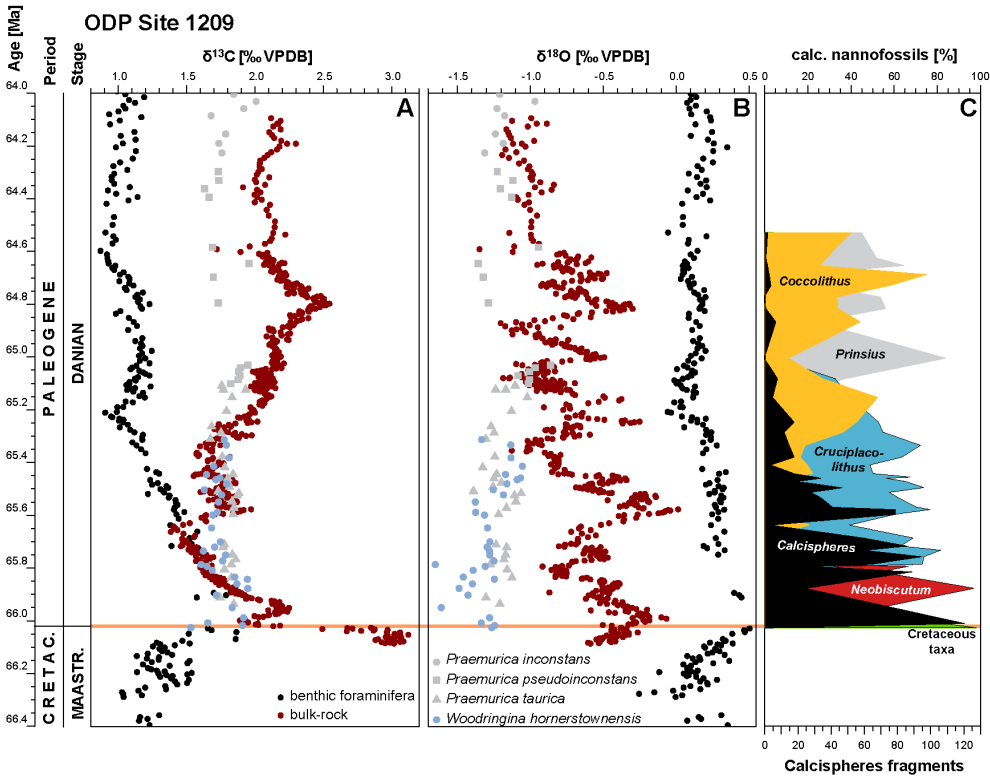
Figure 4. Records from ODP Site 1209, Central Pacific support patterns and inferences from IODP Site 1403. The K/Pg boundary coincides with a collapse (to inversion) in (a) the carbon isotopes of bulk carbonate (red) and planktonic foraminifera (grey, blue) relative to benthic foraminifera (black), a $\delta^{13}C$ gradient typically maintained by the biological pump. In (b) the relative stability of benthic foraminiferal (black) and planktonic foraminiferal (grey and blue) $\delta^{18}O$ (b) support the inference that earliest Paleocene of bulk carbonate (red) $\delta^{18}O$ values are strongly influenced by vital effects reflecting the rapid turnover in dominate nannofossil taxa (c) Data from Tables S11, S18 and refs. (*56, 60*).

474   **Table 1. Model parameters for four main Deccan outgassing scenarios tested in LOSCAR.**

475

	Case 1: Leading	Case 2: 50/50	Case 3: Lagging	Case 4: Spanning
Volcanic Outgassing				
Pulse 1 (Pre): Volume	87% of total high: 8305 Gt C, 7395 Gt S low: 3559 Gt C, 2784 Gt S	50% of total high: 4773 Gt C, 4250 Gt S low: 2045 Gt C, 1600 Gt S	13% of total high: 1241 Gt C, 1105 Gt S low: 532 Gt C, 416 Gt S	100% of total high: 9545 Gt C, 8500 Gt S low: 4091 Gt C, 3200 Gt S
Timing	Starts: -358 kyr Ends: -218 kyr	Starts: -358 kyr Ends: -218 kyr	Starts: -358 kyr Ends: -218 kyr	Starts: -358 kyr Ends: 355 kyr
Pulse 2 (Post): Volume	13% of total high: 1241 Gt C, 1105 Gt S low: 532 Gt C, 416 Gt S	50% of total high: 4773 Gt C, 4250 Gt S low: 2045 Gt C, 1600 Gt S	87% of total high: 8305 Gt C, 7395 Gt S low: 3559 Gt C, 2784 Gt S	
Timing	Starts: 0 kyr Ends: 355 kyr	Starts: 0 kyr Ends: 355 kyr	Starts: 0 kyr Ends: 355 kyr	
Impact Outgassing				
Volume	100% of total 115 Gt C, 325 Gt S	100% of total 115 Gt C, 325 Gt S	100% of total 115 Gt C, 325 Gt S	100% of total 115 Gt C, 325 Gt S
Timing	Starts: 0 kyr Ends: 0 kyr	Starts: 0 kyr Ends: 0 kyr	Starts: 0 kyr Ends: 0 kyr	Starts: 0 kyr Ends: 0 kyr
Biotic Change				
Organic ExportFlux Δ	50% reduction	50% reduction	50% reduction	50% reduction
CaCO₃ Export Flux Δ	42.5% reduction	42.5% reduction	42.5% reduction	42.5% reduction
Intermediate-depth C_{org} remineralization fract. Δ	22% increase	22% increase	22% increase	22% increase
Timing	Starts: 0 kyr immediately begins taper Ends: 1770 kyr	Starts: 0 kyr immediately begins taper Ends: 1770 kyr	Starts: 0 kyr immediately begins taper Ends: 1770 kyr	Starts: 0 kyr immediately begins taper Ends: 1770 kyr

476

19

Science

AAAS

Supplementary Materials for

Constraining the Role of Impact and Volcanism in Marine Extinctions across the Cretaceous-Paleogene Boundary

Pincelli M. Hull, André Bornemann, Donald Penman, Michael J. Henehan, Richard D. Norris, Paul A. Wilson, Peter Blum, Laia Alegret, Sietske Batenburg, Paul Bown, Timothy J. Bralower, Cecile Cournede, Alexander Deutsch, Barbara Donner, Oliver Friedrich, Sofie Jehle, Hojung Kim, Dominik Loroch, Peter Lippert, C. Brenhin Keller, Dick Kroon, Iris Moebius, Kazuyoshi Moriya, Daniel J. Peppe, Gregory E. Ravizza, Ursula Röhl, Philip Sexton, Julio Sepúlveda, Jonathan D. Schueth, Elizabeth Sibert, Kasia K. Sliwinska, Roger Summons, Ellen Thomas, Thomas Westerhold, Jessica Whiteside, Tatsuhiko Yamaguchi, James C. Zachos

correspondence to: pincelli.hull@yale.edu

This PDF file includes:

Materials and Methods
Supplementary Text
Figs. S1 to S38
Tables S1 to S2

Other Supplementary Materials for this manuscript includes the following:

Tables S3 to S30

Materials and Methods

<u>Sites and materials</u>

Here we present highly resolved, multiproxy records from three ocean drilling localities: J-Anomaly Ridge, North Atlantic (Integrated Ocean Drilling Program [IODP] Site U1403), Shatsky Rise, North Pacific (Ocean Drilling Program [ODP] Site 1209, Deep Sea Drilling Program [DSDP] Site 577), and Walvis Ridge, South Atlantic (ODP Site 1262 & 1267).

This is the first detailed study of Cretaceous-Paleogene (K/Pg) sediments from IODP Site U1403, which was drilled on the flank of the J-Anomaly Ridge in 2012 at 39°56.60′N by 51°48.20′W and a present water depth of 4,949 m (*1*). Shipboard scientists immediately recognized that the two K/Pg spanning holes (U1403A and U1403B) were remarkably complete, with an intact ejecta layer and all nannofossil biozones present (*2*). The results presented here include a highly resolved bulk carbonate stable isotope record sampled shipboard at a resolution varying from ~20 cm in the Danian, to 2 cm across the boundary, and ~10 cm in the late Cretaceous (Table S12). This bulk carbonate carbon and oxygen isotope record is the longest highly resolved record of its sort across the K/Pg boundary (Fig S17), spanning the last 2.5 million years of the Cretaceous and the first 3 million years of the Paleocene. Additional samples for complementary measurements (i.e., sedimentology, magnetostratigraphy, biostratigraphy, cyclostratigraphy, iridium measurements, faunal and organic geochemistry analyses) were sampled during the post-cruise sampling party and in subsequent sampling requests and are detailed below in the relevant subsections.

We also present new K/Pg records from two of the best studied deep sea K/Pg boundary localities, Walvis Ridge and Shatsky Rise, while leveraging existing resources from these sites. Shatsky Rise sites include the well-studied ODP Site 1209 on the Shatsky Rise (*3, 4*) at 32°39.1001′N by 158°30.3560′W and 2,387 m current water depth and DSDP Site 577 at 32°26.5′N by 157°30.4′W and 2,685 m current water depth (*5*). Walvis Ridge sites include ODP Site 1262 at 27°11.15′S by 1°34.62′E and 4,759 m current water depth (*6*) and ODP Site 1267 at 28°5.89′S by 1°42.66′E and 4,355 m current water depth (*7*). ODP Sites from Shatsky Rise and Walvis Ridge have been used along with the deep-sea sediments outcropping in Zumaia, Spain, to develop and refine a complete astrochronological age model for the Paleocene and latest Cretaceous (*8-12*). With a biostratigraphically complete K/Pg boundary section, and a globally aligned cyclostratigraphic age model spanning from the very latest Cretaceous through the

Paleocene, ODP Site 1209 and the nearby ODP Sites 1210 and 1211 have been extensively studied across the boundary, with existing studies including a resolved benthic foraminiferal and, in the Cretaceous, bulk carbonate stable carbon and oxygen isotope record (*13-15*), community dynamics across the boundary in nannoplankton (*16-21*), foraminifera (*22-24*), and fish (*25*), productivity change (*26*), environmental change (*27, 28*), extinction drivers (*29*), and in global compilations of boundary sections and dynamics (*30*). The new high-resolution records presented here include a highly resolved boundary record of bulk carbonate oxygen and carbon isotopes (shown in part in: *22*) (Table S11), complementary records of early Paleocene foraminiferal oxygen and carbon isotopes (Table S11), and a resolved earliest Danian record of nannoplankton community composition (Table S18). These new and existing records from ODP Site 1209 allow us to test the generality of patterns and explanations derived from Site U1403 records in the context of the much broader body of work from Shatsky Rise, including studies on the historic DSDP 577 holes (e.g., *5, 31-40*) at the same location. The same is true of Walvis Ridge. From Walvis Ridge we present a new resolved bulk isotope record (Tables S9) and weight percent coarse fraction record from ODP Site 1267 (Table S13), to test the generality of these existing resources from ODP Site 1262 (*41*), with the underlying records published here for the first time Tables S10, S14).

The high-resolution records at J-Anomaly Ridge, Shatsky Rise, and Walvis Ridge are shown in Fig. 2. The data in this figure is provided in Tables S9-S15 and refs. (*13-15, 22, 41-44*) and age models are from (*12, 45, 46*).

Together these records (Fig. 2 and S18), are the most temporally resolved and finely sequenced records of the K/Pg boundary and they offer the opportunity to finely detail the temporal sequence of change in open ocean sites relatively far from the impactor: the central equatorial Pacific (ODP Site 1209, DSDP Site 577), the mid latitude North Atlantic (IODP Site U1403), and the South Pacific (ODP Sites 1262 and 1267). Distance from the impactor was an important criterion because proximal sites in the Caribbean and in some locations along the eastern seaboard of North America are stratigraphically complex, and include some combination of the following: expanded ejecta deposits, tsunami deposits, mass wasting deposits, and hiatuses (*30, 47-53*). Part of the historic debate on the timing of boundary related events in open marine sediments, and the possibility of multiple impacts or impacts asynchronous with the boundary, has arisen from studies that interpret the depositional history (in particular, the timing of

3

deposition) in proximal sites as if they reflected processes and rates typical of normal marine sedimentation (*54-56*). Our study focuses on records from the relatively open ocean basins in the latest Cretaceous (the Atlantic and Pacific) in order to capture the open ocean response to the events of the K/Pg boundary.

Age model overview

Two main types of age models are used in this study: cyclostratigraphic age models and bio- or magnetostratigraphic age models. Data from the three high resolution localities (J-Anomaly Ridge: IODP Site U1403, Shatsky Rise: ODP Sites 1209 & 1210, and Walvis Ridge ODP Sites 1262 & 1267) are shown in the geologic time domain using cyclostratigraphic age models. For Site U1403 we combined a completed cyclostratigraphic age model for the Maastrichtian (*57*) with a new cyclostratigraphic age model for the Danian (detailed below). The Site U1403 age model is tied to a K/Pg boundary age of 66.022 Ma to be consistent with the boundary used by Dinarès-Turell et al. (2014) in other cyclostratigraphic age models for this interval for Walvis Ridge and Shatsky Rise (*12, 14, 15, 45, 46*). This boundary age differs from the most recent radiometric ages for the K/Pg boundary of 66.016 ± 0.05 Ma (*58*) for U-Pb and 66.052 ± 0.008 Ma (*59*) for ^{40}Ar/^{39}Ar, but falls within the error bounds for those estimate (including systematic error). We use the existing cyclostratigraphic framework for the K/Pg boundary sections at Sites 1209, 1210, 1262, and 1267 from Dinares-Turrell et al. (2014) (*12*), with its extension further into the Maastrichtian by Woelders et al. (2017) (*44*).

GTS 2012 (K/Pg boundary age 66.04 Ma) forms the framework for the other age models used in this study and shown in the compilation Figure 1 (*60*). The data in Figure 1 are a compilation of temperature estimates from marine and terrestrial sites around the world (Fig. S1-S16), updated to a common timescale (primarily) by updating the bio- and magnetostratigraphic marker ages to match those of GTS 2012. In order to construct GTS 2012-compliant age models for all localities (detailed below and shown in Tables S2-S4), the records from Sites U1403, 1209, 1210, 1262, and 1267, which were on the Dinarès-Turell et al. (2014) (*12*) age model, were shifted to match the K/Pg boundary age in the global compilation.

Cyclostratigraphic age model for U1403

The Maastrichtian to Danian interval of Site U1403 was analyzed by XRF-scanning (X-Ray Fluorescence) in the MARUM XRF Core Scanner Lab in Bremen, Germany. The AVAATECH instrument, serial no.11, with an Oxford Instruments 100W Neptune Rh X-Ray tube and a Canberra X-PIPS Silicon Drift Detector (SDD, Model SXD 15C-150-500) was set to a step-size of 15 mm, a slit down-core of 10 mm, and a slit cross-core of 12 mm. A first run was applied with 10Kv, 1.0 mA, for 20 s, and a second run at 50 Kv, 0.2 mA, for 20 s. The data were processed with WIN AXIL batch software using a 10Kv_Cl-Rh model and a 50Kv model, respectively. Outliers as a result of an uneven core surface were removed. The Danian XRF record is presented in Supplemental Table S21and compliments the already published Maastrichtian record (*57*).

Two holes were drilled at IODP Site U1403: Holes U1403A and U1403B. A shipboard splice, subsequently updated slightly by Batenburg et al. (*57*), was used to generate a common depth scale between these two holes (classically known as meters composite depth [mcd] but called CCSF [core composite depth below sea floor] at Site U1403). The K/Pg impact ejecta layer was not used as an anchor point in building the composite splice between these two holes. Because of the highly resolved sampling across the K/Pg boundary, this omission created numerous issues with regards to building an accurate relative stratigraphy of the event for the samples that were collected off the main splice in the boundary cores (342-U1403A-26X, 342-U1403B-28X) due to a 20cm CCSF offset between the ejecta layer in the two holes on the CCSF scale. To address this problem in the relative depth scale and age model, we adjusted the splice to include the impact ejecta layer as the tie point between the boundary cores at the two sites. The secondary tie point linked the K-Pg boundary in Hole B (which is not in the splice) with 247.7 rCCSF (revised CCSF) in Hole A. We then recalculated the CCSFs for Hole B, Core 28 by a linear interpolation between the boundary and the neighboring splice tie points. Only the coarse fraction, fish teeth and iridium records contain samples that required a CCSF revision as described above. The effect of this adjustment is shown in Table S22.

To obtain detailed age control for the Danian interval of U1403, we correlated the iron record and the sedimentary banding pattern to the existing cyclostratigraphic framework of Site 1209(*12*). A direct cyclostratigraphic interpretation of the interval above the K/Pg at U1403 is hampered by the relatively short length of the record and the complex nature of orbitally forced sedimentation patterns directly following the K/Pg, which is documented in records worldwide

(*12, 61*). A detailed comparison of Site U1403 to Site 1209 was made using the banding patterns in the core photographs and the Fe counts from XRF analysis (expressed as log Fe, Fig. 7), supported by variations in magnetic susceptibility(*62*). In addition, a bandpass filter was applied using AnalySeries (*63*) to the log Fe record, centered at 2.2 m with a bandwidth of 1.7 to 3.3 m (Fig. S22). The 2.2 m filter follows the oscillations of the log Fe record and the sedimentary banding patterns, with maxima in the bandpass filter coinciding with groups of dark bands, likely representing maxima in the 405-kyr cycle of eccentricity-modulated precession. An age model for the Danian of U1403 was constructed by assigning ages of long-eccentricity (405 kyr) maxima and minima in the La2011 eccentricity solution (*64*) to levels in U1403 corresponding to interpreted 405-kyr extremes in Site 1209 (*12*). An additional cyclostratigraphic investigation of Site 1209 (*61*) proposes the same number of interpreted long-eccentricity cycles post-K/Pg and a similar interpretation of the position of 405-kyr cycle extremes, except for the placement of the second 405-kyr maximum above the K/Pg boundary. The age model for the Danian of U1403 was combined with the existing Maastrichtian cyclostratigraphic age model (Table S23, Fig. S22). The resulting age model is broadly consistent with shipboard based nannofossil biostratigraphy in the Maastrichtian (*57*), updated Danian nannofossil biostratigraphy (Tables S24 & S25), and osmium isotope stratigraphy (see below).

The comparison of bulk isotope records from J-Anomaly Ridge, Shatsky Rise, and Walvis Ridge highlight the relative certainty in the age models for the three sites (Fig. 2). IODP Site U1403 on J-Anomaly Ridge is relatively poorly constrained in the latest Maastrichtian due to lack of magnetostratigraphic control (see below) and changes in sedimentation rates within long eccentricity cycles. At ODP Site 1209, the latest Maastrichtian is likewise disturbed by drilling. These uncertainties and offsets show in differences in the timing of the peak $\delta^{18}O$ excursion in the Cretaceous portion of C29R. At Shatsky Rise, the minimum in $\delta^{18}O$ of benthic foraminifera precedes that at Walvis Ridge by ~87 kyrs, although this offset is primarily due to a single anomalously low $\delta^{18}O$ value at Shatsky Rise. In bulk isotope space, the minimum values at Walvis Ridge precede those at J-Anomaly Ridge by ~37 kyrs. In the early Danian, the agreement between the three sites generally seems better (Fig. 2), although slight differences in the relative timing of peaks and troughs in bulk carbonate $\delta^{18}O$ attest to the uncertainty in current time constraints and provide a new tool for evaluating age models in this contested interval.

Bio- and Magnetostratigraphy at Site U1403

The construction of cyclostratigraphic age models depends on reliable indicators of geologic time like geological boundaries (i.e., the impact markers used to align the boundary cores between U1403A and U1403B), biostratigraphically important datum levels, magnetochron boundaries, and chemostratigraphically important events. For Site U1403, nannofossil biostratigraphy, osmium isotope stratigraphy, and light stable isotope stratigraphy provided additional constraints for the construction and/or testing of the cyclostratigraphic age model.

Although the sedimentary weight percent carbonate at Site U1403 is typically above 50% in the late Maastrichtian, the sediments are devoid of planktonic foraminifera –a common biostratigraphic marker. Calcareous nannoplankton, however, are abundant in the upper Maastrichtian and lower Danian and provided critical constraints on the Maastrichtian cyclostratigraphic age model (*1, 57*) (Figs. S23). With minor updates to the shipboard biostratigraphy (Tables S24 & S25), the nannofossil datums in the Danian are generally consistent with the cyclostratigraphic age model (Figs. S22). Other taxa were not well-enough preserved to be of use in biostratigraphy. Silica was not well preserved during this time period (*1*), and radiolarian datums were not provided or used in shipboard age models for sediments older than ~63 Ma. Organic matter preservation was similarly poor, so no dinocyst or palynomorph zonation was possible (Table S26).

Shipboard pass-through magnetometry during Expedition 342 failed to collect reliable magnetochron data for the late Maastrichtian to early Paleocene of Site U1403. Discrete, high-resolution paleomagnetic samples were collected during the post-cruise sampling party in order to attempt to identify the highly important magnetochron spanning the K/Pg boundary (magnetochron C29R). Seventy-two discrete samples were taken from the splice in XCB cores between U1403A25X1-124cm (233.97 m ccsf) and U1403B30X2-84cm (271.09 m ccsf). Samples were obtained ~0.30 m (excepting a disturbed interval around 254 m ccsf) from the split core sections by pressing 7 cm^3 plastic cubes into the sediment in the least disturbed, central region of the core. All magnetic measurements were performed at CEREGE (Aix-en-Provence, France) using a SQUID cryogenic magnetometer (2G Enterprises, model 755R, with noise level of 10^{-11}Am^2) with an attached automatic alternating field 3-axis degausser system (maximum peak field 170 mT) placed in a magnetically shielded room (field of ~nT). The natural remanent

magnetization (NRM) was measured and samples were demagnetized using step-wise alternating field (AF) up to 60 mT. All discrete sample data were volume corrected (7 cm^3). Data visualization and analysis were realized using Paleomac software (*65*) and correlated to the magnetic polarity timescale (GTS 2012) (*60*).

A small overprint (< 10-15 mT), possibly due to viscous remanent magnetization (VRM) or an isothermal remanent magnetization (IRM), was removed by using a progressive alternating field to isolate only one component of magnetization (or Characteristic Remanent Magnetization, ChRM). For 42 samples, a normal or reverse polarity was attributed using the direction of the ChRM because of their unequivocal behavior. For 13 samples, a polarity was tentatively assigned, although some caution should be taken because of their behavior upon AF treatment (large alpha95 and/or low intensity). The 17 remaining samples were excluded for the final interpretation because of their ambiguous or erratic behavior upon AF (alpha 95>20). In the end, ChRM inclination allowed us to define 7 magnetozones (Fig. S24).

 Paleomagnetic data from the discrete analyses unfortunately failed to provide additional time constraint around the K/Pg boundary. Overall, the polarity sequence appears sound for the Paleogene magnetochrons C27R to C29N, where a continuous normal and reverse polarity scale was established. However, magnetochron C29R, the short chron bracketing the K/Pg boundary and spanning the Deccan trap eruptions (*66, 67*), could not be defined due to unclear paleomagnetic results (Table S27, Fig. S24). Similar issues (lower NRM intensities, possibly disturbed sediments) continued in the Cretaceous portion of the core where chrons C30N and C30R were only tentatively attributed.

Osmium isotope geochemistry

Osmium isotope chemostratigraphy provides a useful geochronometer around the K/Pg boundary because of two globally recognized features in the osmium isotope record: a drop of ~0.13 ^{187}Os/^{188}Os beginning around the C30N/C29R magnetochron boundary and a drop of ~0.25 ^{187}Os/^{188}Os coincident with the K/Pg boundary iridium anomaly (*68-70*). These two osmium isotope events are attributed to the onset of Deccan volcanism and the extraterrestrial impact, respectively, as has been discussed at length in the literature (e.g., *68, 69-71*).

An osmium isotope record spanning the uppermost Cretaceous through lowermost Paleocene was generated for IODP Site U1403 on the leachable osmium following the method of

Ravizza 2007 (*72*) (Fig. S25). Leached osmium (from clays) was favored over the bulk digest methods (e.g., *69*) to minimize contamination from abundant detrital components. This choice, combined with the low Os content, a blank correction of 0.02-0.03, and an unquantified Re contribution, combine to mean that the Site U1403 record presented here (Fig. S26, Table S16) can be interpreted in terms of the relative shape of the osmium profile but likely does not accurately capture the absolute values, although the values are similar to those obtained from other sites (Fig. S26a). The large uncertainty ($\approx \pm 2.5\%$) in $^{187}Os/^{188}Os$ compared to previously reported Os isotope records is mainly the result of low concentration of leachable Os in these samples, and the associated correction for procedural blank, which can reach up to 10% of total analyte.

The osmium record at IODP Site U1403 is very similar to other existing K/Pg boundary records from Bottacione Gorge, Shatsky Rise, Walvis Ridge, and Maud Rise (Fig. S26). Namely, osmium isotope ratios decline in the upper Cretaceous, plateau during magnetochron C29R, and then drop again the K/Pg boundary before settling into a lower Paleocene baseline than occurs in the Cretaceous. Unfortunately, IODP Site U1403, like the Walvis Ridge record, does not show a stable Cretaceous baseline or abrupt transition to declining osmium values coincident with the C30N/C29R boundary as in 'classic' records like Bottacione Gorge and Shatsky Rise. This means that osmium at Site U1403, like the magnetochron boundary, provides a poor time constraint. Even so, the current cyclostratigraphic age model extends the relative duration of the upper Cretaceous plateau in osmium (highlighted in green in Fig. S26b) as compared to other sites. This pattern would suggest that the current age model is overestimating the amount of time in this interval.

Iridium geochemistry

Iridium was measured across the U1403 K/Pg boundary using laser-ablation inductively coupled plasma–mass spectrometry as described and published in Loroch et al. 2016 (*73*).

Oxygen and carbon isotope geochemistry

We generated resolved and temporally expanded records of stable carbon and oxygen isotopes to consider the relative role of Deccan volcanism and impact in marine extinctions. This section discusses the methods used to collect new stable isotope data (carbon and oxygen) from

carbonates at IODP Site U1403 and ODP Sites 1209, 1262 and 1267. We discuss published stable isotope records (shown in Fig. 1) in the section 'Temperature proxy compilation' below, including new $\delta^{18}O$ records from stable carbon isotope data published for Sites 1210, 1262, 1267, and 465 (i.e., records in Tables S5-S9)(*29*).

For IODP Site U1403 we generated a high resolution, ~5 million year long record of bulk carbonate stable carbon and oxygen isotopes comprising 646 measurements across four laboratories as indicated in Table S12. The Maastrichtian bulk samples from Site U1403 were analyzed at the Goethe-University Frankfurt (Germany) using a Finnigan MAT 253 coupled online to a Gasbench II or at Kanazawa-University (Japan) using a Finnigan Delta V Advantage coupled with Gasbench II (for details see (*74*)) and were published in Batenburg et al. 2017 (*57*). K/Pg boundary samples were analyzed at the Yale Analytical and Stable Isotope Center using a Thermo DeltaPlus XP and Paleocene sample were analyzed at the Friedrich-Alexander Universität Erlangen-Nürnberg with a Gasbench II connected to a ThermoFinnigan Five Plus mass spectrometer. All isotope values are reported in ‰ relative to the Vienna Peedee belemnite standard (VPDB). For all systems used, the analytical precision of replicates of standard measurements is better than 0.06 and 0.08 ‰ for carbon and oxygen, respectively. At Yale, weight percent carbonate (Table S19) was calculated by the deviation of the measured signal intensity from that predicted for a pure carbonate of the same mass, as determined by in-house standards. These weight percent carbonate measurements were combined with shipboard measurements of weight percent carbonate (*1*), to calculate a weight % carbonate record (shown in Fig. 2) from XRF measurements of Ca and Fe (Table S20). The sedimentary weight % coarse fraction (i.e., the mass proportion of the sample greater than 38 μm in size) was also determined for Site U1403 (as shown in Fig. 1), during sample preparation at Yale University (Table S15).

For ODP Site 1209, four new isotope records are presented in Table S11for bulk carbonate, bulk foraminifera, *Praemurica*, and *Woodringina*. Each are described in turn. The bulk carbonate record from ODP Site 1209 was generated with a Thermo-Finnigan MAT 253 mass spectrometer coupled to a Kiel Device at the University of California Santa Cruz, with analytical precision (1σ) of ± 0.05 ‰ for $\delta^{13}C$ and ± 0.08 ‰ for $\delta^{18}O$ based on repeated analyses of in-house standards. The boundary portion of this record was published in part previously in Hull et al. 2011 (*22*), but the data is provided here for the first time. To isolate the potential cause of the high amplitude $\delta^{18}O$ dynamics in the bulk carbonate in the early Paleocene, we generated a novel

type of 'bulk' record: bulk foraminifera. Bulk foraminifera were analyzed as a homogenized 38-125 μm size fraction, a size fraction dominated by immature and microperforate planktonic foraminifera (*22, 75*). For the same time interval (the earliest Paleocene) we also analyzed *Woodringina* and an evolutionary series of *Praemurica*. The bulk foraminifera and *Woodringina* records were analyzed at the MARUM (the Center for Marine Environmental Sciences) at the Universität Bremen on a Thermo-Finnigan MAT 251 mass spectrometer coupled to a Kiel Device. The MARUM lab analytical precision (1σ) for carbonate mass spectrometry is ± 0.05 ‰ for δ^{13}C and ± 0.07 ‰ for δ^{18}O, based on replicate analysis of in-house and international standards. The *Praemurica* series was generated at the Scripps Institution of Oceanography using a Caroussel-48 automatic carbonate preparation device and a common acid bath (i.e., a Fairbanks device) coupled to a Finnigan MAT 252 mass spectrometer, with an analytical precision (1σ) of ± 0.04 ‰ for δ^{13}C and ± 0.09‰ for δ^{18}O, respectively.

Organic geochemistry

The targeted analysis of aliphatic hydrocarbons in selected samples from Site 1403 across the K/Pg boundary provides qualitative information about the sources and preservation of organic matter in these sediments. Most algal steranes and bacterial hopanes were present below the limit of detection, while the signal of detected biomarkers was close to, or slightly above laboratory blanks and background contamination. This observation is consistent with the overall low total organic carbon (TOC%) of samples near the K/Pg boundary (0-0.3%;(*1*)). Thermal maturity indices based on the stereochemistry of algal steranes and bacterial hopanes indicate a degree of thermal alteration that ranges between early and peak oil window (Table S29). However, the elevated degree of thermal maturity obtained from biomarkers is inconsistent with the low thermal alteration inferred from the burial history of the Newfoundland sediment drifts. Indeed, older, organic-rich sediments across the Cenomanian-Turonian boundary in site 1407 contain organic matter that is thermally immature and relatively well preserved, as shown by high hydrogen indexes and low Tmax values (*2*). Given the low TOC% near the K/Pg boundary, it is likely that the prevalent organic matter preserved in these sediments is dominated by previously fossilized, thermally mature, allochthonous organic matter derived from the erosion of source rocks on the continent, similar to previous reports across the K/Pg in Stevns Klint, Denmark (*76*) and in Quaternary sediments (*77*). Furthermore, although we did not measure the

functionalized precursors of steranes and hopanes, our result is consistent with the lack of functionalized lipids such as archaeal glycerol dialkyl glycerol tetraethers (GDGTs) in the same samples. Thus, given the low abundance of hydrocarbon biomarkers detected across the K/Pg boundary in site 1403, and because of their non-indigenous source, they are not reliable indicators of changes in biological sources and environmental conditions in the overlying water column during this time.

Lipid Extraction and Analysis: Metal tools were rinsed with organic solvents, while all glassware, aluminum foil, silica, quartz wool and quartz sand were combusted at 500ºC for 12 hours to remove any organic contamination. About 5-10 g of powdered sample was extracted with a Dionex ASE 250 using DCM:MeOH (9:1 v/v). 100 ng of d4 C_{29} ααα (20R)-ethylcholestane was added as an internal standard before extraction. Elemental sulfur was removed using acid-activated copper powder for 12 hours. Asphaltenes were removed (3x) by precipitation in 10-40 ml of hexane at ~4ºC overnight, following centrifugation at 2500 rpm for 30 min. Aliphatic hydrocarbons were separated from the maltene fraction on a silica gel column using *n*-hexane (3/8 dead volume). Samples were analyzed by gas chromatography – mass spectrometry in full scan and metastable reaction monitoring (GC–MRM–MS) modes on a Micromass AutoSpec Ultima mass spectrometer interfaced to an Agilent 6890 N gas chromatograph at the Massachusetts Institute of Technology as described elsewhere (*78*). MRM-MS is a sensitive analytical technique that provides an elevated signal to noise ratio for the identification of compounds that are normally unresolved, co-eluting, or present in very low abundance.

Temperature proxy compilation

In order to assess the similarity of the LOSCAR model run temperatures with global temperature change across the K-Pg boundary, we compiled relatively resolved records of temperature across this time interval and updated the temperature calculation and age model as needed. Although our compilation represents the most comprehensive database (Table S4) of temperature estimates across the K-Pg boundary, and allows us to examine the relative similarity of temperature dynamics across sites and proxy types, in does not include every record ever published in the Maastrichtian and Paleocene nor does it attempt to estimate a global-absolute temperature through this interval. We choose to include records with relatively high temporal

resolution in order to assess a relative temperature change across the K-Pg boundary. Temperature records from a small portion of the compilation time frame (i.e., the Paleocene) were not included because we were not able to calculate a temperature relative to the latest Cretaceous in such instances (e.g., some low-resolution foraminiferal isotope records). So while there are more published paleotemperature proxy records around this time (e.g., *79, 80*), they were excluded if they lacked the temporal resolution around the boundary needed to express these data in this way with confidence. Furthermore, our compilation and analyses are based on relative temperature change because our focus is on understanding relative change in temperatures through time. The use of absolute temperatures from sites with different starting temperatures would obscure the detection of changes in temperatures (i.e., 2-4°C warming is less the differences in temperature expected with latitude, across the marine/terrestrial divide, and across proxy types). Temperature change within each dataset is calculated relative to the latest Cretaceous values, rather than the mean of a time frame, in order to minimize the effect of sparse or changing sampling densities across intervals of interest. Finally, global temperature change through time is estimated using a 60-pt fast Fourier transform smoother across all datasets. With aligned age models and updated temperature estimates (in some cases), we hope this compilation serves a starting point for future work on global temperature dynamics across this time interval.

Data and transformations include:

- **Benthic foraminiferal $\delta^{18}O$** measurements from Shatsky Rise ((*13, 33*), and this study: Table S5), Hess Rise (this study: Table S7) in the low-latitude Pacific, Walvis Ridge in the mid-latitude South Atlantic (*81, 82*), and this study: Tables S6 & S8), Maud Rise in the high-latitude South Atlantic (*83*), and Blake Nose (*84*), J-Anomaly Ridge (*85*), and Bass River (*86*) in the North Atlantic. For details of the revised age models used for each site, see Tables S2-S4. Temperatures were calculated via the equation of ref. (*87*) with species offsets, where necessary, taken from ref. (*88*), after (*13*). For these calculations, we assume an ice-free mean ocean seawater value of -1.2 ‰. We note though that since we are considering relative changes in temperature rather than absolute values, the assumptions should have a minimal biasing effect on data interpretation.
- **Planktonic foraminiferal $\delta^{18}O$** measurements from Walvis Ridge in the mid-latitude South Atlantic (*82, 89*), Maud Rise in the high-latitude South Atlantic (*90, 91*), and Blake Nose (*84*) and Bass River (*86*) in the North Atlantic. For details of age models, see

Tables S2-S4. As with benthic foraminiferal data, we use the δ^{18}O-temperature calibration from ref. (*87*), assuming ice free conditions.

- **Palaeosol carbonate δ^{18}O** measurements from continental USA (*92, 93*). We use ref. (*93*) option 2 for calculated temperatures, as preferred by the original authors. Sample ages are assigned according to a comprehensive new age model for this formation derived from biostratigraphy, magnetostratigraphy and geochronology from ref. (*94*).

- **Bivalve and gastropod carbonate δ^{18}O** measurements from Seymour Island, Antarctica (*95*) omitting those samples with evident trace metal contamination indicated by Sr, Mn and Fe concentrations. Data shown are averages of several measurements for each time interval. Ages are assigned based on linear interpolation between magnetochron boundaries (*95*), updated to the 2012 geological timescale (*60*).

- **Clumped isotope** measurements from bivalves from Hell Creek, USA (*96*) and brachiopods from Seymour Island, Antarctica (*97*). Note we bin clumped isotope data as in the original studies, and omit those samples with evident trace metal contamination indicated by Sr, Mn and Fe concentrations. We also omit gastropod and carbonate vein measurements from ref. (*96*), as they display more signs of diagenetic alteration/thermal resetting. Age models for Hell Creek and Seymour Island data are based on linear interpolation between magnetostratigraphic reversals from refs. (*95, 98*).

- **TEX$_{86}$** measurements from the New Jersey Margin (*99*) and Brazos River (*100*) in the USA, and Bajada del Jagüel, Argentina (*44*). Datapoints flagged as displaying high BIT index (> 0.3) were omitted. Age models for ref. (*99*) were constructed using dinoflagellate biostratigraphic datums (*99, 100*), while for Bajada del Jagüel ages are as published (*44*). At Bass River (*101*), ages are assigned according to the age model of ref. (*86*)

- **Leaf Margin analyses** from the Williston Basin, continental USA (*91, 102-106*). Where necessary, temperatures were recalculated using the temperature calibration and uncertainty model of ref. (*107*). Age models for these floras are based on magnetostratigraphic tie points (*108*) with ages reassigned according to ref. (*60*).

- **Mg/Ca temperatures** from Bass River, New Jersey Margin (*44*). Temperatures are as calculated by the original authors, omitting those from the bioturbated interval around the K/Pg boundary. Ages are assigned according to the age model in ref. (*86*).

In addition, in a few cases not all data provided in a given study was included in the compilation here, when very poor preservation, reworking, or a lack of stratigraphic control affected a part of the record. However, it should be noted that these exclusions have no visible effect on the estimates of global temperature change. In the case of Bass River (*44*), the uppermost 15cm of the Maastrichtian is heavily bioturbated (*109*). For this reason we do not include Mg/Ca or $\delta^{18}O$ data from the uppermost 15cm of the Cretaceous in our composite, following Woelders et al. (*44*). In addition, Woelder et al.'s earliest TEX_{86} data point (at 18cm below the K-Pg boundary) is anomalously high, which could also be the result of sediment mixing. As such we also exclude this data point from our compilation.

We also omit some New Jersey Margin data from ref. (*86*). Specifically, we do not plot the anomalously light data from the indurated or heavily reworked sections at Bass River at and above the K-Pg boundary. In addition, we do not plot data from the shallower Ancora hole from the same study, at which the uppermost Maastrichtian cooling seen elsewhere on the New Jersey margin appears to be missing. This, we suggest, may be the result of a fall in sea level of ~50 m in the very latest Maastrichtian C29r, as indicated by benthic foraminiferal assemblages and planktic:benthic foraminiferal ratios (*109-111*) at the downslope Bass River site. Since prior to this sea level fall the estimated water depth at Ancora was ~45m (*86*), it is likely that such a sizeable sea level change would have exposed Ancora to erosion, especially since rip-up clasts at many New Jersey margin sites at this time suggest the area may have been subject to tsunami or megastorm events (*109*). The absence of a discrete spherule bed at Ancora despite its presence at Bass River downslope (*110*) supports this interpretation.

Finally, as already discussed in the main text, two proxy types (fish teeth $\delta^{18}O$ and bulk carbonate $\delta^{18}O$) record dynamics unique to that proxy type for reasons that we suspect are due to biological responses of the living organisms to life in the early Paleocene Ocean (Fig. S10c, S11, S12), and are thus excluded from the global temperature compilation. In the case of the $\delta^{18}O$ of fish teeth, this proxy alone (from a single site) indicates an average warming of up to 4-5°C during the first 100,000 years of the early Paleocene as compared to background values of the uppermost Cretaceous (Fig. S10c). This would be an extraordinarily large and prolonged warming event to miss in other proxies, especially given the exceptional preservation of carbonate (for instance) in the earliest Paleocene (*112*), and would be similar in magnitude to the

largest known global warming event of the Cenozoic –the Paleocene Eocene Thermal Maximum– which is readily detected across a range of temperature proxies and sites (*113*). In addition, faunal analysis of dinoflagellates from the very same locality suggest the occurrence of cold-water taxa multiple times over the same interval (*114*), contradicting the fish tooth $\delta^{18}O$ signal, although this signal might also reflect biology (high-latitude origins) more than temperature. Thus, we suspect that fish shifted their depth habitat shallower on average in the earliest Paleocene in response to changing environmental conditions. There is also a change in the dominant fish tooth types making up ichthyolith debris in open ocean sites across the K/Pg boundary (*115*) and a wholesale turnover in near coastal taxa (*116, 117*), and the new dominant taxa may have simply occupied a different depth habit than the former dominants.

Similarly, bulk carbonate records show unique dynamics (i.e., high amplitude oscillations in $\delta^{18}O$; Fig. S11-S12) during an interval with large amplitude oscillations in the nannoplankton species comprising the majority of deep sea carbonate oozes (e.e., Figs. 3-4). Although bulk carbonate $\delta^{18}O$ oscillations are coherent across sites (Figs. 2, S11-S12), and generally correspond to turnover in the dominant nannoplankton taxa present (Figs. 3 & 4) and do not match temperature dynamics in any other temperature proxy (Figs. S1-S16). This and the conflict with stable $\delta^{18}O$ values in planktonic foraminifera from the same time period and locations (including species specific records and bulk foraminiferal records, Fig. 4), further suggests that bulk carbonate is not a reliable temperature proxy at this time. We therefore suspect this dynamic reflects the changing composition of the carbonate ooze (although it is perplexing to see the oscillations more strongly expressed in $\delta^{18}O$ than in $\delta^{13}C$), rather than a temperature signal not capture by single (and bulk) records of planktonic foraminifera from the same time and place. For these reasons, both fish teeth and bulk carbonate $\delta^{18}O$ values were excluded from estimates of global temperature change.

Four records are provided here for the first time as part of this global compilation and include benthic foraminiferal $\delta^{18}O$ records from ODP Site 1210 (Table S5), ODP Site 1262 (Table S6), DSDP Site 465 (Table S7), and benthic foraminiferal and bulk carbonate $\delta^{13}C$ and $\delta^{18}O$ records from ODP Site 1267 (Table S8). The carbon isotope records from the first three sites (Tables S5-S7) were published in Alegret et al. 2012 (*29*). The data from ODP Site 1267 is being published here for the first time, and was generated at the University of California Santa Cruz, after the methods described in Alegret et al. 2012 (*29*). This record (also shown in Fig.

16

S1c) is expanded across the very earliest Danian, as is also apparent from XRF core scanning comparisons of ODP Site 1267 vs. 1262 in Westerhold et al. 2008 (*8*).

LOSCAR earth system modeling

We use the LOSCAR (Long-term Ocean-Sediment CArbon Reservoir, v 2.0.4 (*118*)) carbon cycle model to investigate the range of pCO$_2$ change caused by several possible scenarios of Deccan volcanic degassing of carbon and sulfur volatiles, in combination with pelagic calcifier extinction and organic carbon export reduction at the K/Pg boundary.

The Paleogene configuration of LOSCAR featuring a Tethys ocean basin (*118*) was employed, incorporating the modifications detailed in (*112*) and described briefly here as follows. Equilibrium constants for carbonate chemistry calculations were determined for K/Pg seawater [Mg^{2+}] and [Ca^{2+}] using Hain et al's MyAMI-based corrections (*119*). A [Mg^{2+}] of 42 mmol/kg and [Ca^{2+}] of 21 mmol/kg were used for all simulations. Seafloor bathymetry was more finely subdivided into 100m depth intervals, increased from the standard 500m interval. The exponential constant (n_{Si}) used in the silicate weathering feedback equation (after Walker and Kasting (*120*)) was 0.6 in all simulations, which is the strongest weathering feedback considered by Uchikawa and Zeebe (*121*). We used this strong silicate weathering feedback to reflect the presence of easily-weathered Deccan basalt exposure at low latitudes during our interval of interest. A pre-event baseline pCO$_2$ of 600 ppm was used after Henehan et al. (*112*).

SO$_2$ degassing from Deccan volcanism (and the impact) is thought to be converted to sulfuric acid in the atmosphere (H$_2$SO$_4$) and subsequently rain out onto the Earth's surface (*122*). The portion falling into seawater would have rapidly dissociated to sulfate anion (SO$_4^{2-}$). This addition of an anionic salt reduces the negative charge deficit of the conservative salts, i.e., total alkalinity (TA). Since neither sulfur nor sulfate is a tracer in LOSCAR, we simulate the acidification of the oceans through sulfate addition by prescribing an equivalent reduction in total alkalinity (TA, which is a tracer in LOSCAR) as 2 mol TA for every mol S emitted, as sulfate is a divalent anion. This TA reduction is applied to the surface ocean reservoirs only, but is subsequently mixed throughout the ocean due to vertical mixing and thermohaline circulation

in LOSCAR. A similar approach was taken by Tyrrell et al. (*123*) when modelling the influx of bolide-derived SO_2 release at the K/Pg boundary.

Three aspects of the LOSCAR modeling were poorly constrained by the available empirical data (biological change, outgassing volume, climate sensitivity) and we addressed this uncertainty by modeling a range of scenarios in each case. We discuss each aspect in turn.

In order to include the biological effects of the mass extinction of many marine taxa and most marine pelagic calcifiers at the K/Pg boundary on the marine carbon cycle, we had to specify a percentage change in the export of organic carbon and of carbonate from the surface to deep ocean and in the rate of organic matter recycling in the water column. Although it is widely recognized that the K/Pg mass extinction affected all three aspects of the marine carbon cycle (i.e., *124*), the amount and duration of change in each continues to be an area of active research (*26, 29, 86, 89*). As a result, we decided to explore the effects of varying each of these parameters on observed changes in temperature, the surface-to-deep $\delta^{13}C$ gradient, and on carbonate saturation state in the ocean for each volcanic emission scenario. During the exploration of varying combinations of biological change, we assumed a climate sensitivity of 3°C/doubling (consistent with early Paleogene proxy estimates, as in *125*), a high Deccan trap total outgassing volume (9545 Gt C, 8500 Gt S), and an immediate gradual taper back to pre-event conditions over 1.77 myr beginning in the earliest Paleocene.

We began our parameter exploration focusing on Case 1 outgassing (Leading: 87% prior to impact) and exploring a range of changes in pelagic organic carbon export (50-70% decrease) and carbonate export (15-25% increase in the ratio of $CaCO_3:C_{org}$, resulting in a 35-65% reduction in pelagic $CaCO_3$ export flux) (Fig. S27). These were coupled to an increase in shallow water remineralization (the fraction of organic carbon export that is remineralized in the intermediate ocean reservoirs rather than the deep) from 78% prior to the K/Pg impact to 95% following the K/Pg impact. A parameterization of -50% C_{org}, +15% $CaCO_3:C_{org}$ rain ratio (i.e., a 42.5% reduction in total carbonate export), with 95% shallow water remineralization post-impact produced early temperatures similar to empirical records (Fig. 1, S27). While this combination had relatively modest effects on the carbonate saturation state of the deep ocean (Fig. S27), it failed to fully collapse the $\delta^{13}C$ gradients between the surface and deep waters as is observed in empirical records (Fig. 2) even accounting for biological change (*89*). Notably, variation in remineralization rate had a relatively minimal effect on CO_2, although more remineralization did

help decrease the $\delta^{13}C$ gradient and a 95% post-K/Pg remineralization rate was used in all subsequent simulations (Fig. S28). With this parameter exploration in hand (Fig. S27-S28), we choose a Case 1 (Leading) biological parameterization -50% C_{org}, +15% $CaCO_3:C_{org}$ rain ratio) with 95% shallow remineralization (Fig. 1).

All Deccan Trap outgassing scenarios explored in this research (i.e., those in Fig. 1) assume an additional K/Pg boundary impact degassing of 325 Gt S and 425 Gt CO_2 (*126*). We explored whether this impact degassing accounted for the small boundary spike in atmospheric pCO2 in our models by running our favored Case 1 biological scenario with and without impact degassing (Fig. S29). Due to its very small volume, impact degassing has an almost negligible effect on atmospheric CO_2 concentrations, and the most significant boundary feature in all our models is a result of the instantaneous collapse of the biological pump (similar feature simulated by biological pump change in Beerling et al. (*127*)). One boundary phenomenon not included in our modeling is the loss and regrowth of the terrestrial biosphere (*128*). Estimates for the duration of this vary but are on the scale of several thousand years to 10,000 years (*128, 129*). The short end estimates are very short relative to our model duration and time step, and the resolving power of most of our empirical records, and would have been be removed from the model in few time steps after being introduced. As a result, the very rapid loss and regrowth of the terrestrial biosphere was excluded from our simulations to avoid model integration issues. A second boundary phenomenon not included in our modelling is the hypothesized dissociation of gas hydrates (*130, 131*) as a result of the continental shelf slope failure (*47-49*). Gas hydrates were excluded because the carbon emission estimates are relatively small (300-1300 GtC (*130*)). At the lower end estimate, these emissions match that of the boundary impact degassing which had no discernable effect on model behavior (Fig. S29). At the upper end, they would effectively increase the post-impact CO_2 release in a Case 2-like scenario by 25-60% should result in visibly elevated temperatures given the short time scale of release. As this is not generally observed in the empirical temperature estimates (Fig. 1), we considered the lower end estimates for methane hydrate release as more likely and, hence, we did not included this factor in the modeled scenarios which were evaluated primarily on the global temperature change record in Fig. 1. That said, a shortcoming of the current series of LOSCAR model simulations (Fig. S27-S35) is that none of the simulations fully collapse the surface to deep carbon isotope gradient without oversaturating carbonates throughout the water column (i.e., see 70% C_{org} reduction scenario in

Fig. S27). While this could reflect the low vertical spatial resolution of the model (i.e., similar model parameters do collapse carbon isotope gradients in cGENIE), even a small contribution of dissociated methane hydrates could fully collapse the carbon isotope gradient in LOSCAR (*130*).

Because we use a global temperature compilation as our primary test to distinguish amongst Cases 1-4, we explore the effect of the extreme ends of Deccan trap outgassing scenarios (4090-9545 Gt C and 3200-8500 Gt S (*66, 132, 133*)) and climate sensitivity from 2°C/doubling to 4°C/doubling, with 3°C/doubling consistent with early Paleogene proxy estimates (*125*) (Fig. S30). The temperature range for Case 1 under differing combinations of total outgassing volume and climate sensitivity in Fig. S30 is the same as that shown in Fig. 1.

For Case 2 (50/50), we began the biological parameter exploration around the best Case 1 outgassing scenario exploring a range of C_{org} change (-25 to -60%) and $CaCO_3$:C_{org} rain ratio change (no change up to +40%) (Fig. S31). To our surprise, the best scenario was identical to our Case 1 exploration: -50% C_{org}, +15% $CaCO_3$:C_{org} rain ratio, with 95% shallow water remineralization. As in Case 1, we then explored the effect of the extreme ends of Deccan trap outgassing and climate sensitivity on this scenario (Fig. S32), with the temperature range in Fig. S32 for Case 2 the same as that shown in Fig. 1. For Case 3 and 4, we simply used the best-case biological scenario from Case 1 & 2 and explored the effect of changing outgassing and climate sensitivity in Figs. S33 and S34 respectively.

To simplify the model exploration and minimize the danger of overfitting, we assumed the same time scale of biological change for all modeled scenarios: an instantaneous biological change at the K/Pg boundary tapering back to the pre-extinction levels of organic carbon and inorganic export (and rates of remineralization) over the subsequent 1.77 myr. There are multiple possible timescales indicated by the empirical records, including i) a ~400 kyr low followed by a ~400 kyr taper back to pre-event levels based on the duration of the peak abundance of the coarse fraction (i.e., planktonic foraminifera fraction) and subsequent recovery, as in Hull et al. (*22*) (Fig. 2); or ii) a ~800 kyr to million year recovery similar to changes in the relative deposition rates of nannoplankton (Fig. 2); or iii) several million years similar to carbonate deposition rates (*8, 124*), or iv) 1.77 million years based on the most recent estimate for the timing of biological pump recovery (*89*). To choose among these different scenarios, we simulated multiple recovery scenarios and timescales (Fig. S35) and found that a protracted

recovery of the biological pump, combined with an instantaneous onset of the biological recovery, led to temperature changes most consistent with the empirical records (Fig. 1).

LOSCAR Modelling and the Schoene et al Timing of Deccan Trap Emplacement

As our initially modelling was being finalized, Schoene et al. (*58*) published a new hypothesis for the timing of Deccan Trap emplacement. The Schoene et al. emplacement scenario is similar to the 50/50 Case 2 scenario, in that there are roughly equal volumes of lava emplaced prior to and following the KPg impact, but differs from traditional hypotheses regarding the timing of emplacement. Namely Schoene et al. show (in Schoene et al. 2019, Fig. 2) that the highest pre-impact emplacement occurred just 20-60 kyrs prior to the impact and most post-impact emplacement occurred within several hundred thousand years post impact and hypothesize that this emplacement coincided with the degassing (and environmental impacts) of the Deccan volcanism. As Schoene et al. (*58*) recognized, without a commiserate increase in terrestrial weathering, this scenario results in appreciable warming of 2°C (Fig. S36), that does not appear in any of the compiled temperature records (Figs. S1-S16). In addition, it leaves far too little CO_2 to drive the late Cretaceous warming event of 2°C given current estimates of total outgassing (Fig. S36), and although increasing total outgassing would solve this issue, it would result in an even greater estimated temperature change just prior to impact. Increasing terrestrial weathering in-step with volcanic degassing and emplacement would negate the warming effect of Deccan volcanism (Fig. S37) as hypothesized by Schoene et al., but should be detectable in a negative carbon isotope excursion in the surface and deep ocean just prior to impact, with is not observed (Fig. S37 vs. Fig. 2). One line of evidence Schoene et al. point to for the plausibility of increased weathering in the latest Cretaceous prior to impact is the decline in osmium isotopes just prior the boundary (*58*). Although this decline in osmium isotopes has classically been attributed to the impact, with downcore smearing due to bioturbation, Schoene postulated it could be reflect increased weathering in-step with very latest Cretaceous Deccan Trap volcanism (*58*). We find this explanation unlikely. The osmium isotope record declines exactly in-step with the iridium (and osmium) anomaly (*69*), a coincidence only possible if both are emplaced in sediments at the same time. If the osmium isotope decline began prior to the impact (and iridium emplacement) then the osmium isotope decline should appear to extend further back into the

21

Cretaceous than the iridium anomaly, given that both are mixed by sediment mixing (*134*), but this is not observed (*69*). In short, although we find the Case 2 scenario plausible (Fig. 1), we do not find the timing or mechanisms proposed by Schoene et al. to be feasible given the data explored here.

Biological change quantification

We considered the relationship between Deccan volcanism and impact and the ecological and evolution of marine species in one of three primary ways: i) indirectly through tracers of the carbon cycle (i.e., $\delta^{13}C$, carbonate deposition, carbonate preservation, etc.) at Sites U1403 and 1209; ii) directly through microfossil records at Sites U1403 and 1209; and iii) directly through a literature search of biological dynamics from the latest Cretaceous through earliest Paleocene (Table S1). In this section we discuss the methods used to collect new microfossil records from IODP Site U1403 and ODP Site 1209.

Sedimentary preservation at Site U1403 favored the preservation of calcareous nannofossils, benthic foraminifera and ichthyoliths over other microfossil groups. Silica preservation was generally poor during this interval thus precluding detailed study of radiolarian or diatom dynamics (*1*). The same was true of organic matter preservation, ruling out dinoflagellates (Table S26) and meaningful biomarker analysis (Table S28). Prior to the K/Pg impact and throughout much of the Paleocene, carbonate preservation was also poor enough to dissolve nearly all planktonic foraminifera, precluding detailed faunal studies of planktonic foraminifera, due to the depth of the carbonate compensation depth relative to Site U1403. Ostracods were not studied in detail at Site U1403, but at the nearby Site U1407 a study of late Cretaceous through Paleocene faunal dynamics reveled no increase in extinction rates across the K/Pg boundary relative to background rates (*135*).

Of the three potential groups at Site U1403 for detailed biotic study (calcareous nannoplankton, benthic foraminifera, and ichthyoliths), we investigated two: calcareous nannoplankton and ichthyoliths. Calcareous nannoplankton provide key biostratigraphic control on Site U1403 due to the preservation and abundance. Large amplitude oscillations in bulk carbonate $\delta^{18}O$ in the earliest Danian at IODP Site U1403 and ODP Site 1209, an interval known for rapid faunal change in both nannoplankton and foraminifera, led us to ask whether the $\delta^{18}O$ signal might simply reflect the dominance and turnover of successive nannoplankton clades. To

test this, high resolution nannoplankton assemblage counts were carried out as described by Bown (*20*) at the University of College London (Site U1403; Table S17) and Penn State University (Site 1209; Table S18). Namely, for each sample listed at least 300 nannoplankton were counted from successive, randomly chosen, fields of view of smears slides. At Site 1209, additional diversity scans of 50-fields of view were carried out to account for rare taxa, which are indicted with an 'x' in Table S18. Characteristic taxa at Site U1403 are show in Figure S23. Because different workers collected the data at Site 1209 (JS, Penn State) and Site U1403 (HK and PB, at University College London) there are slight differences in taxonomy (e.g., *Coccolithus cavus* and *Coccolithus pelagicus* are grouped at Site 1209), although every effort was made to minimize differences in taxonomic concepts and naming. In both sites, reworking across the boundary (and downcore) was noted by a comparison of Cretaceous, Survivor and Incoming taxa and of the biostratigraphic age of rare down-smeared individuals (at Site 1209: *Fasciculithus*, *Sphenolithus primus*, and *Cruciplacolithus edwardsii*).

We also generated new records of the mass accumulation rate of ichthyoliths at Site U1403 as follows. Bulk samples were dried, weighed, and digested with 5% acetic acid. All ichthyoliths in the >106 μm size fraction were subsequently picked to determine the ichthyoliths per gram sediment (methods as detailed in *136*). The mass accumulation rate of ichthyoliths was then determined using the new cyclostraigraphic age model (i.e., Table S29) and a constant (1.08 g/cm^3) or variable dry bulk density (linearly interpolated from shipboard measurements). Ichthyolith mass accumulation rates were relatively insensitive to the dry bulk density used (Table S29), and the constant dry bulk density calculation is figured in Fig. 3.

Supplementary Discussion

Biological change in the Ocean

      Deccan Trap outgassing in the latest Cretaceous is notable for the biological impacts it did, and did not, have on marine biota (Table S1). Biogeographic range changes in the late Cretaceous includes the extension of tropical and subtropical plankton to higher latitudes during peak warming (*137*). At the same time, open ocean calcareous phytoplankton community structure suggests increased oligotrophic conditions (*138*). In our records, fish tooth abundance increased at Site U1403 in step with warming (Fig. S21, Table S29) and decreased at the K/Pg boundary. In contrast to abundant evidence for ecological responses to Deccan Trap outgassing in the marine realm, there is no evidence for increased extinctions in the widespread open ocean taxa used for biostratigraphy (e.g., foraminifera, coccolithophores, dinoflagellates, ammonoids, ichtyolitahs, etc) as us apparent from the scarcity of biostratigraphic markers. In planktonic foraminifera, the single marker during this period is a short-lived species (*Plummerita hantkeninoides*) that originates in C29R and goes extinct at the K/Pg boundary. Given the intense interest pertaining to the timing and consequences of volcanism in the K/Pg boundary extinction, increasing age control around the boundary is a top priority. If Deccan volcanism caused significant extinctions, these would provide greater biostratigraphic control during this key time interval, and the lack of markers based on last occurrences is thus notable and underscores the minimal effect of the late Cretaceous warming on the viability of species. It has been argued that a mass extinction did occur in the shallow water marine fauna of Seymour Island (*95*), but more extensive records do not support this (*139*). In addition, the relatively modest decline in marine $\delta^{13}C$ during late Maastrichtian warming is of the magnitude expected for a volcanogenic driver (Figs. 2-4, S27-S35), without appreciable feedbacks from the marine carbon pump (organic and/or inorganic). Some studies have argued on the basis of observed ecological changes that Deccan volcanism has destabilizing effect on communities (*140*), particular in terrestrial communities (*141, 142*), but the rapid rebound of marine plankton ranges and community structure within the latest Cretaceous and the lack of pronounced carbon cycle feedbacks in $\delta^{13}C$ suggest otherwise for the ocean.

      The K/Pg boundary differs by coinciding with extensive evidence for marine extinctions, including the extinction of ammonites and mosasaurs (*143, 144*) and the near complete

extinction of planktonic foraminifera and coccolithophores (>95% species-level extinction) (*39, 145-147*). At Site U1403, only the coccolithophores could be analyzed throughout the uppermost Cretaceous and lowermost Paleocene due to preservation, but a striking reduction in nannoplankton abundance, the disappearance of most Late Cretaceous species (there is some cross-boundary reworking; reworked specimens identified by criteria as in (*19, 20*)), and the first appearance of small, abundant calcispheres (calcareous dinoflagellates) all clearly coincide with the spherule layer (Fig. 3,4, Tables S17, S24, S25). The near-complete extinction of coccolithophorids likely accounts for the ~500,000 year interval in the earliest Paleocene when bulk carbonate $\delta^{18}O$ records (typically a tracer of mixed-layer temperatures by coccolithophores) diverge from all other marine temperature estimates at Sites 1209, 1262, 1267 and U1403 (Figs. 3, 4, S11, S12). At Sites 1209 and U1403, the incoming Cenozoic taxa form a succession of acmes, with miniscule early forms (<3 μm) quickly replaced by larger taxa within the same lineages (e.g., *Cruciplacolithus*, *Prinsius*, *Coccolithus*), with the termination of rapid biotic succession coinciding with the stabilization of the bulk $\delta^{18}O$ values, similar to the rapid succession of foraminiferal taxa in the same interval (Fig. S20) (*20, 22, 40, 148*).

Following the impact, the collapse in $\delta^{13}C$ between planktonic and benthic species was so extraordinary when first observed that a total cessation of marine productivity was hypothesized (the Strangelove Ocean hypothesis) (*149*). Although more modest changes in the biological pump are now thought to account for the pattern (*26, 37, 38, 86, 89, 150*), this collapse to reversal in carbon isotope gradients stands out as the largest carbon cycle perturbation in the pelagic carbonate fossil record for over 150 million years. Following the impact, surface to deep ocean $\delta^{13}C$ gradients recovered to ~75% of pre-extinction values within ~500,000 years, coinciding with the first major change in plankton community structure (*39*). Notably, the timing of $\delta^{13}C$ gradient collapse and partial recovery occurs in step with changing carbonate preservation conditions in the Atlantic and Pacific Oceans (Fig. 2, (*38*)) and major changes in plankton community structure (*39*). In the Late Maastrichtian, Site U1403 appears perched just above the carbonate compensation depth (i.e., the maximum depth below which carbonate is not preserved in sediments). Moderately well-preserved coccolithophores are abundant but the relatively dissolution-prone planktonic foraminifera are almost entirely absent (Figs. 3, 5)(*1*) until the earliest Paleocene when sediments go from nearly barren to ~30% planktonic foraminifera by weight. The pronounced change in carbonate preservation at Site U1403 reflects

a global phenomenon, with distinct improvement in the quality of carbonate preservation in the deep-sea and a 1-2 km deepening of the CCD in the earliest Paleocene (*112*). However, the wt % coarse fraction dynamics differs among the three best resolved sites (Fig. 2), possibly due to orbitally paced changes in circulation.

Exceptions to the Global Temperature Compilation

The global temperature compilation documents fairly stable, roughly Cretaceous-like temperatures in the earliest Paleocene. There are three exceptions to this statement that necessitate discussion: very brief excursions, the Dan-C2 event, and the long-term warming trend.

The time-integrated nature of most of the samples in the compilation mean that they do not capture very short-term excursions including the impact winter and warming rebound. A 1-cm thick interval at most deep sea sites in the early Paleogene spans several thousand years due to low sedimentation rates, and up to 10,000 years when one includes sediment mixing (*134*). Recent modeling work has emphasized the severity of the impact winter due to sulfur (*151*) and soot (*152*) in the years following the impact. This modeling work is generally consistent with empirical evidence from (TEX$_{86}$) for impact winter in the months to decades following the impact in highly expanded, coastal sections (*99, 100*). The same studies provide evidence of a warming overshoot of first few thousand years following the impact winter (*99, 153*). This few thousand year-long warming of ~1-2°C is consistent with a biospheric driver (like the loss and regrowth of biomass). Interestingly, bulk carbonate records of $\delta^{13}C$ appear to have a two-step decline in values after the K/Pg impact, with the first step lasting a few thousand years (Figs. 3,4, S38) consistent with a short-lived perturbation like the loss and regrowth of terrestrial biomass. However, planktonic foraminifera from the same sites do not show this two-step $\delta^{13}C$ drop (Fig. 4), either because foraminiferal records are less temporally resolved (with individuals carried beyond their stratigraphic range due to mixing (*134*)) than bulk carbonate or because the bulk carbonate record reflect changes in the composition of carbonate fine fraction rather than the global carbon cycle (*75*). Similarly, TEX$_{86}$ records from shallow coastal locations must be interpreted with caution due to the confounding effects of different environmental factors on the distribution of archaeal GDGTs , and the possibility of terrestrial sources of GDGTs not captured by the BIT index (*154, 155*), like oxygen concentration (*156*) and ammonia oxidation rate (*157*)

both of which can vary widely in shallow water settings. Regardless, if a brief post-impact warming of a few thousand years did occur as in (*99, 153*), it cannot be attributed to Deccan degassing and subsequent weathering feedbacks because the rate at which the warming signal is removed (less than one thousand years) is far too fast for the weathering feedbacks that typically drawdown volcanogenic CO_2 inputs. This point is important because it also means that it is very unlikely that any very short warming burst was driven by Deccan Trap volcanism.

The Dan-C2 event (recognized on the basis of a carbon isotope excursion in some localities) is hypothesized to be an earliest Paleocene global warming event that occurs ~250,000 years after the K/Pg boundary (*84, 158*). The magnitude and duration of the Dan-C2 event would be consistent with a Deccan volcanism related driver if outgassing were delayed relative to the impact as previously hypothesized (*159*), although the evidence for global warming during the Dan-C2 remains scant. This is an intriguing possibility, and would tie Deccan volcanism to the recovery of biotic diversity rather than the loss, as this event occurs near a turning point in many geochemical and assemblage records from the open ocean, as they begin to return to pre-impact like values and diversities. The appeal of this idea is that volcanic outgassing from a large igneous province is hypothesized to drive some later hyperthermal events (like the PETM (*160*)). However, as we show in our modeling here, extensive changes to the carbon cycle due to the K/Pg mass extinction should mask and/or mute the climate effect of volcanic degassing during the earliest Paleogene (Fig. 1, S31-S33). However, it is possible that if Deccan outgassing occurred over a relatively shorter time interval than we modeled, and at a turning point in the strength of the biological pump, that it would have the carbon cycle effects attributed to the Dan-C2, with the relatively muted (or non-existent) evidence for coincident global warming that is observed (*84, 158*).

Finally, perhaps the most unexpected finding of our modeling regards the gradual long-term warming trend in the early Paleocene (Fig. 1) of about 1°C over the first 600,000 years. Our modeling demonstrates that the recovery of the biological pump in the aftermath of the K/Pg extinction results in a gradual increase in atmospheric pCO_2. In fact, this effect was so strong, that many of the scenarios for the timing of biological pump recovery results in far too sudden (and pronounced) warming in the earliest Paleocene (Fig. S35). The immediate, gradual, and prolonged pump recovery (starting immediately in the K/Pg impact aftermath and continuing over 1.77 million years) was overall the best scenario for the warming trends observed. The

difference in amongst biological pump recovery scenarios in the pattern of ocean saturation state, pCO$_2$, and temperature change (Fig. S35), suggest a clear path forward for advancing our understanding of the timing of marine carbon cycle recovery after the K/Pg impact.

A.

B.

C.
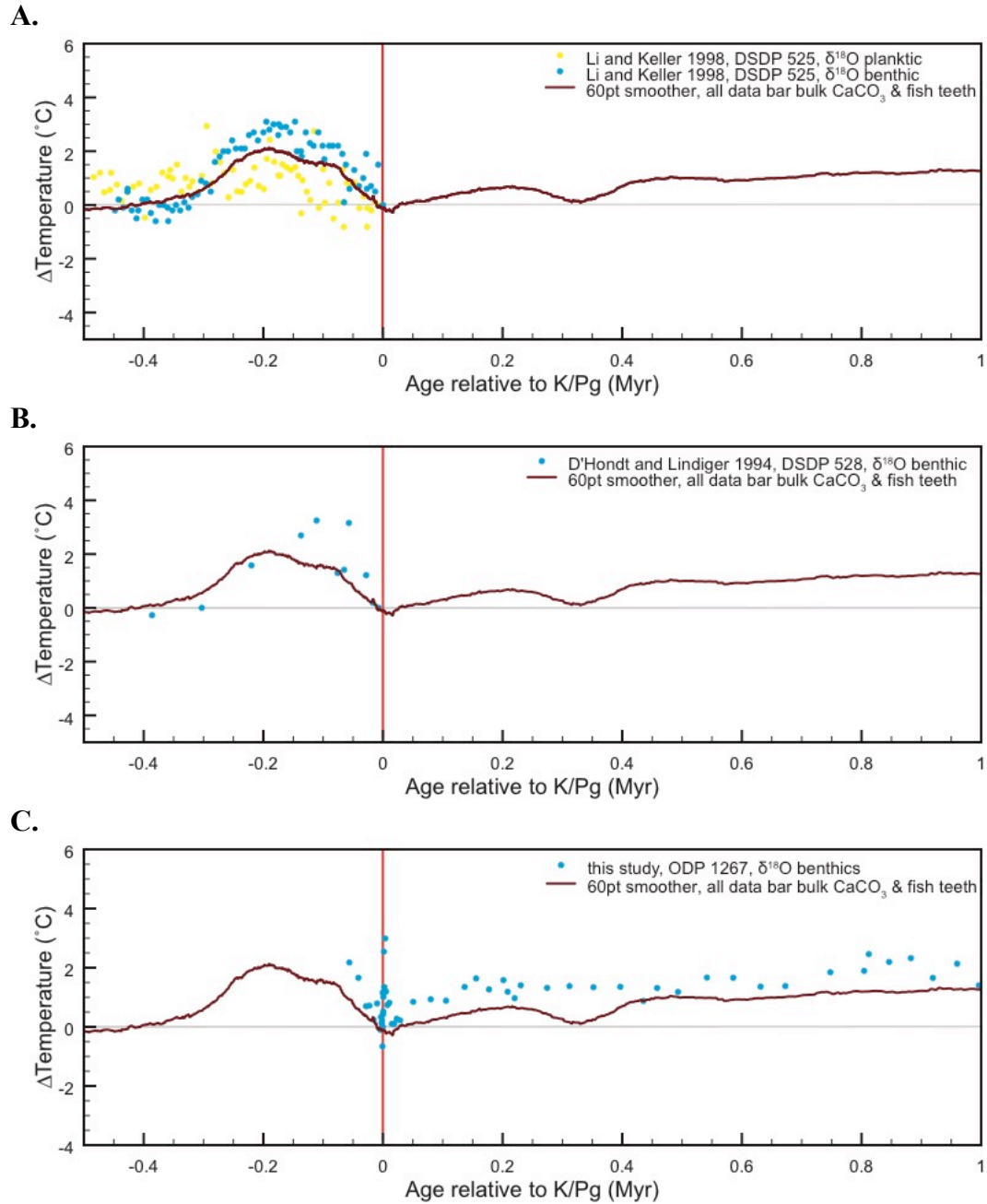
Fig. S1.
Temperature records from Walvis Ridge sites: (A) DSDP Site 525 (*82*), (B) DSDP Site 528 (*81*), and (C) ODP Site 1267 (*this study*), on unified age models and a common δ^{18}O-temperature equation.

A.

B.

C.
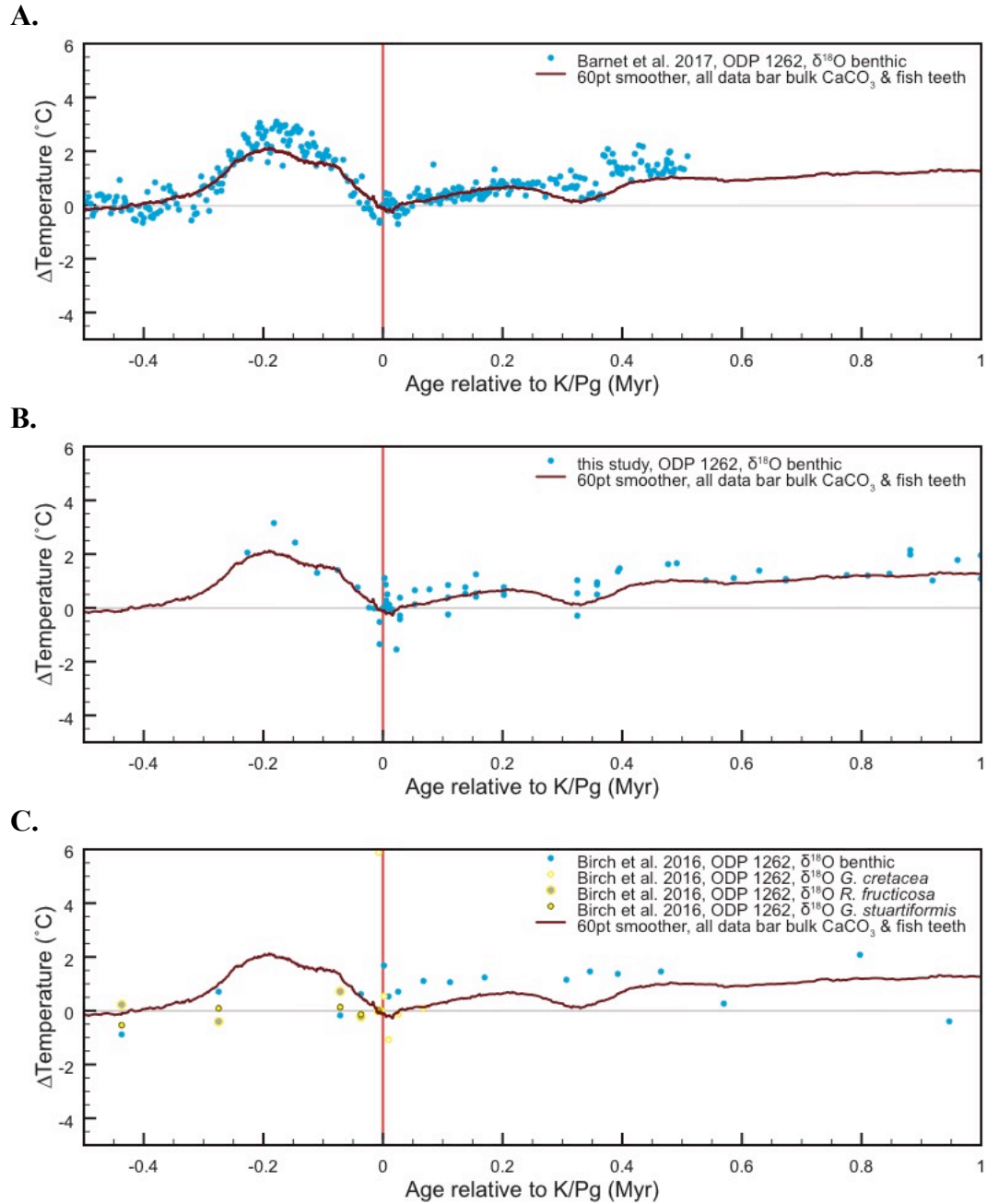
Fig. S2.
Temperature records from Walvis Ridge sites: (A) ODP Site 1262 (*42*), (B) ODP Site 1262 (*this study*), and (C) ODP Site 1262 (*89*), on unified age models and a common δ^{18}O-temperature equation.
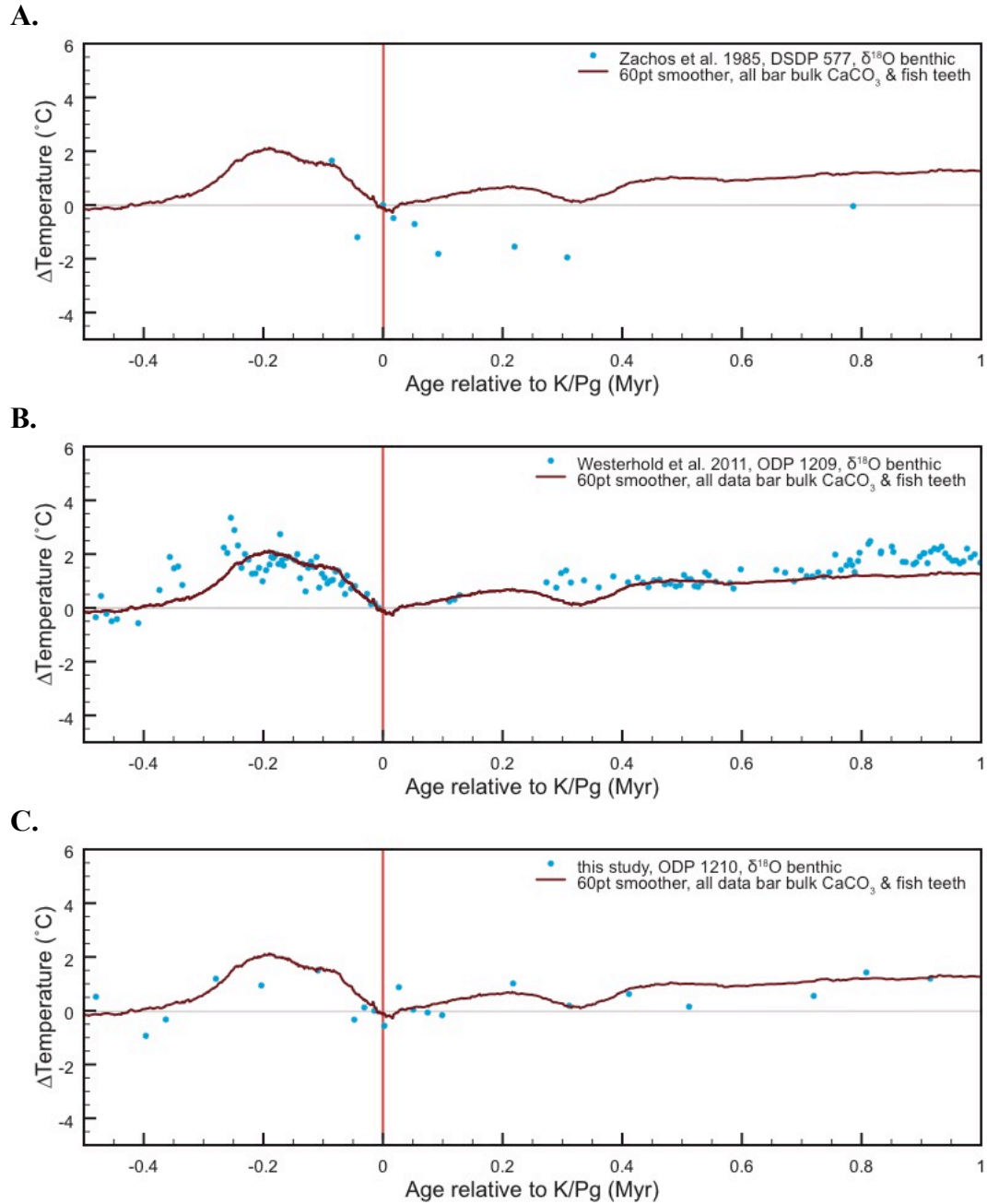
A.

B.

C.

Fig. S3.
Temperature records from Shatsky Rise sites: (A) DSDP Site 577 (*33*), (B) ODP Site 1209 (*13*), and (C) ODP Site 1210 (*this study*), on unified age models and a common δ^{18}O-temperature equation.

A.

B.

Fig. S4.
Temperature records from Shatsky Rise, ODP Site 1209 (A) bulk foraminifera, i.e., homogenized 38-125μm sieve size fraction material (*this study*), and (B) mixed *Woodringina* species (*this study*), on unified age models and a common δ^{18}O-temperature equation.

Fig. S5.
Temperature records from (A) Blake Nose, ODP Site 1049 (*84*), (B) J-Anomaly Ridge, DSDP Site 384 (*85*), and (C) Hess Rise, DSDP Site 465 (*this study*), on unified age models and a common δ^{18}O-temperature equation.

A.

B.

C.

Fig. S6.
Temperature records from Maud Rise ODP Site 690 (A) (*83*), (B) (*161*), and (C) (*91*), on unified age models and a common δ¹⁸O-temperature equation. Note for data in panel A, ΔTemperature is calculated relative to a measurement of *Nuttallides truempyi* at the K-Pg boundary from ref. (*91*).
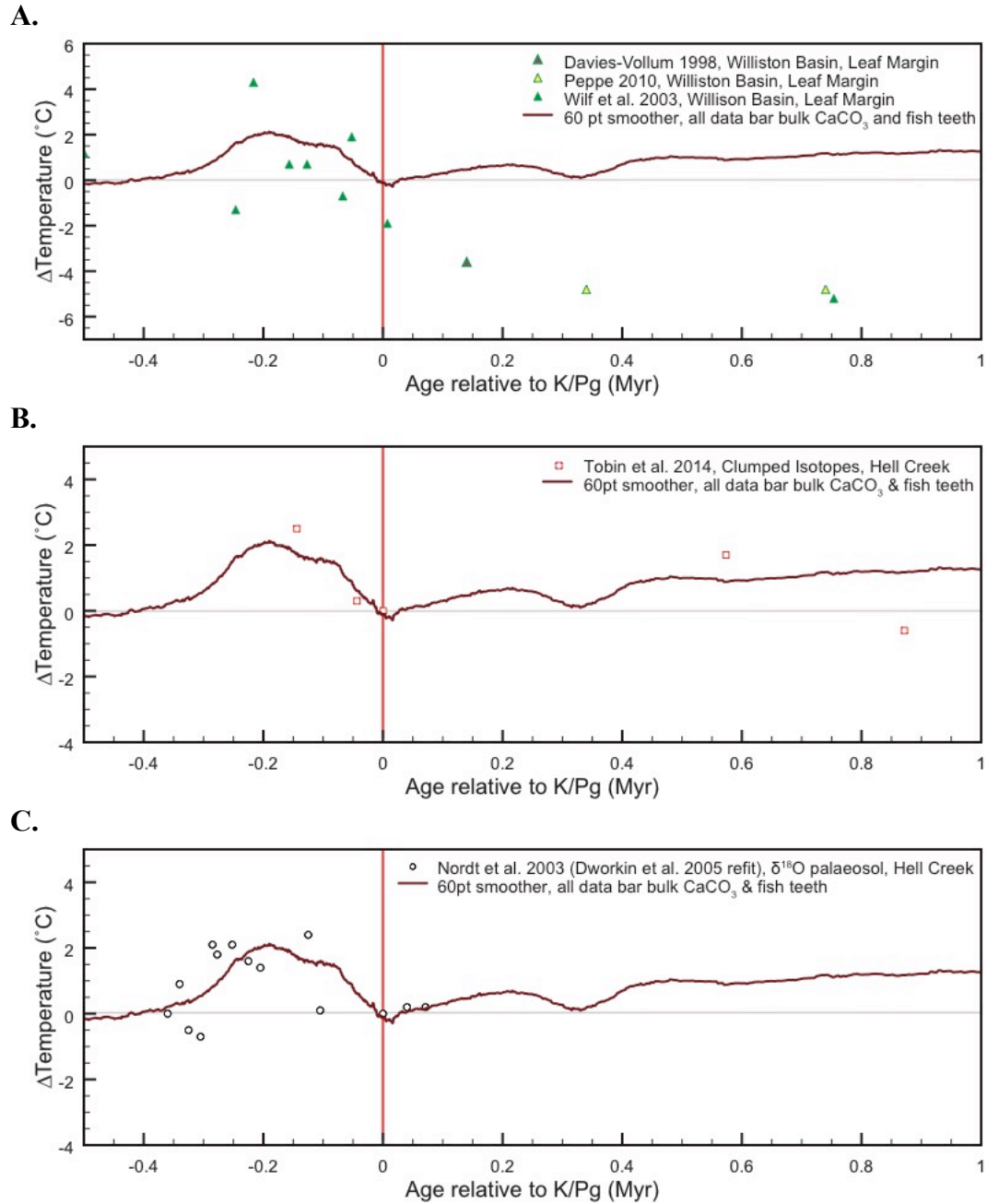
Fig. S7.
Temperature records from (A) the Williston Basin leaf margin data set (*91, 102-105*), (B) from
Hell Creek, clumped isotopes of mollusks (*96*), and (C) Dawson Creek $\delta^{18}O$ of paleosols (*92,
93*), on unified age models.

A.

B.

C.
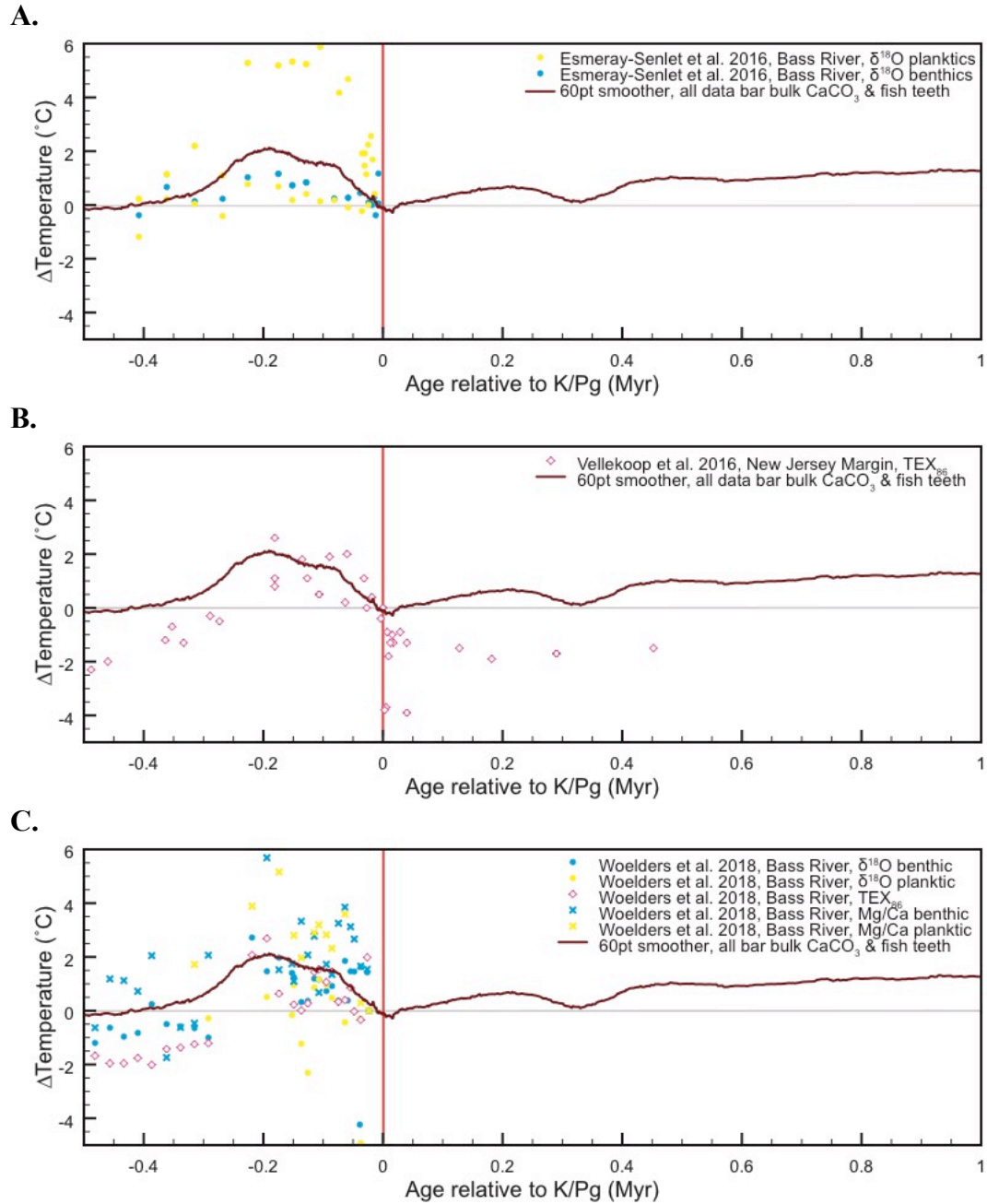
Fig. S8.
Temperature records from Bass River (A) δ^{18}O of foraminifera (*86*), (B)TEX[86] (*99*), and (C) mixed proxies (*101*), on unified age models and a common δ^{18}O-temperature equation.

A.

B.

Fig. S9.
Temperature records from (A) Bajada del Jaguel (*44*), and (B) Brazos River (*100*), on unified age models.

A.
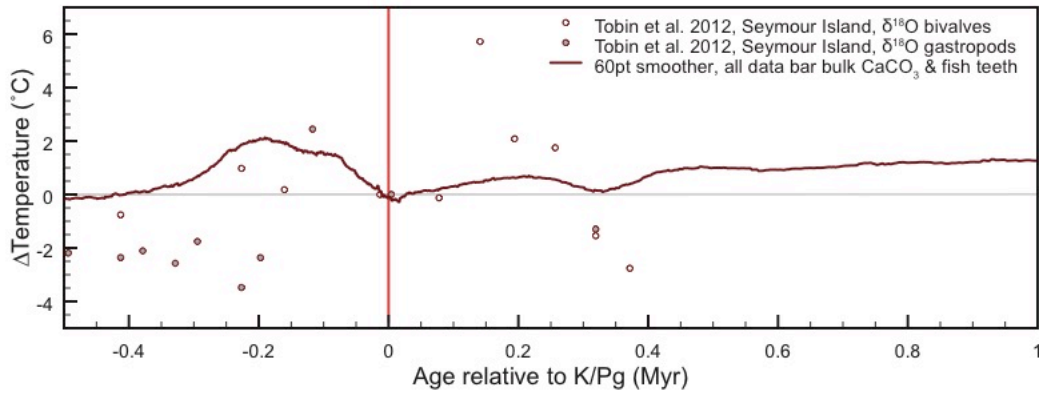
B.
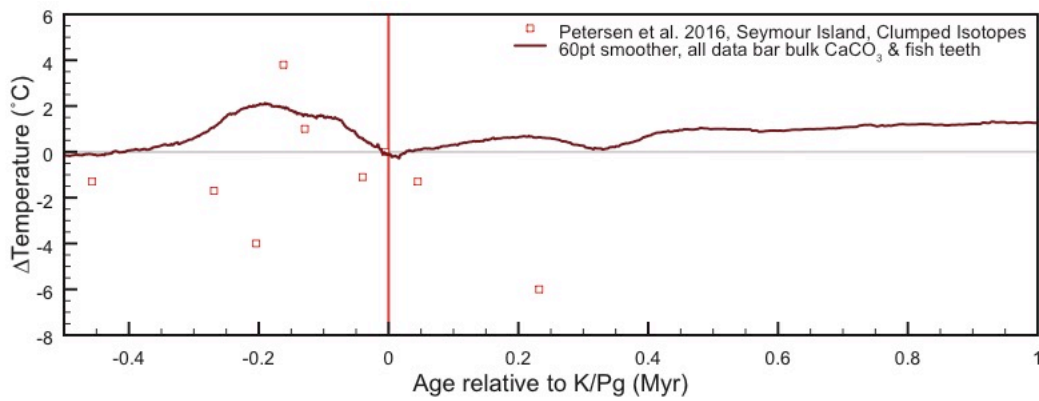
C.
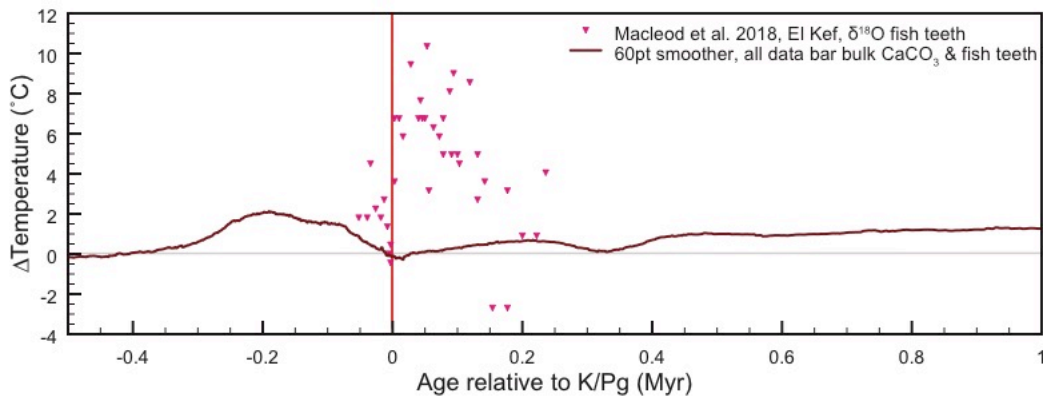
Fig. S10.
Temperature records from Seymour Island, Antarctica (A) $\delta^{18}O$ of mollusks (*95*) and (B) clumped isotopes of mollusks (*162*), and fish teeth at El Kef (*163*), on unified age models.
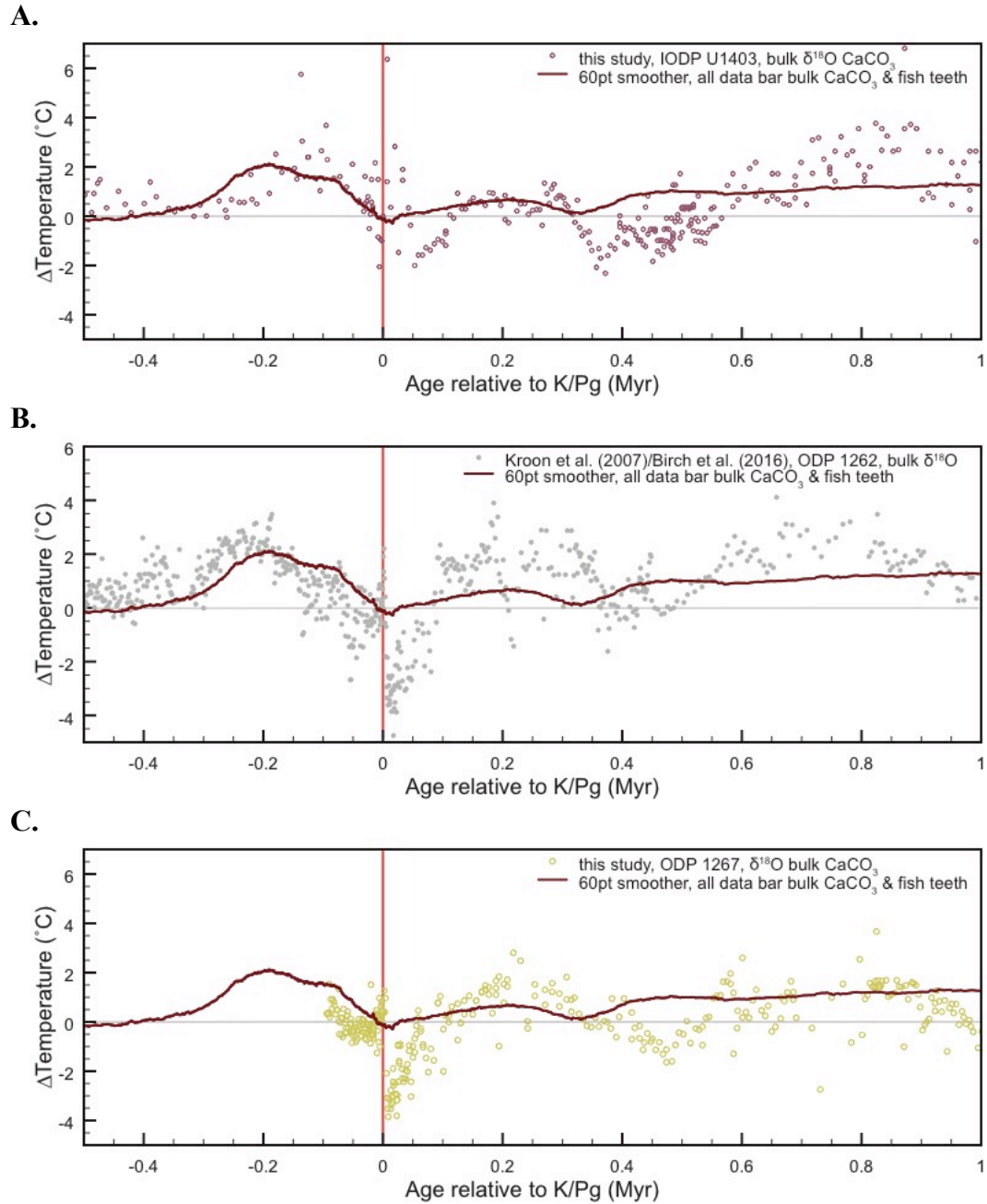
Fig. S11.
Temperature records from bulk carbonate at (A) IODP Site 1403 (*this study*), (B) IODP Site 1262 (*41, 89*), and (C) IODP Site 1267 (*this study*), on unified age models and a common δ^{18}O-temperature equation.
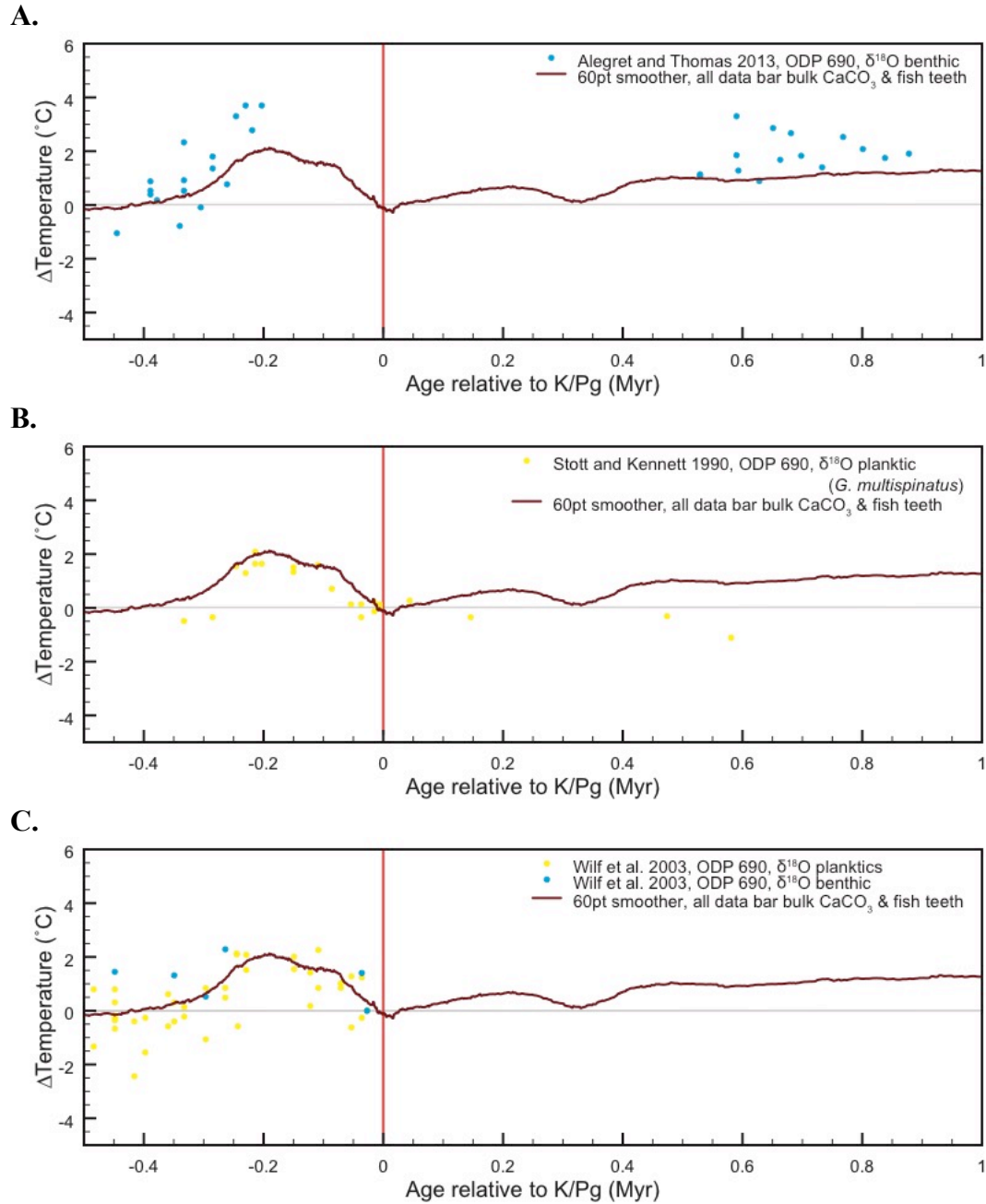
A.

Fig. S12.
Temperature records from bulk carbonate at (A) ODP Site 1209 (*this study*), on unified age models and a common $\delta^{18}O$-temperature equation.

A.

- ● Barnet et al. 2017, ODP 1262, δ¹⁸O *N. truempyi*
- ▫ D'Hondt & Lindiger 1994, DSDP 528, δ¹⁸O '*Gavelinella*' sp.
- △ Alegret and Thomas 2013, ODP 690, δ¹⁸O
  S. beccariiformis/N. truempyi
- ▼ this study, ODP 1262, δ¹⁸O *N. truempyi*
- ▼ this study, ODP 1210, δ¹⁸O *N. truempyi*
- ▽ this study, DSDP 465, δ¹⁸O *S. beccariiformis*
- ◆ Quillévéré et al. 2008, ODP 1049, δ¹⁸O *S. beccariiformis*
- ● Berggren and Norris 1997, DSDP 384, δ¹⁸O
  S. beccariiformis/N. truempyi/Cibicidoides
- ▪ Westerhold et al. 2011, ODP 1209, δ¹⁸O *S. beccariiformis*

- ◇ Zachos et al. 1985, DSDP 577, δ¹⁸O *Aragonia* sp.
- ▪ Esmeray-Senlet et al. 2016, Bass River, δ¹⁸O *A. midwayensis*
- ▼ Wilf et al. 2003, ODP 690, δ¹⁸O *S. beccariiformis/N. truempyi*
- ◆ Woelders et al. 2018, Bass River, δ¹⁸O *A. midwayensis*
- ✕ Woelders et al. 2018, Bass River, Mg/Ca *A. midwayensis*
- ◆ Li and Keller 1998, DSDP 525, δ¹⁸O *A. acuta*
- ◆ this study, ODP 1267, δ¹⁸O *N. truempyi*
- ▲ Birch et al. 2016, ODP 1262, δ¹⁸O *N. truempyi*
- —— 60pt smoother, all data bar bulk CaCO₃ & fish teeth
- – – 40pt smoother, Benthic foram data only

B.

- ● this study, ODP 1209, δ¹⁸O *Woodringina* sp.
- ● Stott and Kennett 1990, ODP 690, δ¹⁸O *G. multispinatus*
- ▽ Wilf et al. 2003, ODP 690, δ¹⁸O *G. prairiehillensis*
- ▼ Wilf et al. 2003, ODP 690, δ¹⁸O *H. globulosa*
- ▫ Li and Keller 1998, DSDP 525, δ¹⁸O *R. rugosa*
- ◇ Esmeray-Senlet et al. 2015, Bass River,
  δ¹⁸O *G. multispinata*
- ◆ Esmeray-Senlet et al. 2015, Bass River, δ¹⁸O *R. rugosa*

- ◇ Woelders et al. 2018, Bass River, δ¹⁸O *Globotruncana* sp.
- ✕ Woelders et al. 2018, Bass River, Mg/Ca *Globotruncana* sp.
- ◇ Birch et al. 2016, ODP 1262, δ¹⁸O *G. cretacea*
- ◆ Birch et al. 2016, ODP 1262, δ¹⁸O *R. fructicosa*
- ◆ Birch et al. 2016, ODP 1262, δ¹⁸O *G. stuartiformis*
- —— 60pt smoother, all data bar bulk CaCO₃ & fish teeth
- – – 20pt smoother, Planktic foram data only

Fig. S13.
Comparison of all foraminiferal temperature datasets (shown individually in Figs. S1-S12) versus the global temperature composite, including (A) benthic foraminifera δ¹⁸O based temperature estimates, and (B) planktonic foraminifera δ¹⁸O based temperature estimates, on unified age models and a common δ¹⁸O-temperature equation.

A.

B.

C.
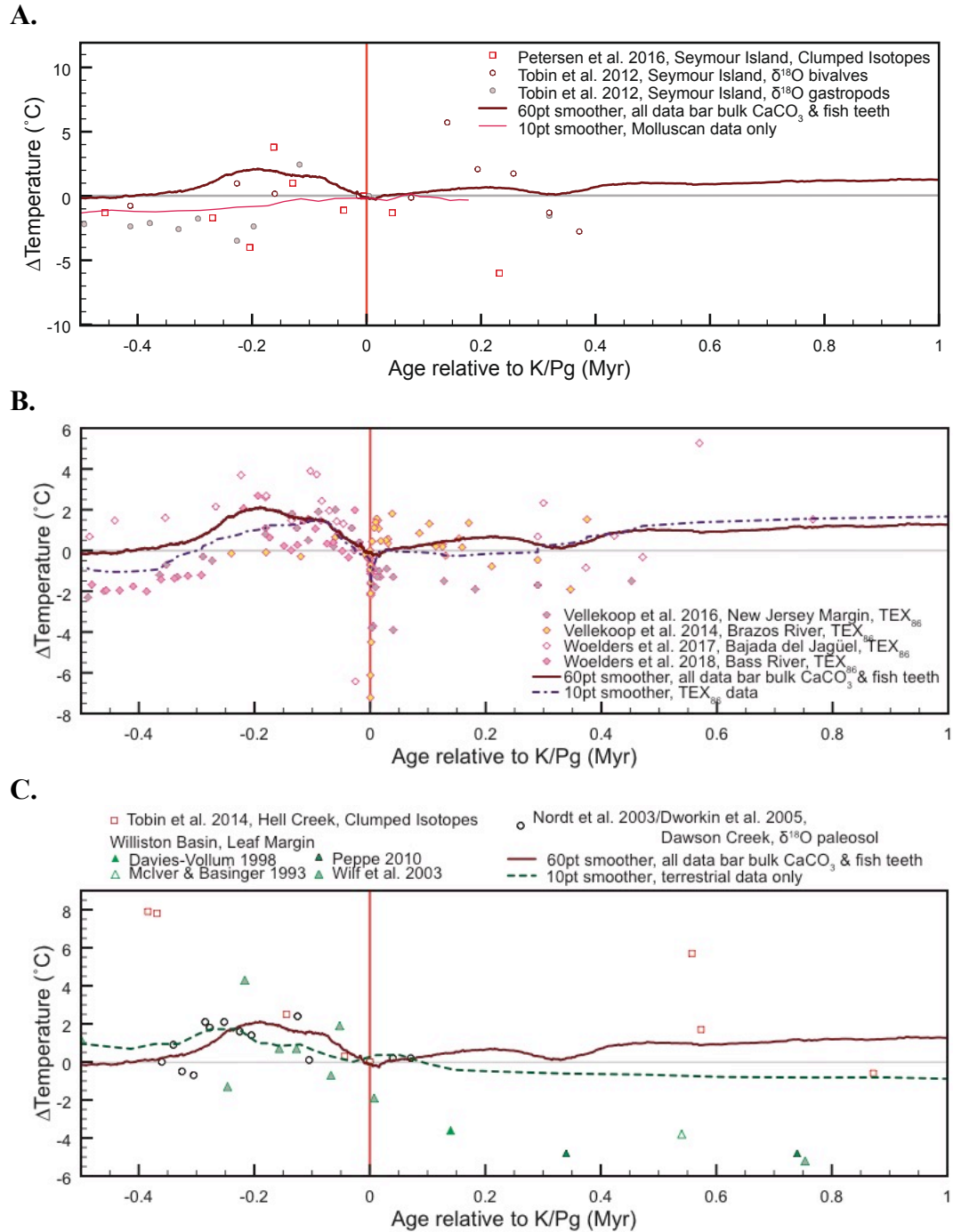
Fig. S14.
Comparison of all (A) mollusk temperature proxy data, (B) TEX$_{86}$ temperature proxy data, and (C) terrestrial temperature estimates, versus the global temperature composite (as shown individually in Figs. S1-S12), on unified age models and a common δ^{18}O-temperature equation.

A.
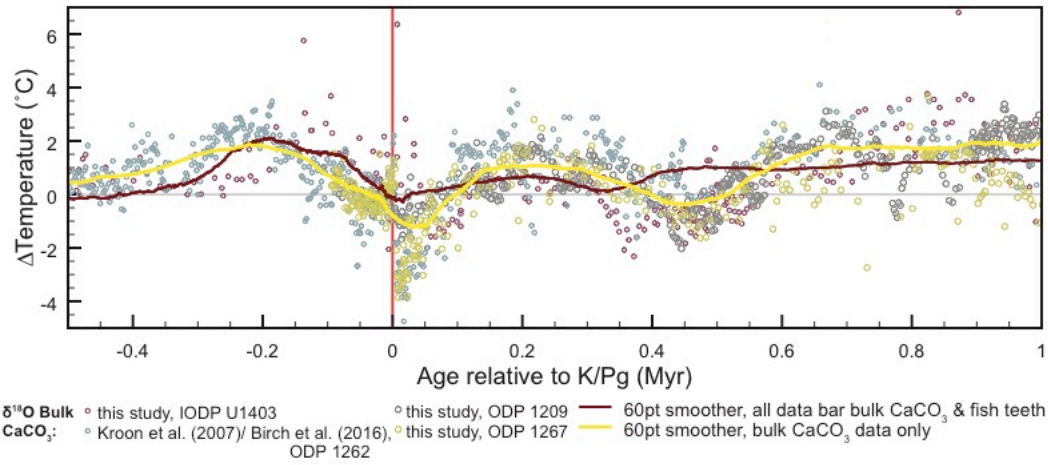
B.
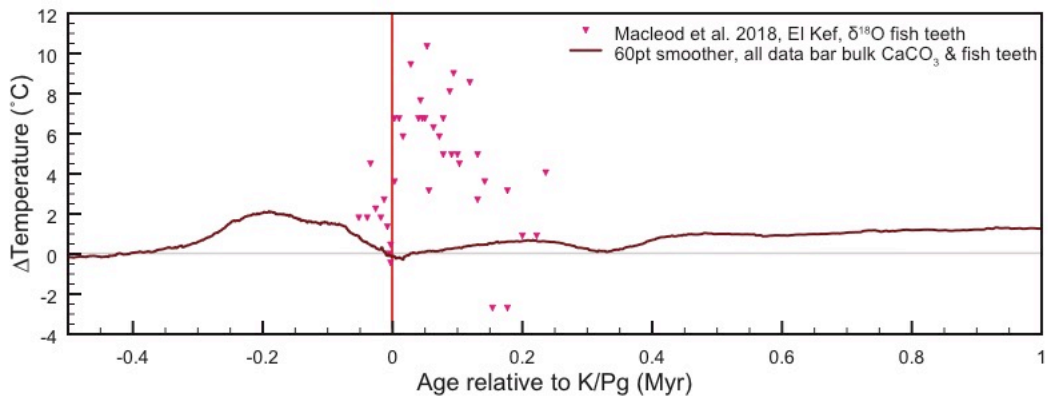
Fig. S15.
Examination of proxies likely not tracking temperature in the earliest Paleocene due to extinction related changes in communities including (A) bulk carbonate δ^{18}O, and (B) fish tooth apatite δ^{18}O (*163*), on unified age models and a common δ^{18}O-temperature equation.

A.
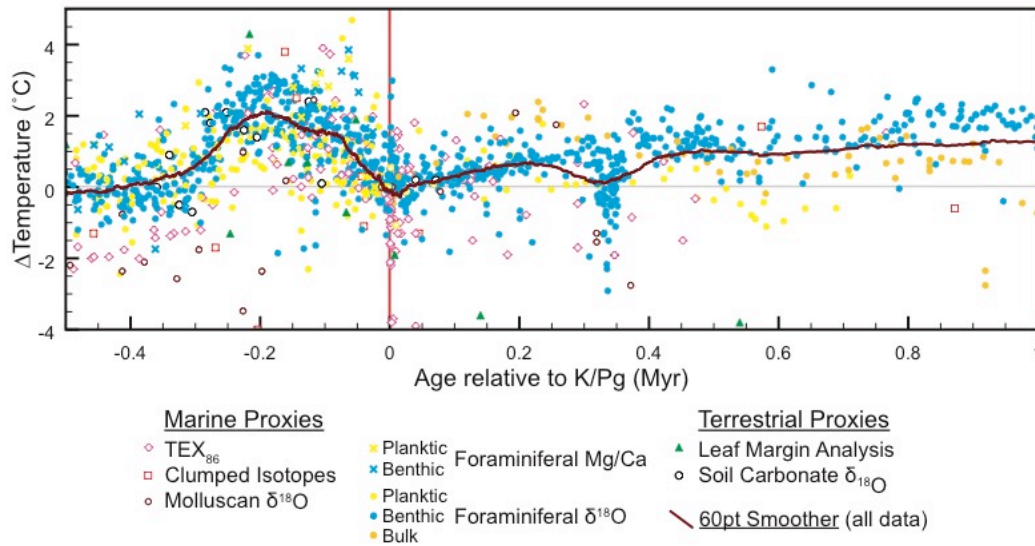
B.
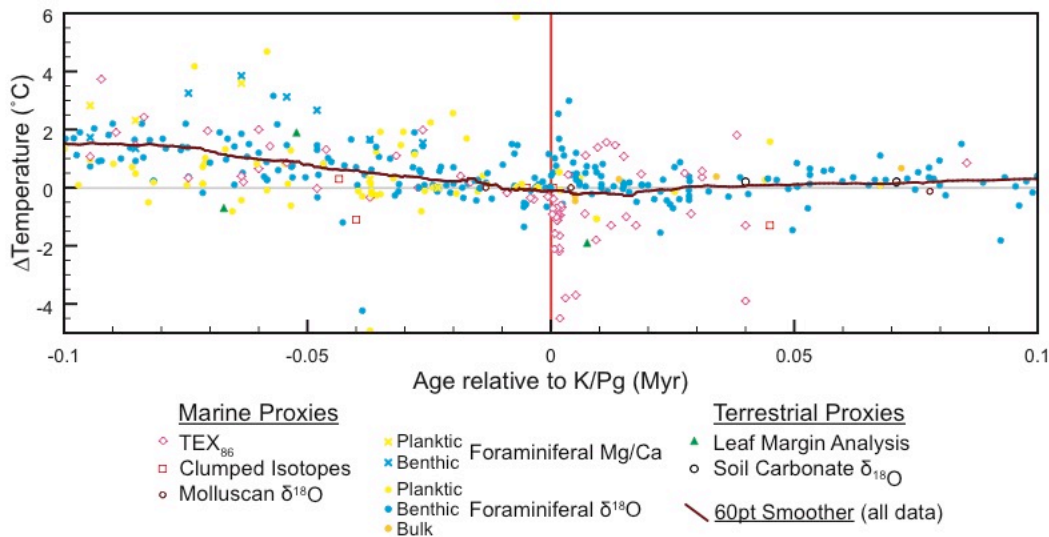
Fig. S16.
Global temperature composite across the K/Pg with a 60pt fast Fourier transform for (A) the full time window, and (B) the K/Pg boundary proper. Data as in Fig. S1-S12, but shown by dataset and proxy type, and excluding bulk carbonate $\delta^{18}O$ and fish teeth $\delta^{18}O$ which are unlikely to be tracking regional temperature change (as shown in Fig. S15). Note that the smoothing approach used naturally weights to the most data-dense records although most individual records of various proxy types do show the major features of the compilation (Figs S1-S12), and it does not account for differences in temporal or paleotemperature proxy uncertainty.
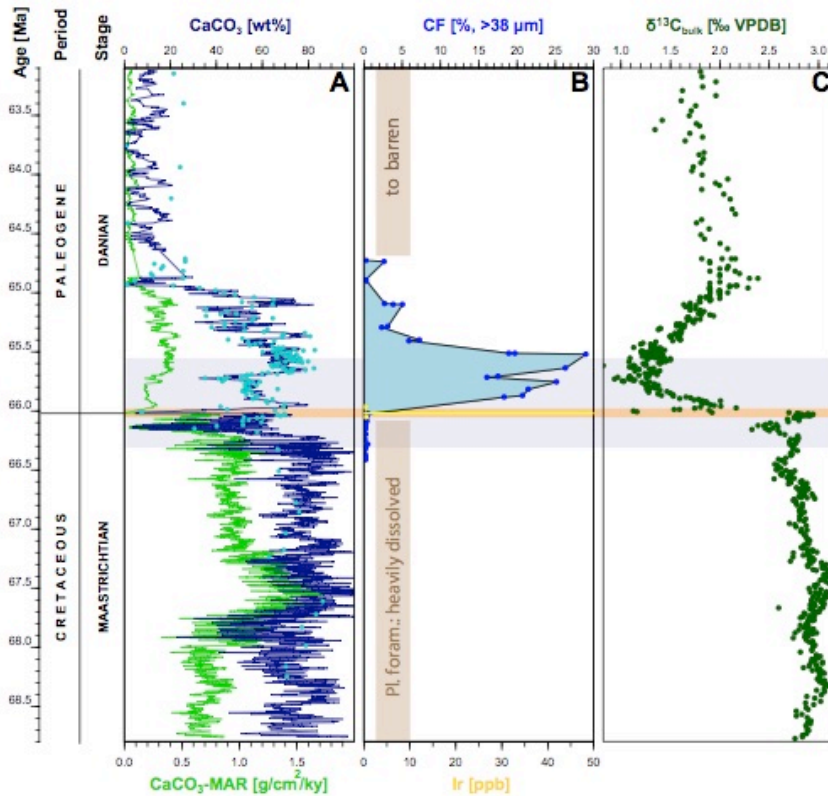
Fig. S17.

**A long, high-resolution Cretaceous baseline at IODP Site U1403 evidences the unusually
large perturbation of the Cretaceous-Paleogene impact.** Multiproxy records from IODP Site
U1403 provide the first expanded (~3 million year) Cretaceous paleoceanographic baseline with
centimeter scale resolution from a site with an intact K/Pg boundary spherule layer include (a)
$CaCO_3$ mass accumulation rate (green) and wt % $CaCO_3$ (blue) inferred from XRF core scanning
of Ca and Fe and calibrated with shipboard and mass-spec based measurements of wt % $CaCO_3$
(light blue), (b) wt % course fraction record from washed core samples (blue) with the interval
barren to intact planktonic foraminifera indicated in brown and iridium concentrations in yellow,
and (c) $\delta^{13}C$ of bulk carbonate (green). The light orange band indicates the K/Pg boundary and
the pale indigo bar indicates the interval of Deccan Trap emplacement. Data in Tables S12, S15,
S19, S20, S21.
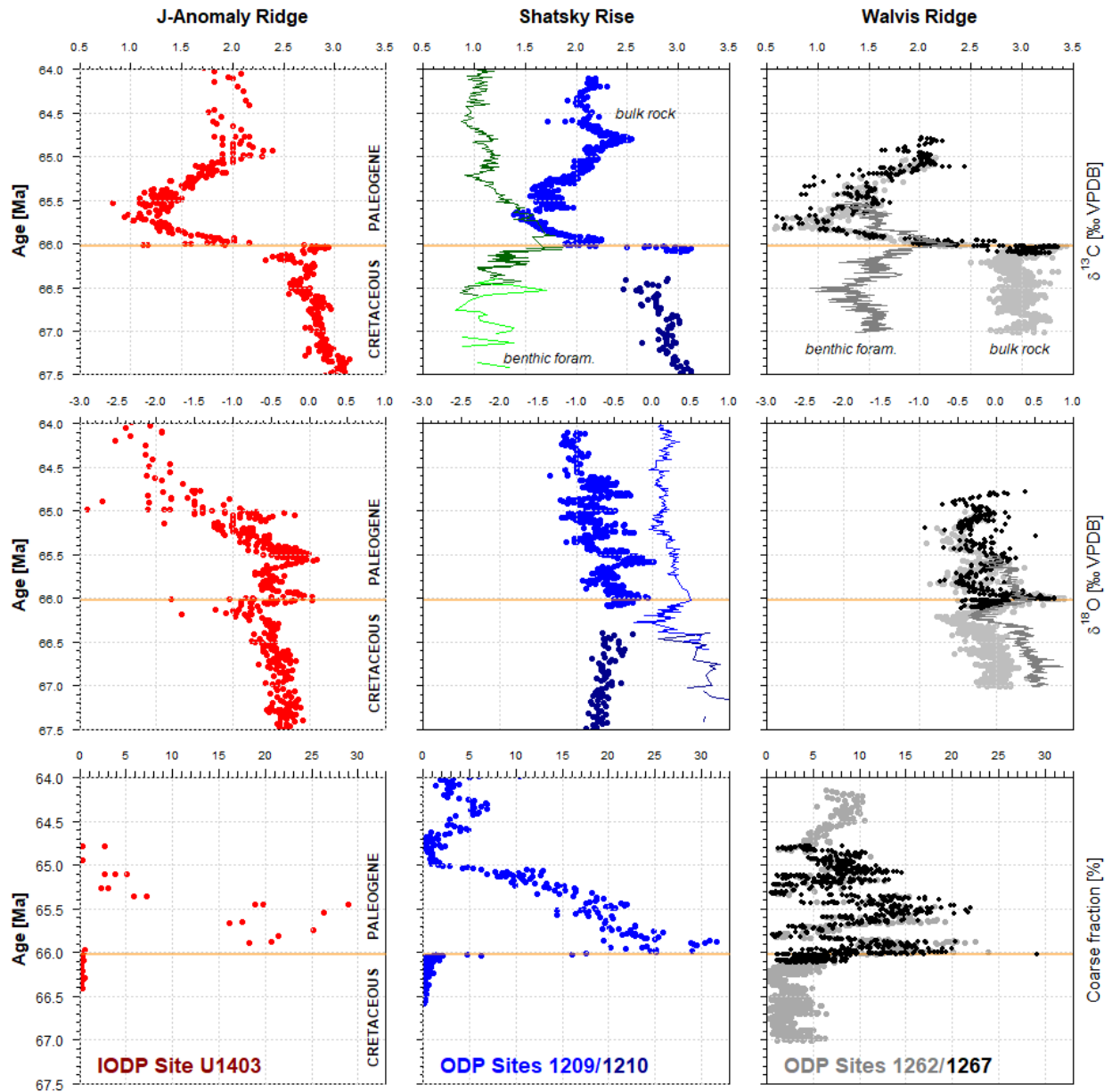
Fig. S18.

New and published (*13-15, 41, 42, 89*) high resolution bulk carbonate and benthic foraminiferal carbon and oxygen records and weight percent coarse fraction records across the K/Pg boundary at the three focal sites (J-Anomaly Ridge, Shatsky Rise, and Walvis Ridge), focused on the last 1.5 million years of the Cretaceous and first 2 million years of the Paleocene.
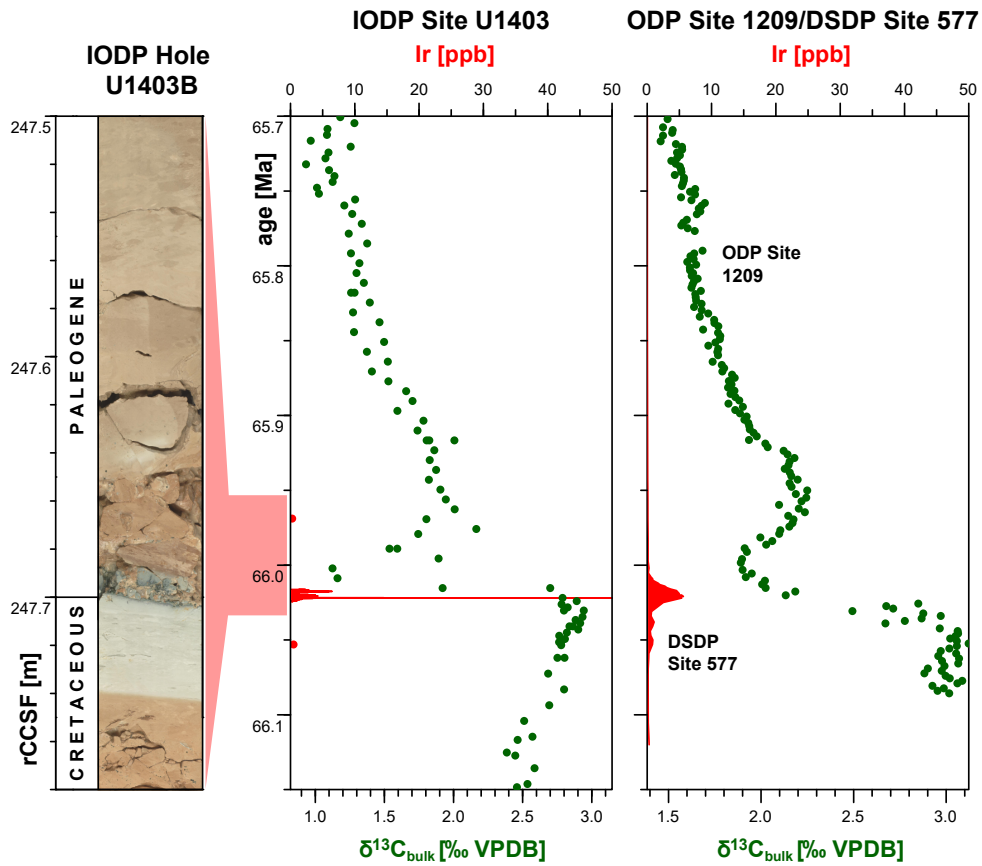
Fig. S19.

Iridium anomalies and the $\delta^{13}C$ gradient collapse in the North Atlantic and Central Pacific. Iridium anomaly (red) and $\delta^{13}C$ excursion (green) at (a) Site U1403, Newfoundland, aligned to core photo of the impact layer, and (b) Shatsky Rise in the North Pacific (iridum anomaly from DSDP Site 577; $\delta^{13}C$ from ODP Site 1209).
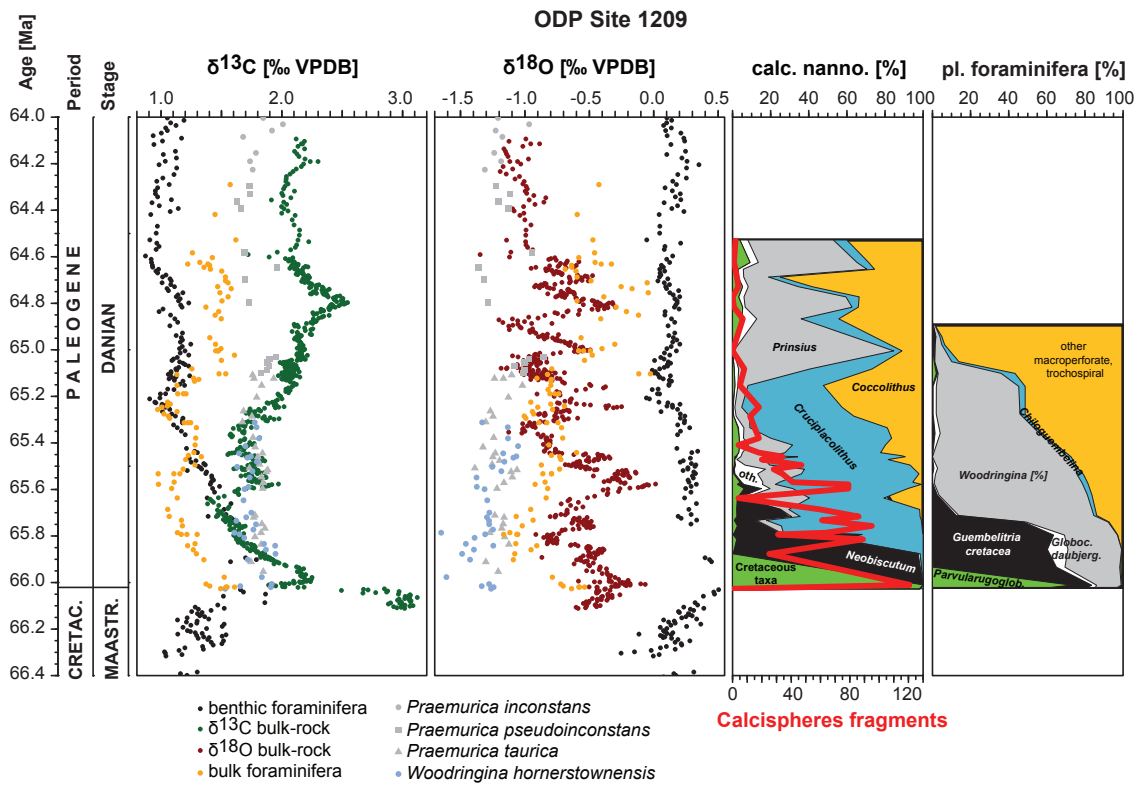
Fig. S20.

Early Paleocene carbon and oxygen isotopes in carbonates versus community turnover in nannoplankton and planktonic foraminifera at IODP Site 1209. Planktonic foraminifera data from Hull et al. (*22*).
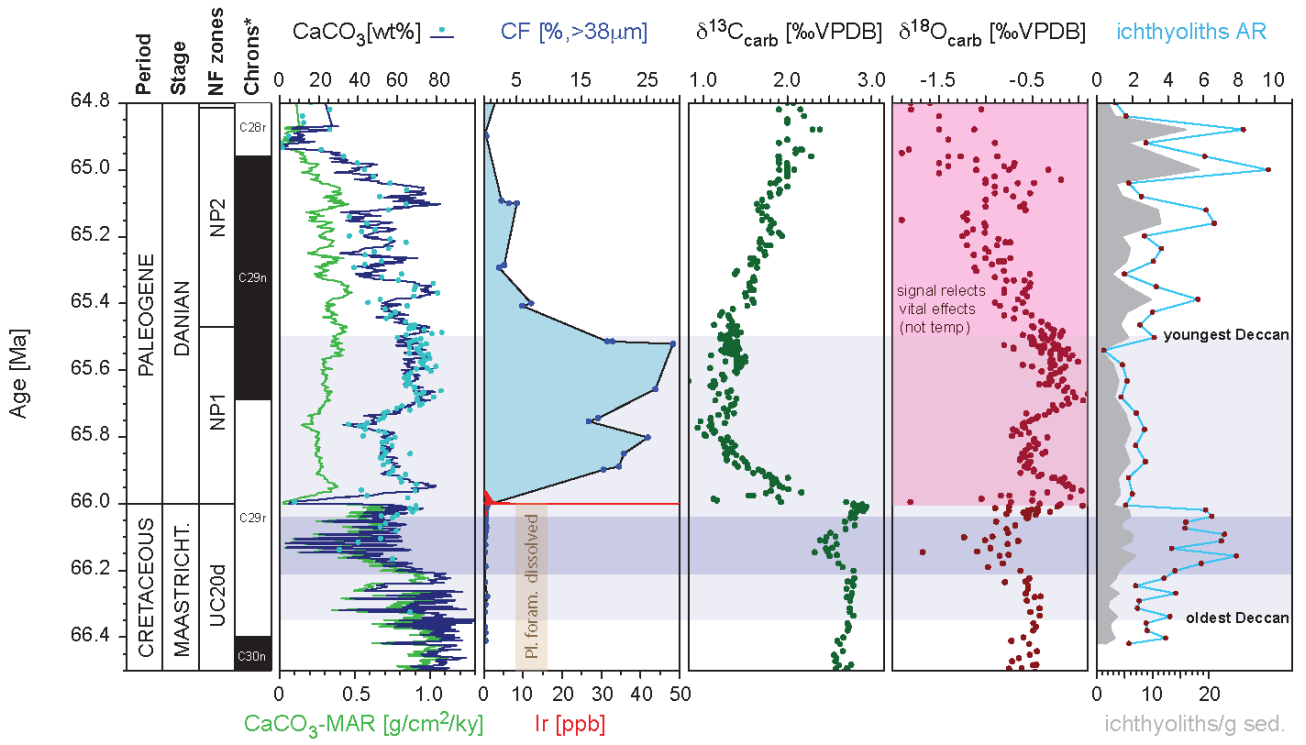
Fig. S21.

IODP Site U1403 K/Pg boundary records from Figs 2,3 with ichthyolith accumulation rate records (far right).
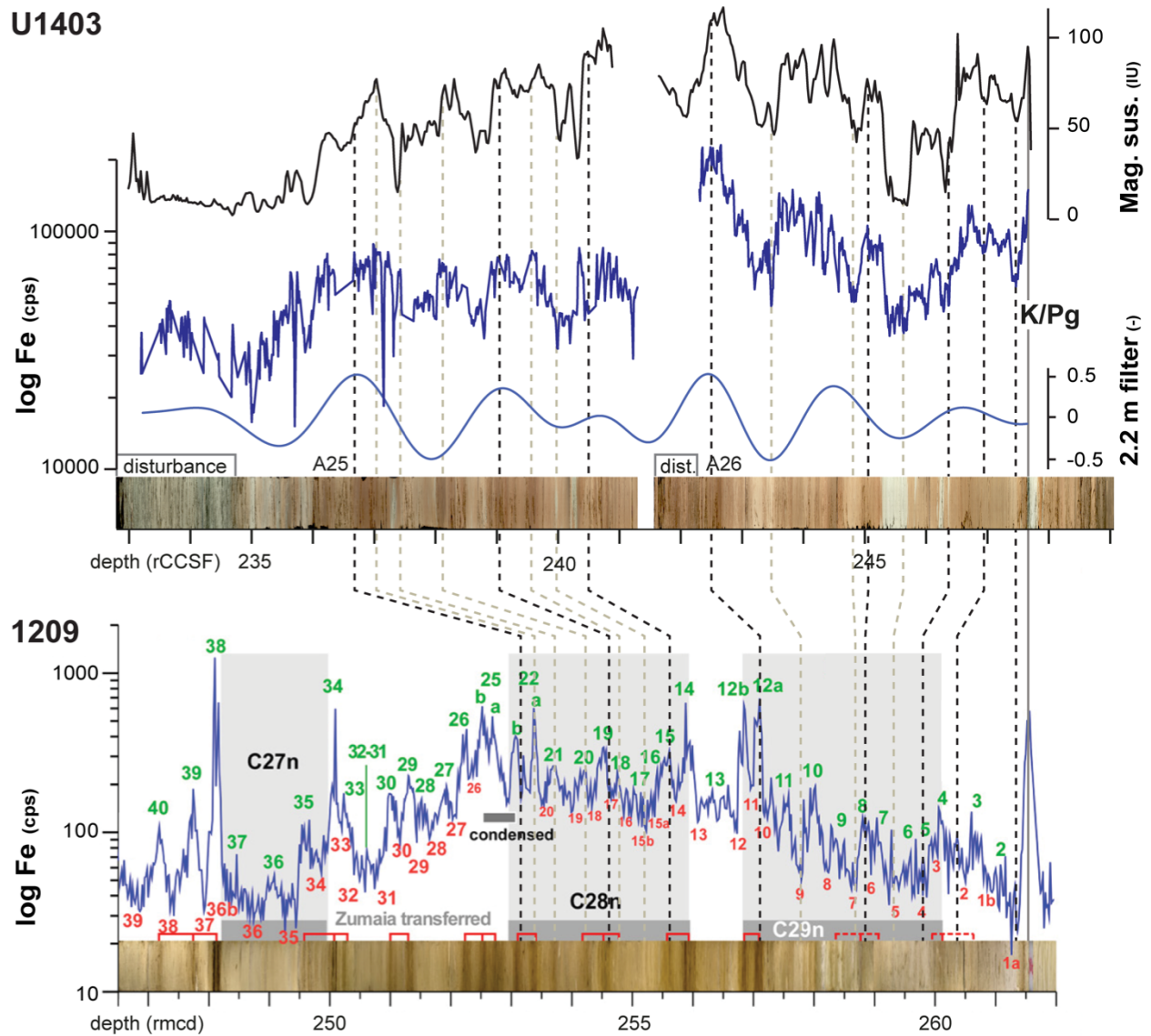
Fig. S22.

Correlation of Site U1403 to Site 1209, based on iron counts from XRF scanning (depicted as log Fe) and sedimentary banding patters, supported by magnetic susceptibility (Mag. sus.) variations. In the lower panel, red bars indicate strongly expressed bands interpreted as long-eccentricity maxima and green and red numbers mark interpreted short-eccentricity (~100 kyr) extremes (*12*). Black dashed lines indicate the tie-points used for the construction of the age model, grey dashed lines indicate additional correlation features. K/Pg: Cretaceous-Paleogene boundary.

IODP 342-1403 K/Pg calcareous nannoplankton
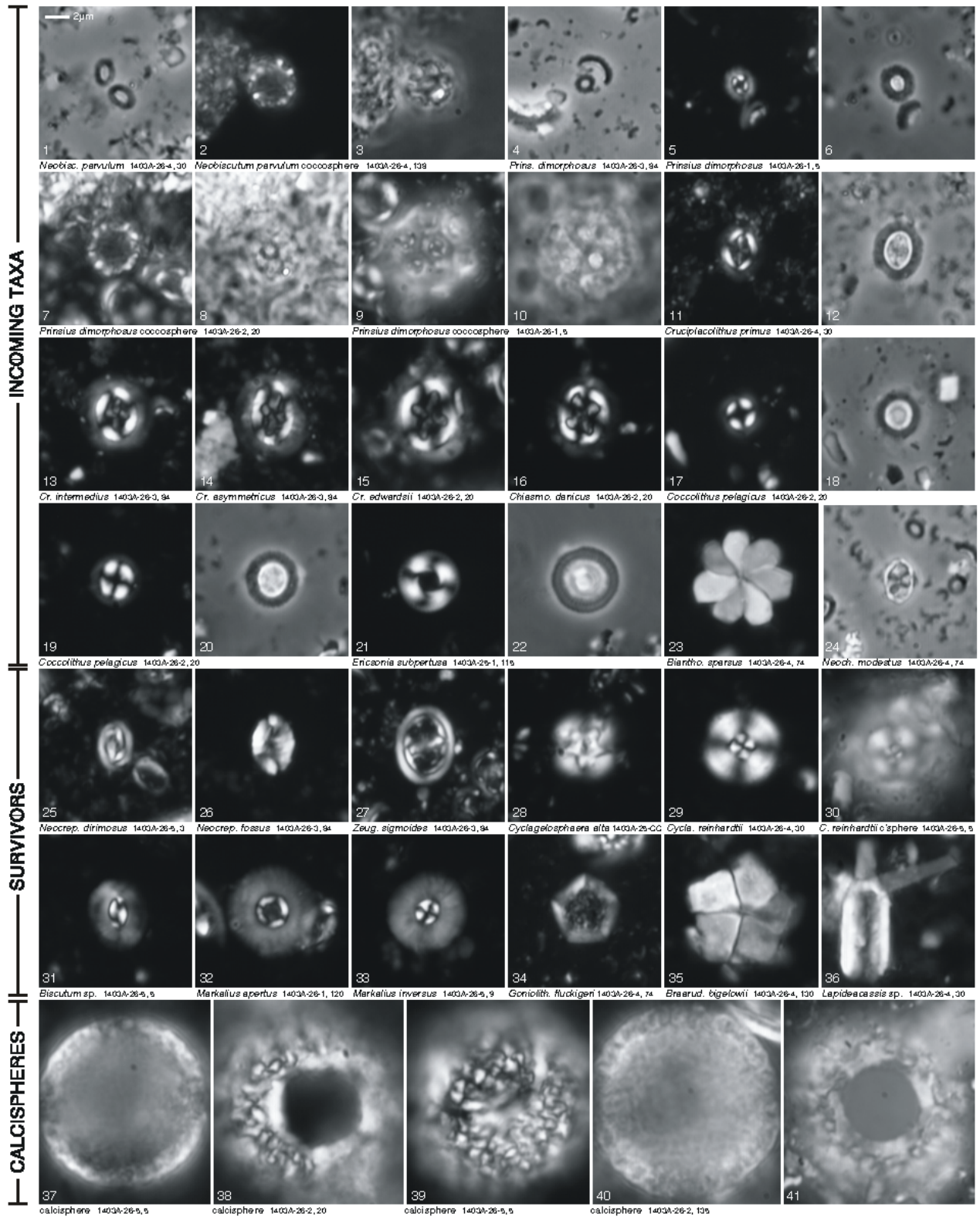
Fig. S23.
Calcareous nannofossils from IODP Site U1403.

51
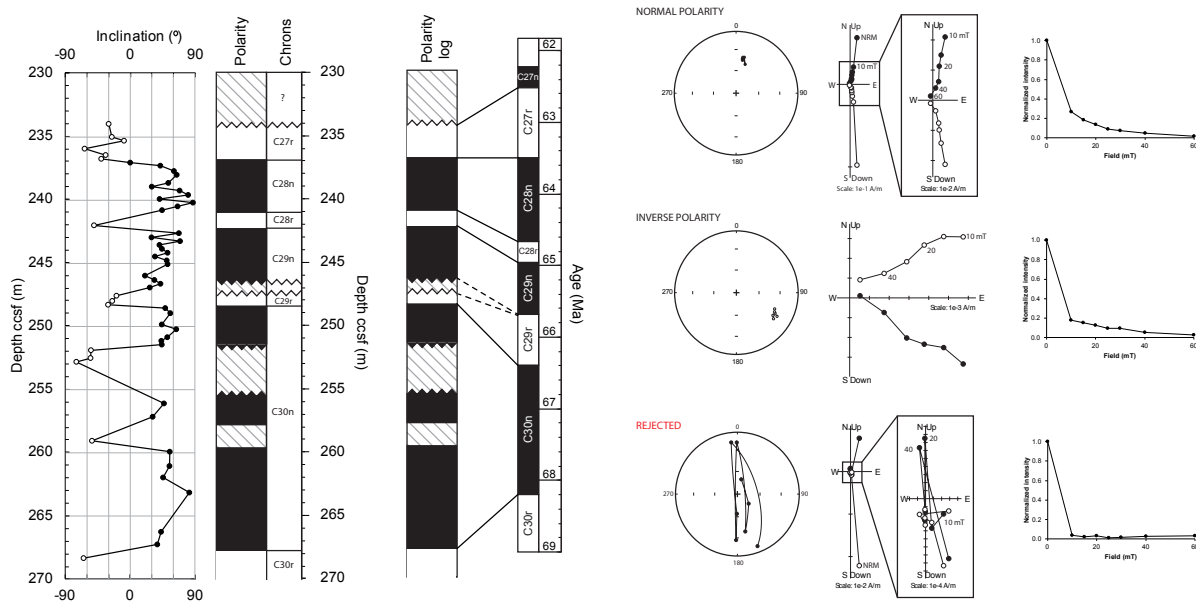
Fig. S24.
Magnetostratigraphy defined for the late Cretaceous to early Paleogene period, covering the K/Pg boundary. All three main types of data obtained to define the magnetostratigraphy are represented, for each one the Zijderveld plot, the stereographic projection and the magnetization versus alternating field are given.
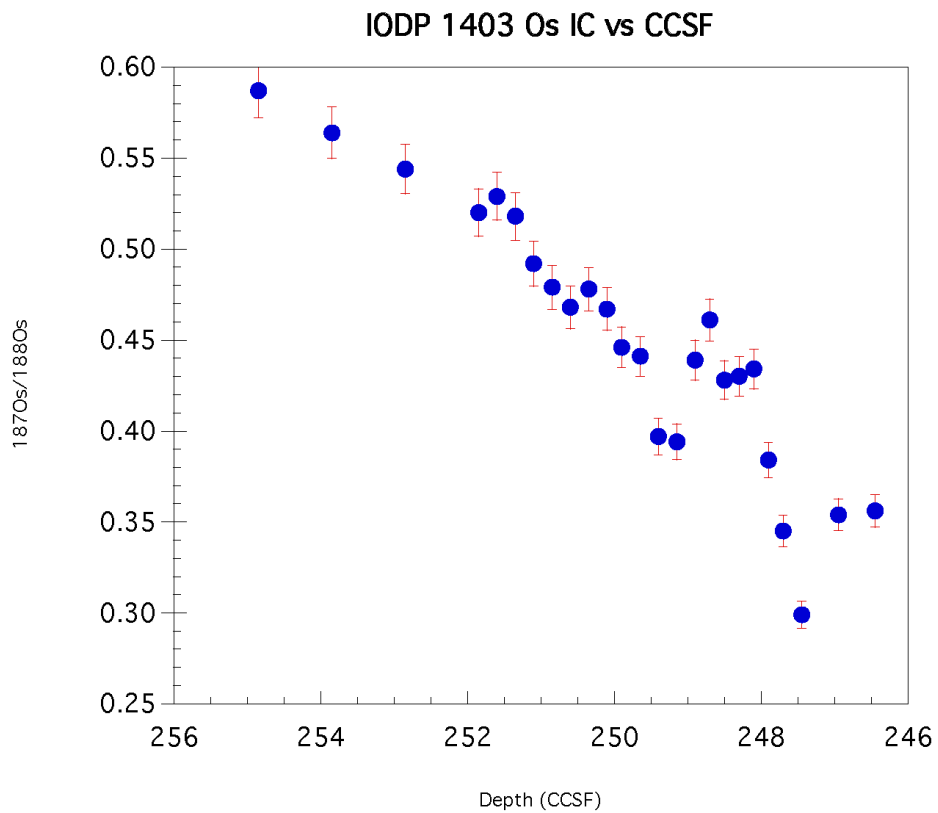
Fig. S25

Osmium isotope record from IODP Site U1403, with 95% confidence intervals.

Panel a
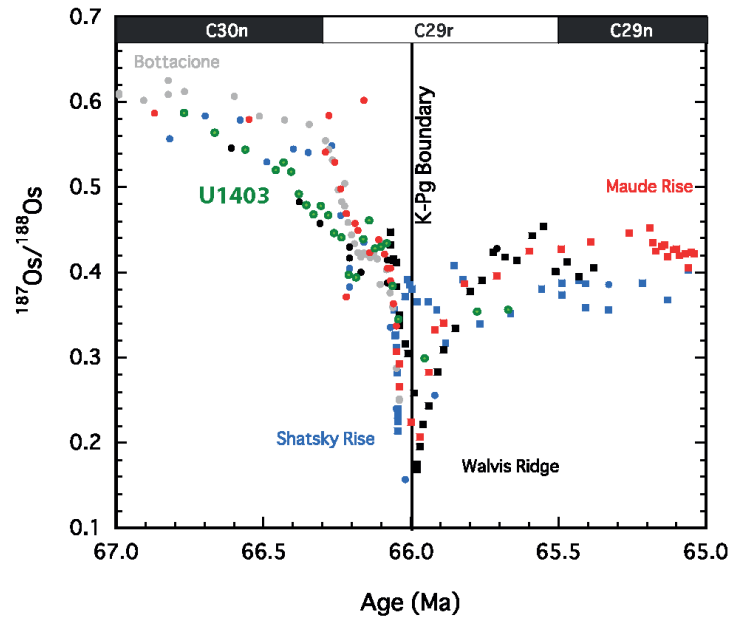
Panel b
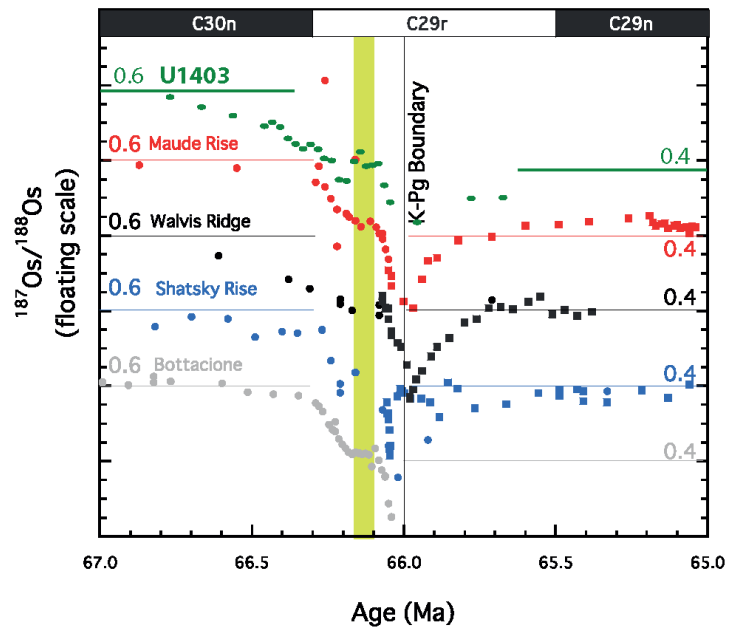
Fig. S26

Osmium isotope record from Site U1403 relative to published records used for isotope stratigraphy (*68-70*), on absolute (a) and floating (b) scales.
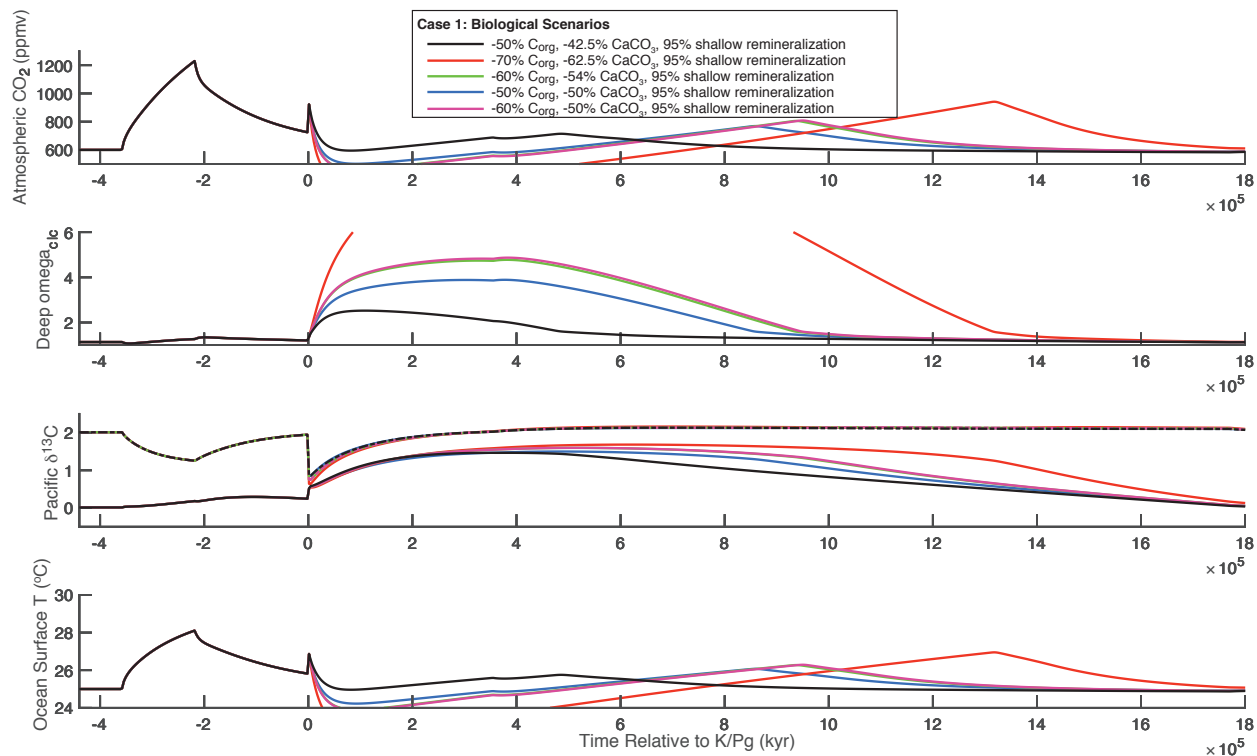
Fig. S27

Biological scenarios explored for Case 1. All tests assume enhanced remineralization rates after the K/Pg (95% shallow water remineralization post-K/Pg and 75% prior to the K/Pg), impact degassing, and a Case 1 outgassing scenario with high Deccan emissions and a climate sensitivity of 3°C/doubling. Biological scenarios explored include a 50-70% reduction in organic carbon export and somewhere between no change and a 25% increase in the $CaCO_3$ to C_{org} export ratio. Even though we explored only increases in the $CaCO_3$ to C_{org} export ratio (to minimize the oversaturation of the deep ocean) these scenarios resulted in dramatic declines in the total export flux of carbonate to the deep sea due to the reduction of organic carbon (between 42.5% and 62.5% reduction in $CaCO_3$ export). The best scenario in terms of minimizing the increase in deep sea carbonate saturation and the decrease in earliest Paleocene temperatures was a 50% reduction in C_{org} with a 15% increase in the $CaCO_3$:C_{org} rain ratio (42.5% $CaCO_3$ export reduction).
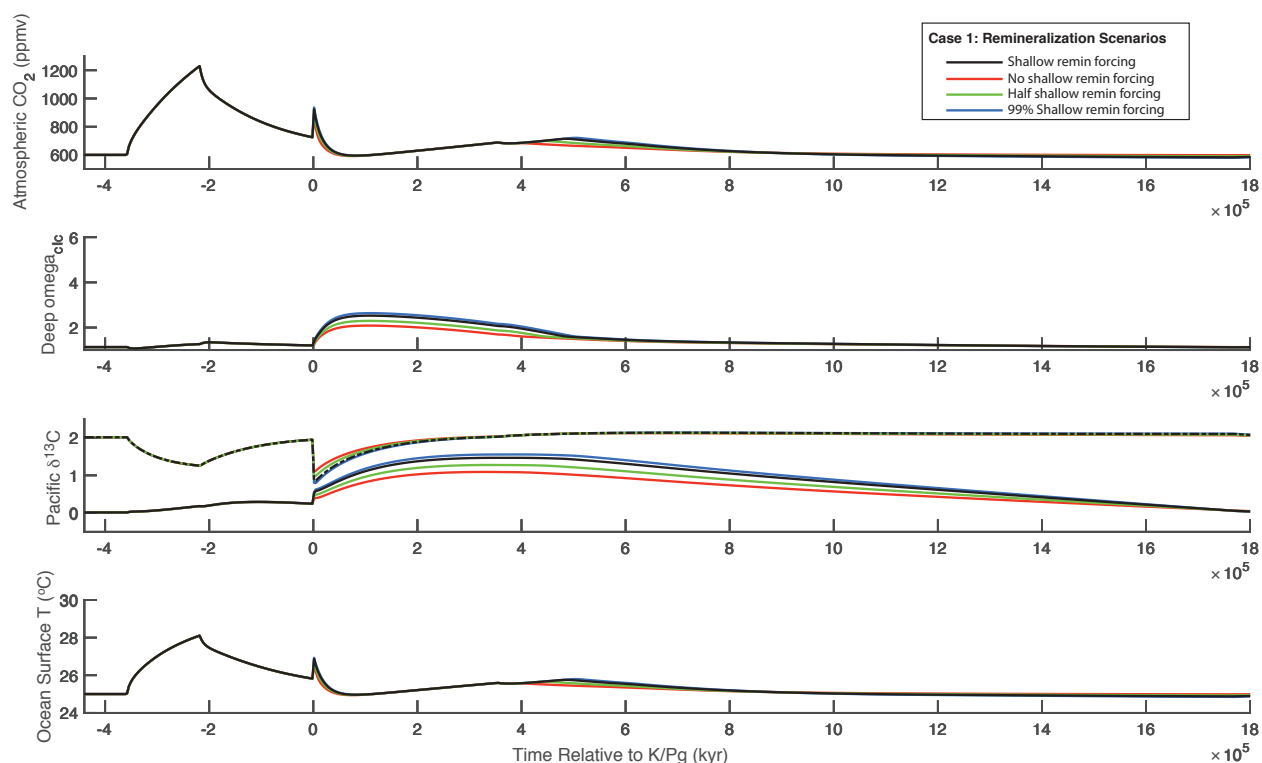
Fig. S28

Exploration of the effect of changes in shallow water remineralization (the fraction of sinking organic carbon that is remineralized in the intermediate ocean reservoirs, as opposed to the deep) on Case 1. All tests assume impact degassing, a Case 1 outgassing scenario with high Deccan emissions and a climate sensitivity of 3°C/doubling, and a biological change scenario of a 50% reduction in C_{org} with a 15% increase in the $CaCO_3$:C_{org} rain ratio. The effect of shallow water remineralization on the early Paleocene marine carbon cycle in LOSCAR was explored by holding remineralization constant across the boundary at 78% ('No shallow remin. forcing'), increasing shallow water remineralization to 86% ('Half shallow remin. forcing'), 95% ('Shallow remin forcing'), and 99% ('99% Shallow remin forcing). Because of the relatively minimal effect of this factor, our initial scenario (and increase from 78% to 95% at the K/Pg) was used in all other modelling scenarios.

56
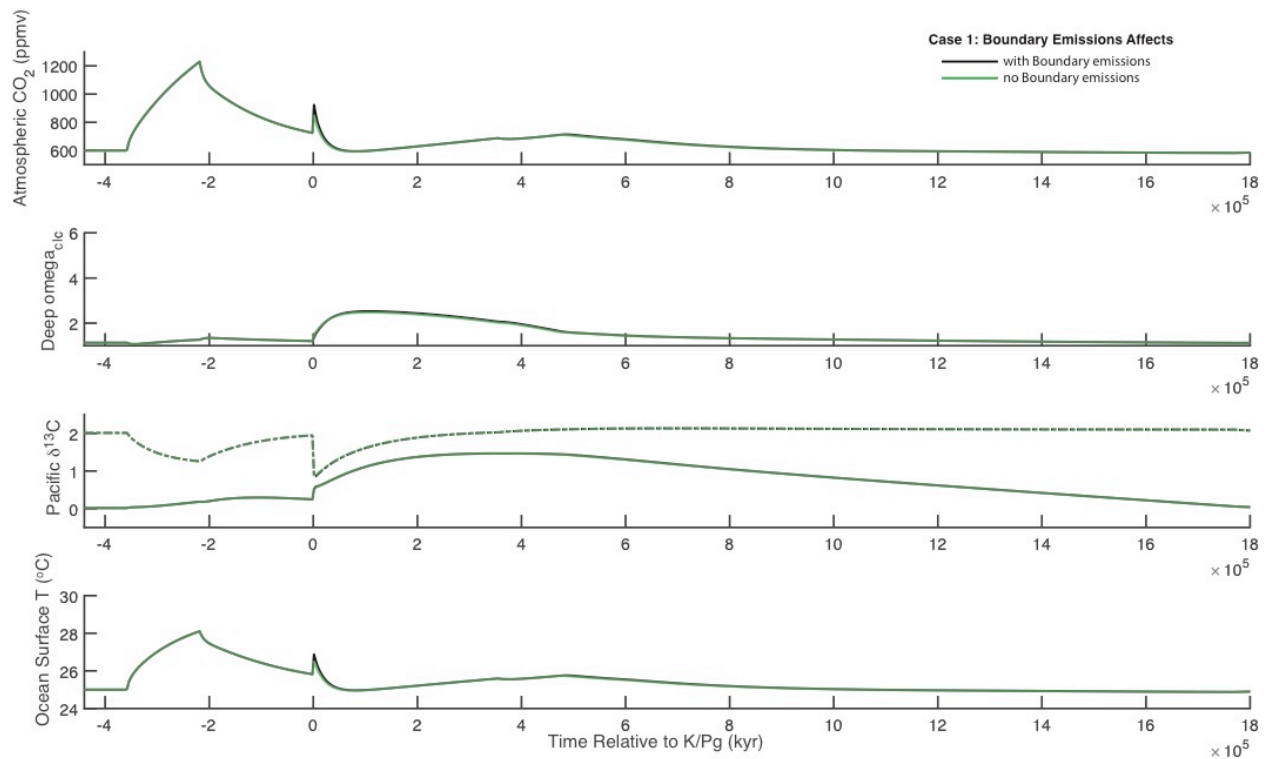
Fig. S29

Effect on including or excluding K/Pg boundary emissions of 325 Gt S and 425 Gt CO_2 (*126*) from impact degassing on Case 1. Case 1 conditions shown here include a Case 1 outgassing scenario with high Deccan emissions and a climate sensitivity of 3°C/doubling, and a biological change scenario of a 50% reduction in C_{org}, a 15% increase in the $CaCO_3$:C_{org} rain ratio, and an increase in shallow water remineralization from 78% to 95% at the K/Pg. Impact degassing has a negligible effect on the simulation behavior, and is included in all other model simulations explored in this study.
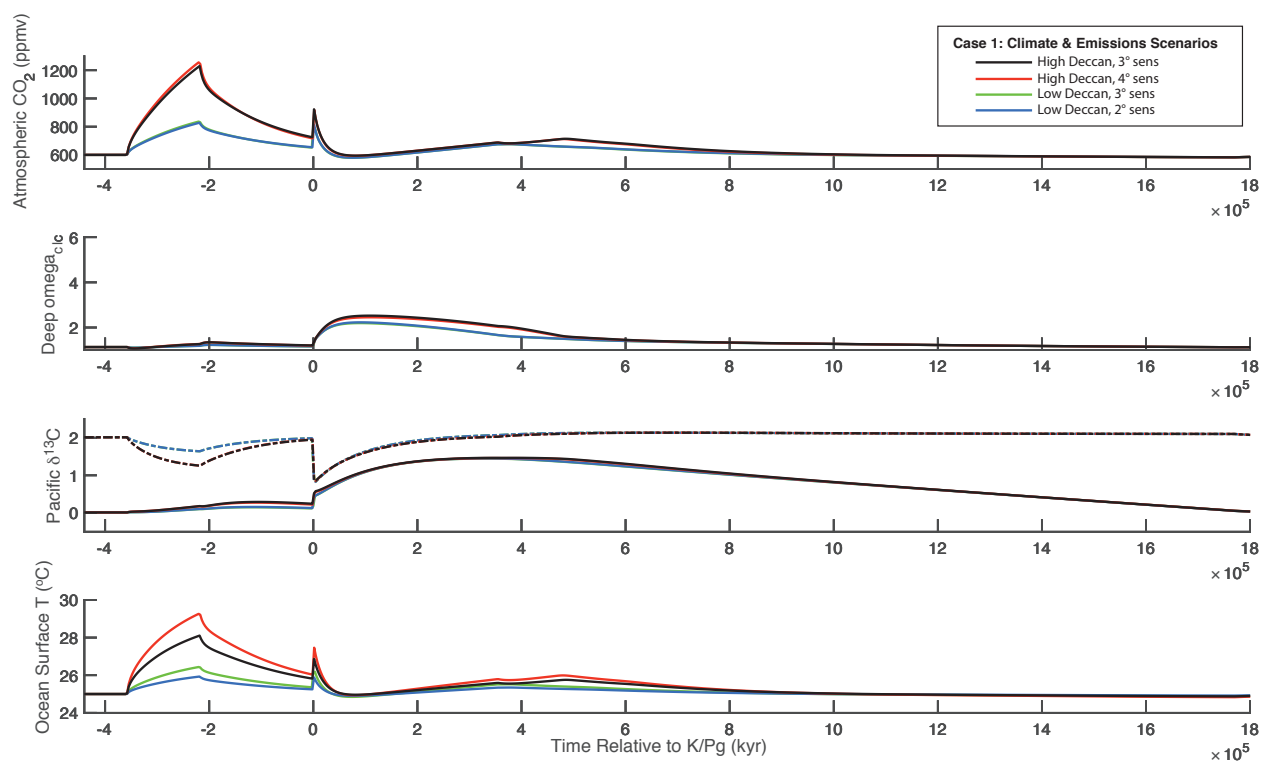
Fig. S30

Effect of volcanic outgassing volume and climate sensitivity on Case 1 simulation behavior. Case 1 conditions shown here include a Case 1 outgassing scenario and a biological change scenario of a 50% reduction in C_{org}, a 15% increase in the $CaCO_3{:}C_{org}$ rain ratio, and an increase in shallow water remineralization from 78% to 95% at the K/Pg. High and low Deccan outgassing scenarios assume upper and lower end-estimates for total volcanic outgassing volumes of 4090 (low) versus 9545 (high) Gt C and 3200 (low) and 8500 (high) Gt S (*66, 132*)), with climate sensitivities (°C/doubling) as described in the legend.
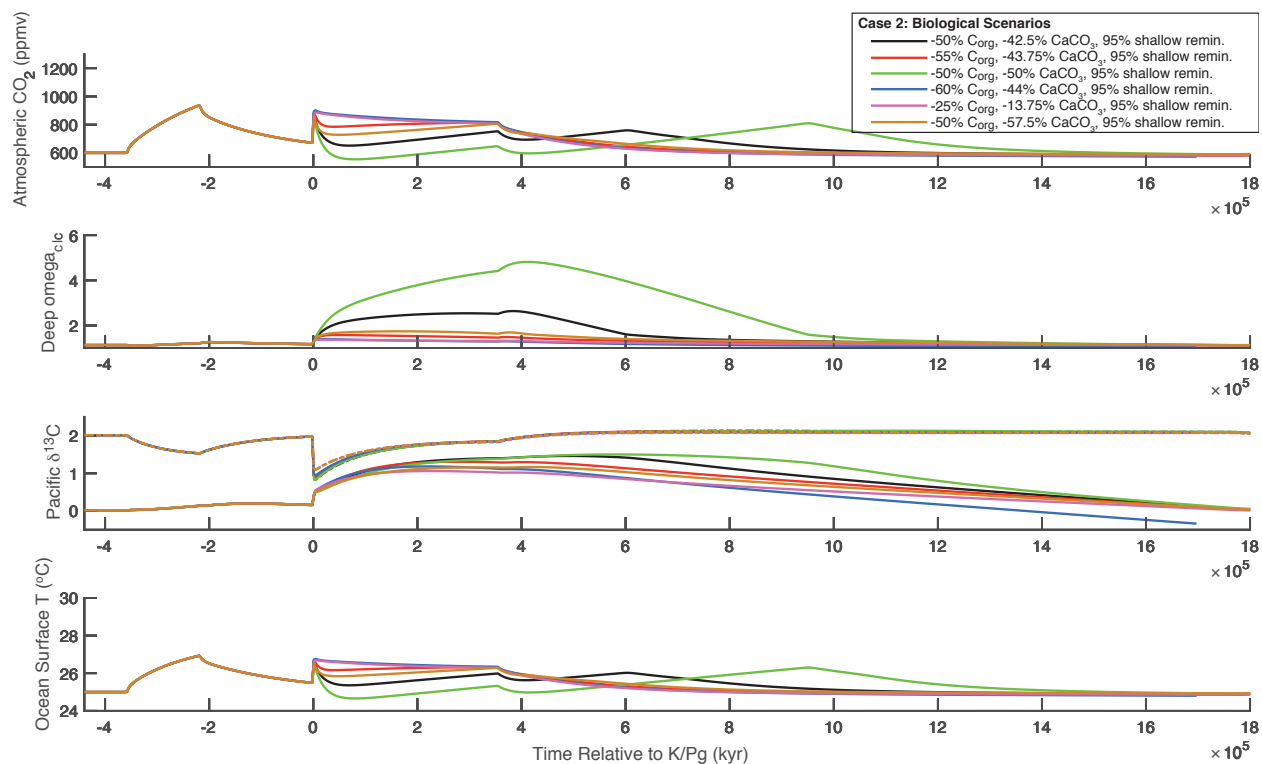
Fig. S31

Biological scenarios explored for Case 2. All tests assume enhanced remineralization rates after the K/Pg (95% shallow water remineralization post-K/Pg and 75% prior to the K/Pg), impact degassing, and a Case 2 outgassing scenario with high Deccan emissions and a climate sensitivity of 3 °C/doubling. Biological scenarios explored include a 25-60% reduction in organic carbon export and somewhere between no change and a 25% increase in the $CaCO_3$ to C_{org} export ratio. Even though we explored only increases in the $CaCO_3$ to C_{org} export ratio (to minimize the oversaturation of the deep ocean) these scenarios resulted in dramatic declines in the total export flux of carbonate to the deep sea (between 13.75% and 57.5% reduction in the $CaCO_3$ export flux) due to the reduction of organic carbon. The best scenario in terms of minimizing the increase in deep sea carbonate saturation and the decrease in earliest Paleocene temperatures was a 50% reduction in C_{org} with a 15% increase in the $CaCO_3$:C_{org} rain ratio (42.5% reduction in $CaCO_3$ export flux).
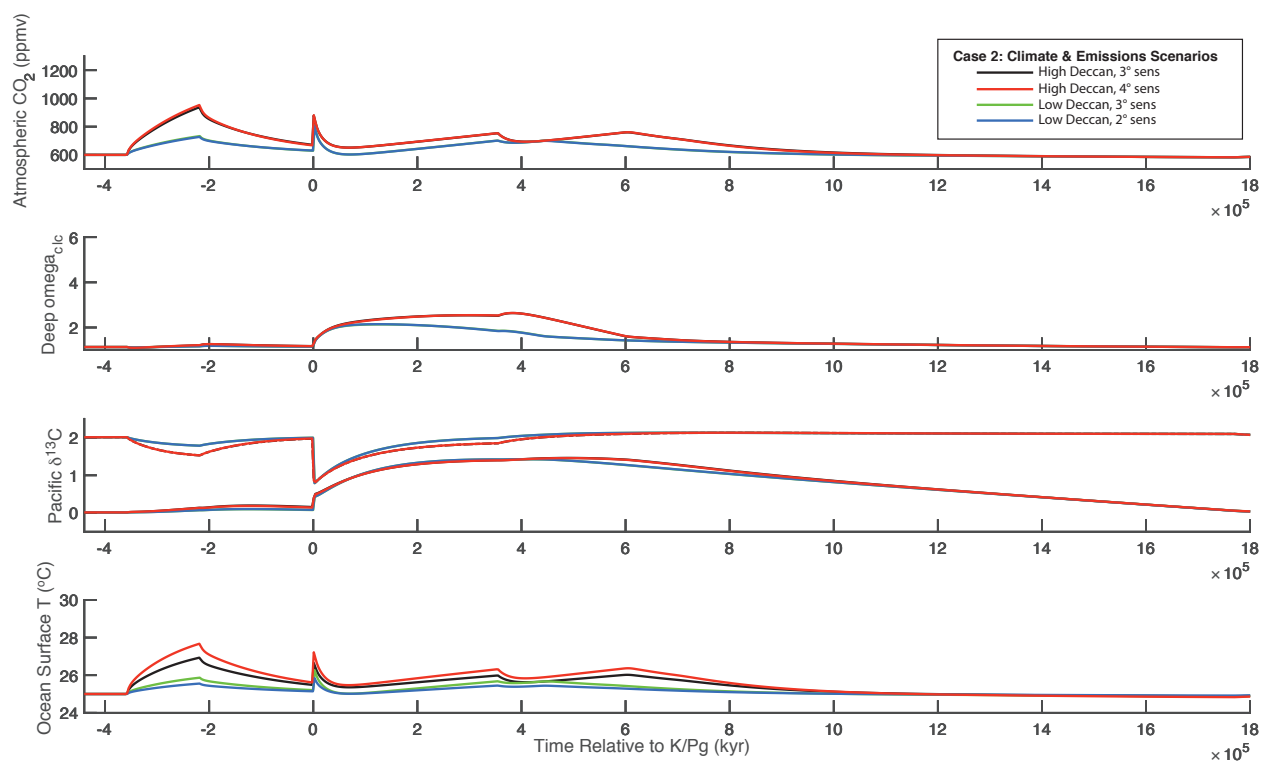
Fig. S32

Effect of volcanic outgassing volume and climate sensitivity on Case 2 simulation behavior. Case 2 conditions shown here include a Case 2 outgassing scenario and a biological change scenario of a 50% reduction in C_{org}, a 15% increase in the $CaCO_3$:C_{org} rain ratio, and an increase in shallow water remineralization from 78% to 95% at the K/Pg. High and low Deccan outgassing scenarios assume upper and lower end-estimates for total volcanic outgassing volumes of 4090 (low) versus 9545 (high) Gt C and 3200 (low) and 8500 (high) Gt S (*66, 132*)), with climate sensitivities (°C/doubling) as described in the legend.

60

Fig. S33

Effect of volcanic outgassing volume and climate sensitivity on Case 3 simulation behavior. Case 3 conditions shown here include a Case 3 outgassing scenario and a biological change scenario of a 50% reduction in C_{org}, a 15% increase in the $CaCO_3$:C_{org} rain ratio, and an increase in shallow water remineralization from 78% to 95% at the K/Pg. High and low Deccan outgassing scenarios assume upper and lower end-estimates for total volcanic outgassing volumes of 4090 (low) versus 9545 (high) Gt C and 3200 (low) and 8500 (high) Gt S (*66, 132*)), with climate sensitivities (°C/doubling) as described in the legend.
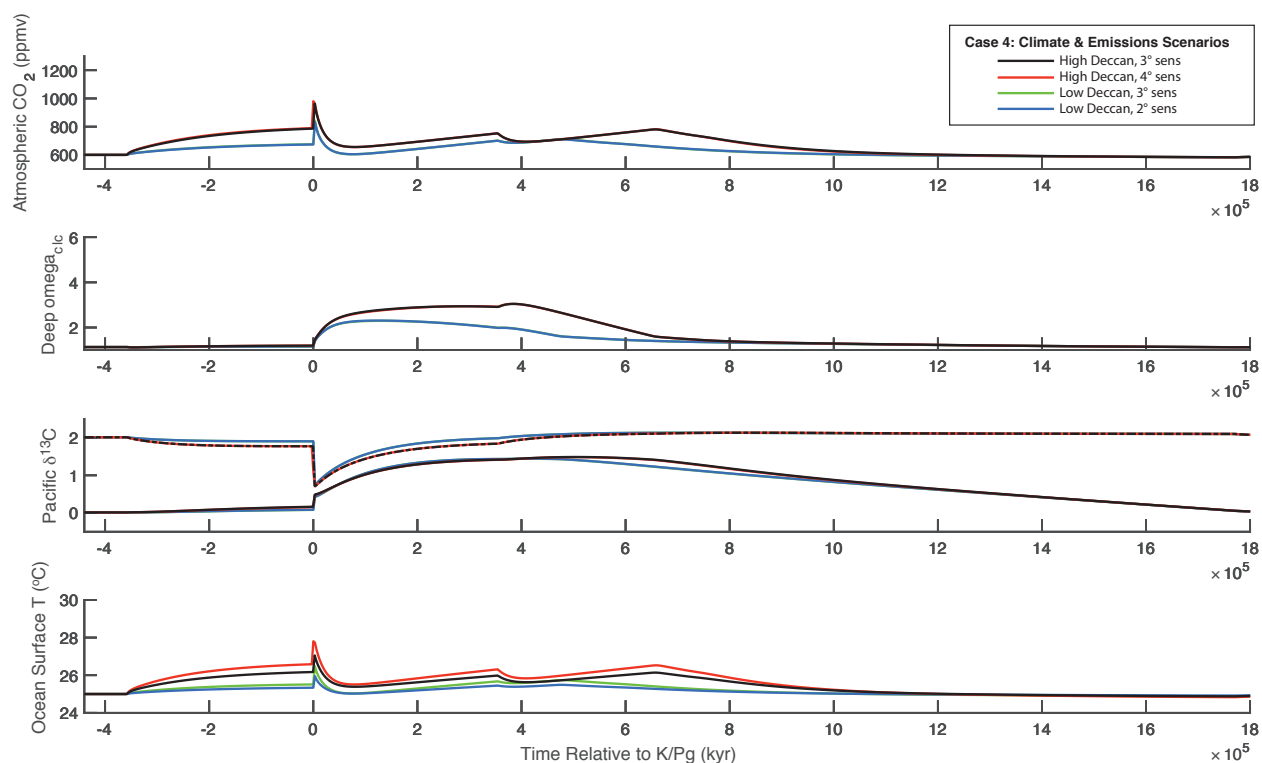
Fig. S34

Effect of volcanic outgassing volume and climate sensitivity on Case 4 simulation behavior. Case 4 conditions shown here include a Case 4 outgassing scenario and a biological change scenario of a 50% reduction in C_{org}, a 15% increase in the $CaCO_3:C_{org}$ rain ratio, and an increase in shallow water remineralization from 78% to 95% at the K/Pg. High and low Deccan outgassing scenarios assume upper and lower end-estimates for total volcanic outgassing volumes of 4090 (low) versus 9545 (high) Gt C and 3200 (low) and 8500 (high) Gt S (*66, 132*)), with climate sensitivities (°C/doubling) as described in the legend.
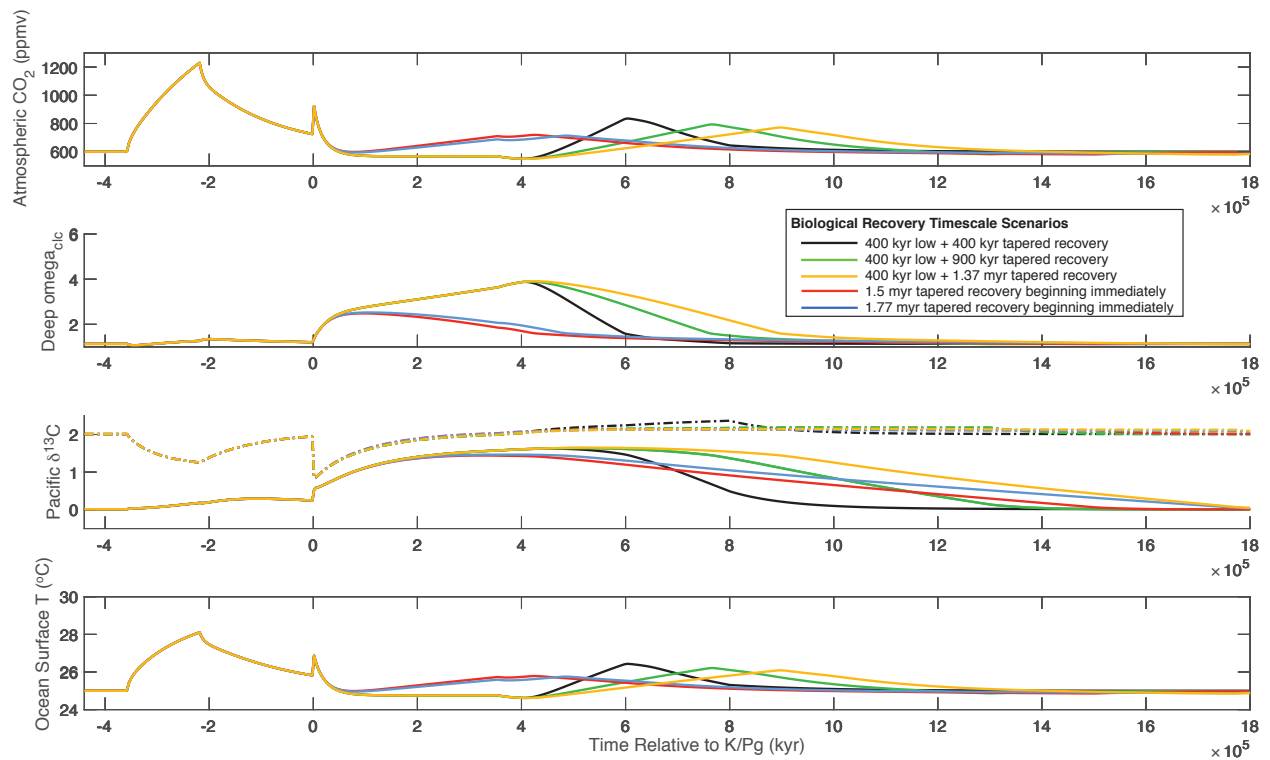
Fig. S35

Biological recovery timescales explored as detailed in the plot legend. All tests assume enhanced remineralization rates after the K/Pg (95% shallow water remineralization post-K/Pg and 75% prior to the K/Pg), impact degassing, and a Case 1 outgassing scenario with high Deccan emissions, a climate sensitivity of 3°C/doubling, a 50% reduction in organic carbon export, and a 42.5% reduction in CaCO₃ export flux.
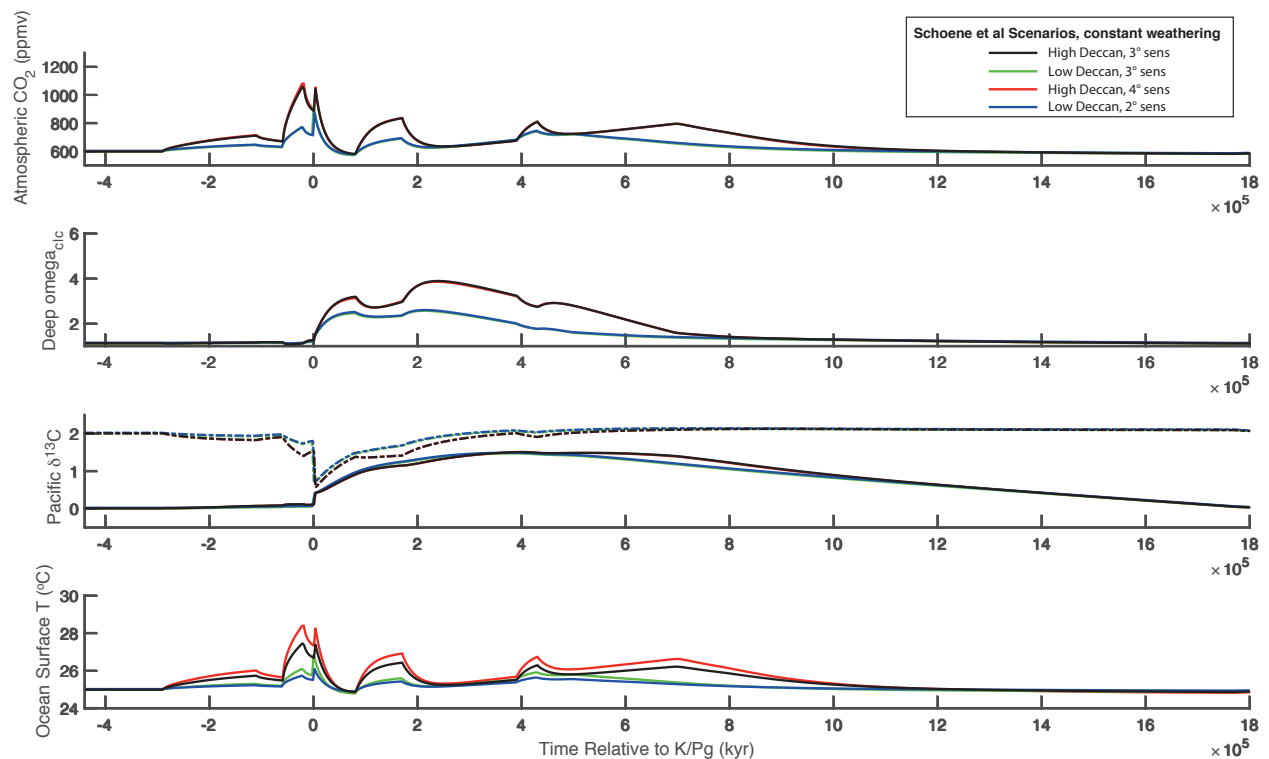
Fig. S36

Effect of volcanic outgassing volume and climate sensitivity on outgassing scenarios following lava emplacement in Schoene et al. (*58*), using the same weathering feedback common to all other simulations. The Schoene degassing timing and volumes are as follows: 20% of emissions between 290 and 110kyr before the boundary, 35% of emissions between 60 and 20kyr before the boundary, 35% of emissions between 80 and 170 kyr after the boundary, and 10% of emissions between 390 and 430kyr after the boundary. All other factors are as in other simulations: a biological change scenario of a 50% reduction in C_{org}, a 15% increase in the $CaCO_3$:C_{org} rain ratio (a 42.5% $CaCO_3$ export flux reduction), an increase in shallow water remineralization from 78% to 95% at the K/Pg, and high and low Deccan outgassing scenarios assuming upper and lower end-estimates for total volcanic outgassing volumes of 4090 (low) versus 9545 (high) Gt C and 3200 (low) and 8500 (high) Gt S (*66, 132*)), with climate sensitivities (˚C/doubling) as described in the legend.

Fig. S37

Effect of volcanic outgassing volume and climate sensitivity on outgassing scenarios following lava emplacement in Schoene et al. (*58*), with silicate weathering doubled during the latest-Cretaceous Deccan pulse to negate warming during that interval. The Schoene degassing timing and volumes are as follows: 20% of emissions between 290 and 110kyr before the boundary, 35% of emissions between 60 and 20kyr before the boundary, 35% of emissions between 80 and 170 kyr after the boundary, and 10% of emissions between 390 and 430kyr after the boundary. All other factors are as in other simulations: a biological change scenario of a 50% reduction in C_{org}, a 15% increase in the $CaCO_3$:C_{org} rain ratio (a 42.5% $CaCO_3$ export flux reduction), an increase in shallow water remineralization from 78% to 95% at the K/Pg, and high and low Deccan outgassing scenarios assuming upper and lower end-estimates for total volcanic outgassing volumes of 4091 (low) versus 9545 (high) Gt C and 3200 (low) and 8500 (high) Gt S (*66, 132*)), with climate sensitivities (˚C/doubling) as described in the legend.
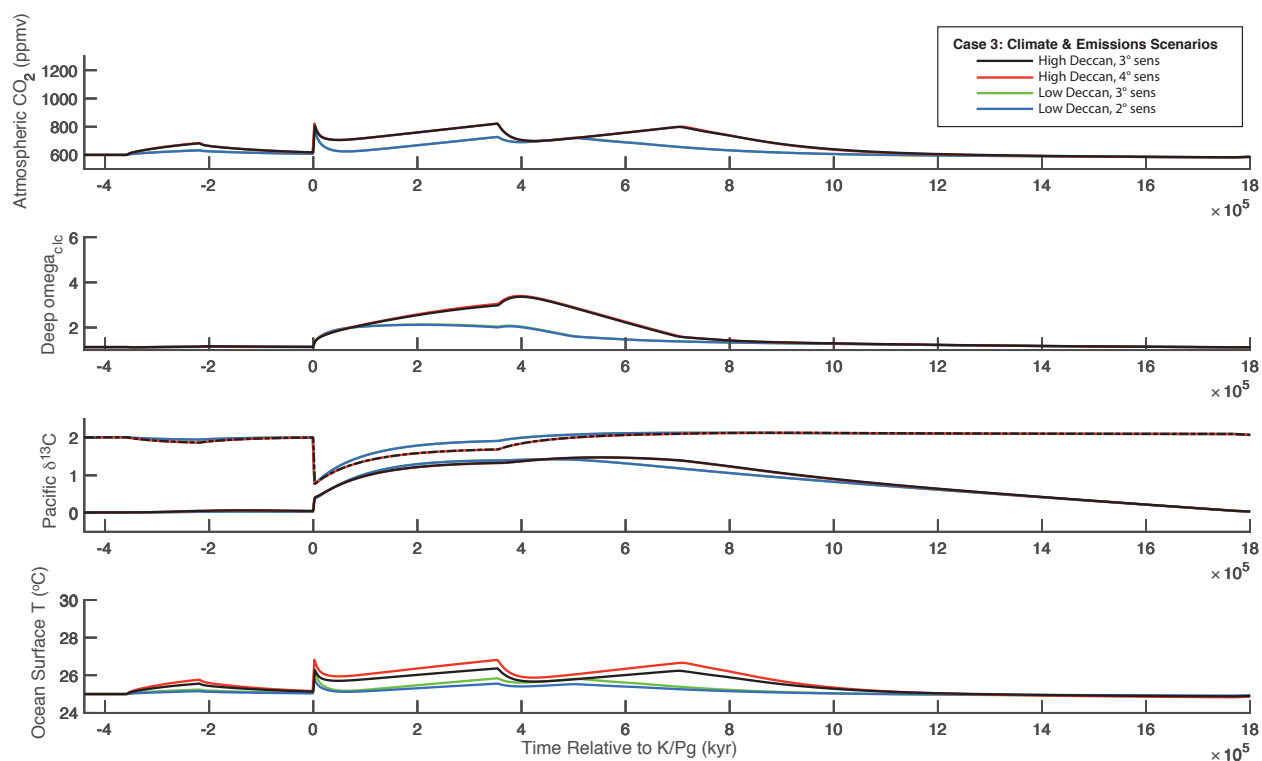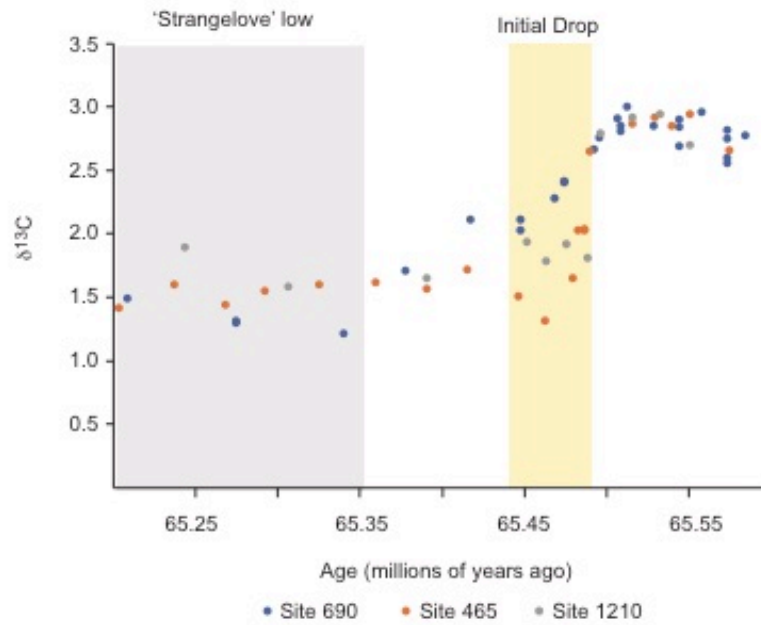
Fig. S38

Evidence for the double drop in $\delta^{13}C$ in the earliest Paleocene is apparent in the published bulk carbonate records of Alegret et al (*29*), shown above on the age scale used in that paper.

Table S1.

Diagnosing a mass extinction requires identifying an exogenous trigger, linking that trigger to a (set of) environmental effects, and linking those environmental effects to extinction. Here we provide an overview of some of the relevant literature regarding the timing, environmental effects, biotic effects of Deccan volcanism and the Chicxulub impact and the ties between these events and the K/Pg mass extinction. This is not a comprehensive review of all literature published on the latest Maastrichtian and earliest Paleocene.

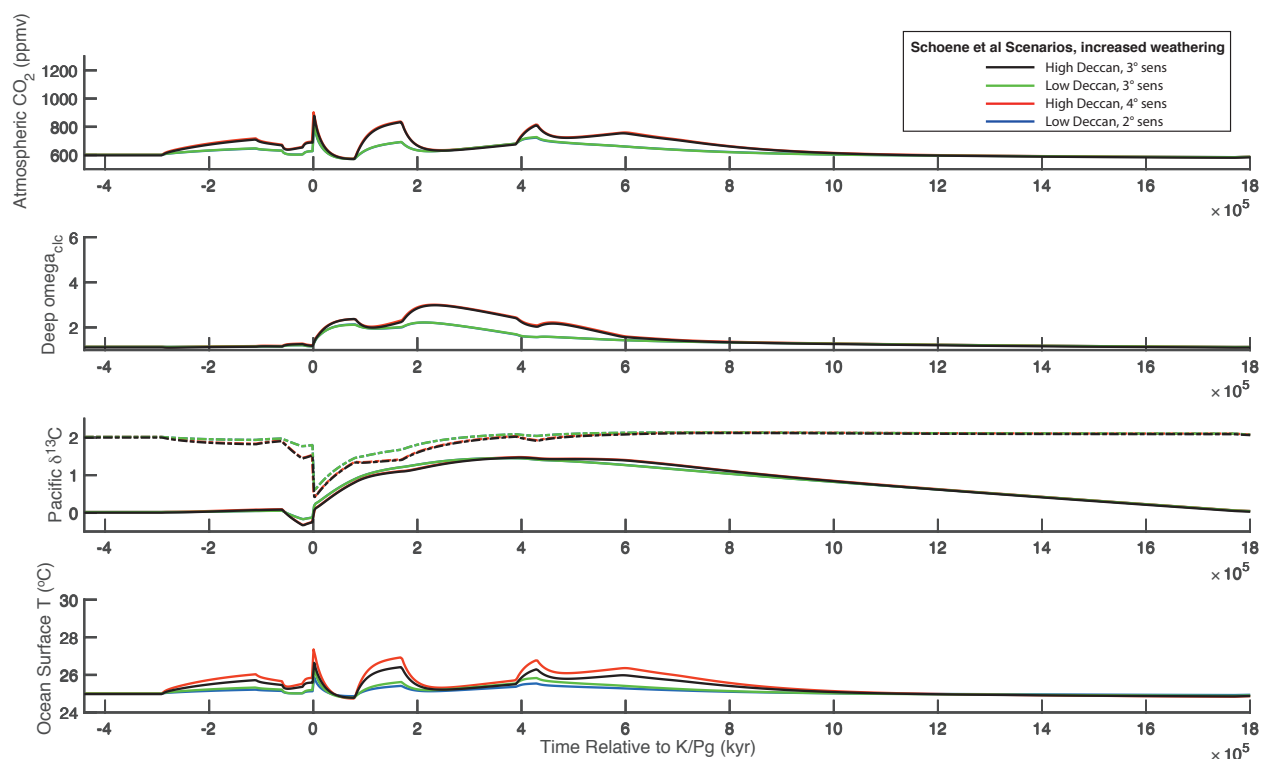| Realm	Evidence for…	Paper Topic	Citation	Ref.
Eruptions	**Deccan:** Volcanism	Vast majority of Deccan flows dated to magnetochron C29R using U-Pb dating (Schoene et al 2015, 2019), K-Ar dating (Chenet et al. 2007), and Ar-Ar dating (Renne et al. 2015; Sprain et al. 2019). Early estimates of a <1myr duration coinciding with C29R based on paleomagnetics, palynology and K-Ar dating (Courtillot et al. 1986), were subsequently debated (Duncan and Pyle 1988, Courtillot et al. 1988, and many others) and only recently confirmed with advanced absolute dating techniques in Schoene et al. 2015, 2019, Renne et al. 2015, and Sprain et al. 2019. Notably, earlier idea of three pulses of volcanism (i.e., Chenet et al. 2007) not supported by recent U-Pb and Ar-Ar work.	Duncan & Pyle 1988; Chenet et al. 2007; Courtillot et al. 1986, 1988; Renne et al. 2015; Schoene et al. 2015, 2019; Sprain et al. 2019	(*58, 66, 67, 164-168*)
		Magnetochron C29r dated to last ~587 ka (Sprain et al. 2018) using Ar-Ar dating, overturning shorter estimates of Sprain et al. 2014, but within error of the GTS 2012 estimate. Key ages from Sprain et al. 2018 include C30n/C29r reversal ~66.311 Ma, K/Pg ~66.052 Ma, C29r/C29n ~65.724 Ma. Accordingly, the C29R Cretaceous duration is ~259+/-52 kyr and Paleocene duration is ~328+/-15kyr (Sprain et al. 2018)	Sprain et al. 2014, 2018; Gradstein et al. 2012	(*59, 60, 169*)
		Paleomagnetic secular variation pins short duration of individual flows, increasing environmental potential	Chenet et al. 2008	(*170*)
		Outgassing potential calculations of Deccan traps for SO_2, CO_2, Cl	Chenet et al. 2009; Self et al. 2006, 2008	(*132, 171*) (*172*)
		Hypothesized link between impact and major Deccan eruptions based on eruptive volumes; new eruptive volume estimates provided	Richards et al. 2015	(*159*)
		Constrain majority of Deccan volcanism to post-K/Pg using Ar-Ar dating (Renne et al. 2015; Sprain et al. 2019)	Renne et al. 2015; Sprain et al. 2019	(*67, 168*)
		Constrains majority of Deccan volcanism to two pulses (one ~30kyr pre-K/Pg, the second ~100 post-K/Pg) using U-Pb dates and lava volume estimates	Schoene et al. 2019	(*58*)
Weathering	**Deccan:** Volcanism	Decrease in Sr isotope ratios ($^{87}Sr/^{86}Sr$) coincident with ^{18}O anomaly in the Cretaceous interval of C29R; attributed to Deccan related increase in weathering	Vonhof and Smit 1997; Olsson et 2002	(*110, 173*)
		Declines in osmium isotope ratios in magnetochron C29r in sites globally suggestion large scale change in terrestrial weathering with Deccan flood basalt volcanism	Ravizza & Peucker-Ehrenbrink 2003; Paquay	(*68, 69, 71*)

			et al. 2008; Robinson et al. 2009	
		Erosional history of Deccan Traps from structure of Western Ghats	Widdowson & Cox 1996	(*174*)
		Mercury anomaly in Bidart, France, coincides w/pre-K/Pg cooling interval (w/evidence for dissolution of foraminifera); and see subsequent discussions	Font et al. 2016a,b; Smit et al. 2016	(*175-177*)
		Increased Sr/Ca ratios in latest Maastrichtian (last 200 kyr) perhaps due to increased chemical weathering during Late Maastrichtian warming & cooling in Elles, Tunisia	Stüben et al. 2003	(*178*)
Pre-K/Pg	**Deccan:** Environment effect	8°C summer temp decrease (Montana)	Tobin et al. 2014	(*96*)
		7°C temp rise & fall (North Dakota)	Wilf et al. 2003	(*91*)
		Clay mineralogical evidence for aridity and alkaline conditions (Deccan volcanic sediments)	Samant et al. 2014	(*179*)
		'Mock aridity' due to volcanically influence local climate (Deccan sedimentary sequence)	Khadkikar et al. 1999	(*180*)
		Intense precipitation inferred from geochemistry of inter-basaltic bole beds (Deccan Traps)	Ghosh et al. 2006	(*181*)
		Longer warm interval (>2 myr span) pre-K/Pg suggested by Seymour Island flora; cool early Paleocene suggested by flora directly countered by evidence of no K/Pg temperature change in organic geochemical proxies	Bowman et al. 2014; Kemp et al. 2014	(*182, 183*)
		High latitude warming (Southern Ocean) coincident with Cretaceous interval of C29r	Tobin et al. 2012	(*95*)
		Antarctic sea ice indicator (dinoflagellate species) present in Maastrichtian is significantly reduced during last ~2 myr before the K/Pg (indicative of significant climatic warming; matches longer interval of warmth in Seymour Island plants as well)	Bowman et al. 2013; Bowman et al. 2014	(*182, 184*)
		Warming (or low oxygen) in Nye Klov, Denmark inferred from bryozoan colonial morphology; matches stable carbon and oxygen records. In both cases the warming occurs right up to boundary (no cooling)	O'Dea et al. 2011; Barrera and Keller 1994	(*185, 186*)
		Regional evidence (biomarker, geochemical and benthic foraminiferal assemblage) towards anoxia in NW Pacific, New Zealand, and a few Tethyan sections	Kajiwara & Kaiho 1992; Kaiho et al. 1999; Alegret & Thomas 2005; Mizukami et al. 2013	(*187-190*)
		Late Cretaceous warming in magnetochron C2r of ~2-3°C (also called the 'Brazos Event')	Henehan et al. 2016; Westerhold et al. 2011; Li and Keller 1998; Barnet et al. 2018, 2019	(*13, 42, 43, 82, 112*)

		Increased oligotrophy suggested by nanoplankton assemblage structure (North Pacific and other sites)	Thibault & Gardin 2010	*(138)*
		Deep sea carbonate undersaturation; minor surface ocean acidification based on fragmentation and wt % CaCO₃ records coincident with warming in open ocean sites (Henehan et al. 2016); dissolution in Dameron et al at Shatsky Ruse begins far earlier (~68-66.Ma) due to local changes in water masses	Henehan et al. 2016; Dameron et al. 2017	*(112)*
		Surface ocean acidification based on robust tests and fragmentation during pre-K/Pg cooling two Tethyian sites (Punekar et al. 2016) (i.e., opposite signal as in Henehan et al. 2016; Dameron et al. 2017)	Punekar et al.	*(191)*
		Decrease in detrital magnetite in Bidart, France section hypothesized to be consequence of acid rains during Deccan volcanism Phase 2 (i.e., the Late Cretaceous warming interval	Font et al. 2014	*(192)*
		Late Cretaceous warming of similar scale to Paleocene warming events; all (including Late Cretaceous warming) hypothesized to be linked to LIPs	Barnet et al. 2019	*(43)*
Post-K/Pg	**Deccan:** Environment effect	No warming or cooling detected with general timing (discussed in Sprain et al. 2019; shown here) in global compilation (but see fish teeth; MacLeod et al. 2018)	This study; Sprain et al. 2019; MacLeod et al. 2019	*(163, 168)*
Pre-K/Pg	**Deccan:** Biotic change	Plant immigration & increased diversity (North Dakota)	Wilf et al. 2003; Wilf & Johnson 2004	*(91, 106)*
		Minor mammalian changes w/climate (body size, relative abundance, evenness) (Montana)	Wilson 2005, 2014	*(142, 193)*
		Declining evenness and diversity in salamander & salamander-like species, Hell Creek Formations (Montana)	Wilson et al. 2014	*(141)*
		Palynoflora community turnover (Deccan volcanic sediments; pre- vs. intertraps)	Samant & Mohabey 2009; Samant & Bajpai 2005	*(194, 195)*
		Molluscan diversity may have decline in the late Maastrichtian (Bay of Biscay)	Marshal & Ward 1996	*(196)*
		Local extinction in Antarctic Seymour Island Section of marine macro-invertebrates coincident with C29R warming; but subsequently debated (Witts et al. 2016; Tobin 2017	Tobin et al. 2012; Zinsmeister et al. 1989; Witts et al. 2016; Tobin 2017	*(95, 139, 197, 198)*
		Pole-ward migration of warm water planktic foraminifera into shelf setting at Bass River section coincident with C29R warming	Olsson et al. 2001	*(199)*
		Morphological changes in bryozoans at Nye Klov; inferred link to environmental change	O'Dea et al 2011	*(185)*
		Upper most Maastrichtian very low diversity shark faunas at Stevns Klint (not extinction, species reappear in the Danian) attributed to regional environmental change (sea level postulated)	Adolfssen and Ward 2014	*(200)*

		Calcareous nannoplankton assemblage change (North Pacific and other sites); peaks with temperature anomaly & recovers before K/Pg boundary	Thibault & Gardin 2010; Thibault and Husson 2016	(138, 201)
		Geographic range extensions (poleward migration) in planktonic foraminifera; recovers before K/Pg boundary	Olsson et al. 2001; Kucera & Malmgren 1998	(137, 199)
		Increased ichthyolith (fish teeth and scale) accumulation rates at one site (Site U1403) and possibly Gubbio but not others (Sites 596, 886, 1209)	this study; Sibert et al. 2014	(25)
		Reduced population abundance of deep dwelling planktonic foraminifera in coastal sites; widespread dwarfing of planktonic foraminifera during warming event	Abramovich and Keller 2003; Keller and Abramovich 2009; Abramovich et al. 2010	(202-204)
		Coastal assemblages of planktonic foraminifera dominated by species thought to be opportunistic and/or tolerant of low oxygen during warming event; reduced diversity in Tethys	Abramovich & Keller 2002, Keller 2003, Keller and Pardo 2004; Pardo and Keller 2008; Abramovich et al. 2010	(202, 205-208)
		Low diversity in Tethys but for longer interval (>1million years of latest Maastrichtian)	Keller 2004	(209)
Post-K/Pg	**Deccan:** Biotic change	The immediate aftermath of the K/Pg mass extinction is similar to that of many extinctions with low diversity (e.g., Coxall et al. 1998), high dominance and turnover communities (e.g., Hull et al. 2011; Bown 2005), unusually functioning ecosystems (D'Hondt et al. 1998, Henehan et al. 2016) persisting for hundreds of thousands to millions of years (e.g., Hull 2015). Although this interval is often attributed the loss of species and the time to re-evolve species and functional communities (Hull 2015), the duration could be paced by volcanic outgassing (as is hypothesized for the P/T). At present, there is not clear tie (or mechanism) for this in the early Paleocene but few studies have looked.	Coxall et al. 2006; Hull et al. 2011; Bown et al. 2005; D'Hondt et al. 1998; Henehan et al. 2016; Hull 2015	(39) (20, 22) (37) (112) (210)
Pre-K/Pg	**Deccan:** Elevated extinction	No, not elevated in mammals	Wilson 2005, 2014	(142, 193)
		No, not elevated in turtles	Holroyd et al. 2015	(211)
		No, not elevated (nor gradually declining in the Late Cretaceous) in dinosaurs	Pearson et al. 2002; Fastovsky et al. 2004; Wang & Dodson 2006;	(212-216)

			Sheehan et al. 1996; 2000	
		Gradual decline in dinosaur richness (in the last several million years in Barrett et al. 2009; so longer than Deccan volcanism); disputed and countered by analysis of Brusatte et al (2015)	Archibald 2012; Barrett et al. 2009; Brusatte et al. 2015	(*217-219*)
		No evidence from rudists; counters earlier interpretations based on different stratigraphic interpretations and patterns in the mostly incomplete carbonate platform sequences	Steuber et al. 2002; Schlüter et al. 2008; Steuber & Schlüter 2012	(*220-222*)
		No evidence in nannoplankton	Bown 2005; Pospichal 1994, 1996; Thibault and Husson 2016	(*145, 201, 223, 224*)
		No evidence in foraminifera	this study; Arenillas et al. 2000a,b, 2002; Norris et al. 1999; Huber et al. 2002; MacLeod et al. 2007	(*225-230*)
		Various single site studies of planktonic foraminifera have reported elevated extinctions prior to the impact (Tunisia: Keller 1988; Keller and MacLeod 1996; Keller 1998; Site 525: Li and Keller). The local nature of these patterns (regardless of whether they reflect local extinctions or local stratigraphic biases) have subsequently been revealed by other studies by the same set of authors (Punkar 2014) that show survivorship up to the K/Pg boundary of the same species at other sites; and by studies of sample biasing by other authors on the same site (Arenillas et al. 2000a,b; Tunsia) showing sudden and catastrophic extinction. Keller et al. 2018 discusses local extinctions (and large scale faunal changes) but not global extinctions prior to the K/Pg boundary; in line with the discussion provided here.	Keller 1988; Keller and MacLeod 1996; Keller et al. 2018; Punekar et al. 2014	(*140, 231-235*)
Impact	**Chicxulub:** Impact	Reviews of K/Pg impact tracers (many hundreds of sites)	Smit 1999; Claeys et al. 2002; Schulte et al. 2010; Hull et al. 2011	(*30, 53, 134, 236*)
		Iridium & osmium anomaly at the K/Pg boundary (North Dakota, Hell Creek and Fort Union formations)	Johnson et al. 1989; Moore et al. 2014	(*237*) (*238*)
		Minerological evidence (shocked quartz & stishovite) for impact at the K/Pg boundary (Western Interior, US)	Bohor et al. 1984;	(*239, 240*)

		McHone et al. 1989	
		Hiatuses common across shallow water K/Pg boundary sections (attributed to tsunami, slumping, and others)	Smith et al. 1996; Olsson et al 2002; Meyers & Peters 2011	*(51, 110, 241)*
		Tsunami deposits around Gulf of Mexico	Bourgeois et al. 1988; Smit et al. 1996, Tada et al. 2002	*(50-52)*
		Iridium layers in multiple sections coincident with K/Pg boundary	Bourgeois et al. 1988; Miller et al. 2010	*(52, 242)*
		Minerological evidence (shocked quartz) for impact at the K/Pg boundary (global)	Bohor et al. 1987	*(243)*
		Mass wasting deposits in the Caribbean and along the Gulf Coastal Plain, triggered by impact associated ground motion (i.e., earthquakes) at the K/Pg boundary	Bralower et al. 1998; Norris et al. 2000; Denne et al. 2013	*(47, 49, 244)*
		Impact ejecta (a few examples) at the K/Pg boundary	Schulte et al. 2010; Sigurdsson et al. 1997; Norris et al. 1999; MacLeod et al. 2007	*(30, 228, 230, 245)*
		Osmium anomalies at the K/Pg boundary	Ravizza et al. 2003; Paquay et al. 2008; Robinson et al. 2009	*(68, 69, 71)*
		Iridium anomalies (a few examples) at the K/Pg boundary	Alvarez et al. 1980; Michel et al. 1981; Alvarez et al. 1990	*(246-248)*
		K/Pg boundary ashes and impact markers (tecktites) dated via Ar-Ar dating to be synchronous within error	Renne et al. 2013	*(249)*

	Chicxulub: Environment effect	Possible paleobotanical evidence for impact winter (Wyoming) (disputed in McIver 1999 among others)	Wolfe 1991;	*(250)*
		Paleobotanical evidence for ecosystem turnover coincident with boundary (Saskatchewan, Canada)	McIver 1999	*(251)*
		Paleobotanical evidence for ecosystem turnover coincident with boundary (Western Interior, US); including fern spike	Tschudy et al. 1984; Nichols 1990	*(252, 253)*
		All early Danian deposits in the western interior in 'coal-bearing, fluvial or paludal deposition settings'(Nichols 1990), with strong evidence for increased 'wetness' (Sweet and Braman 1992) across the boundary	Nichols 1990; Sweet and Braman 1992	*(253, 254)*

		Impact winter suggested by TEX$_{86}$, with sea surface cooling of as much as 7°C in Brazos River, Texas	Vellekoop et al. 2014	(*100*)
		Decrease in export productivity suggested along New Jersey margin	Esmeray-Senlet et al. 2015	(*86*)
		Decreased oxygenation in northwestern Pacific (sulfur isotopic evidence) and some localities in the Tethys	Kajiwara & Kaiho 1992; Coccioni and Galeotti 1994	(*188, 255*)
		Tsunami deposits in Caribbean and Gulf coast	Smit et al. 1996	(*51*)
		Biological selectivity suggestive of impact-associated ocean acidification	Alegret et al. 2012	(*29*)
		Multiple lines of evidence (carbonate geochemistry, other productivity proxies, and biomarkers) for a decline productivity or the efficiency of the biological pump (estimates of the magnitude, geography, and timing vary)	Zachos et al. 1989; D'Hondt et al. 1998; Sepulveda et al. 2009; Hull & Norris 2011	(*26, 37, 38, 76*)
		Prolonged (>500,000 yr) alkalinity pulse	Henehan et al. 2016	(*112*)
	Chicxulub: Biotic change	Extinction selectivity in mammals (against large carnivores and herbivores) suggest loss of primary productivity; recovery fueled by immigration	Sheehan and Hanson 1986; Robertson et al. 2013; Wilson 2013	(*256-258*)
		Wide-spread evidence for floral turnover at the boundary, including a fern spike throughout the western interior	Tschudy et al. 1984; Nichols 1990; Fleming and Nichols 1990; Sweet and Braman 1992	(*252-254, 259*)
		Persistent (>2 million year) shift in floral ecological strategies (North Dakota)	Blonder et al. 2014	(*260*)
		Drastic turnover in leaf miners (insect trace fossils) & decouple leaf to miner diversity (western interior N. America)	Donovan et al. 2014; Wilf et al. 2006	(*261, 262*)
		Recovery of plant community structure in phases. Initial communities of opportunistic 'bloom' taxa (i.e., fern/spore spike) replaced by pioneer communities, and then by diverse communities including new taxa.	Vajda & Bercovici 2014; Nichols and Johnson 2008	(*263, 264*)
		(Note: temporal resolution is too low to distinguish Late Maastrichtian warming from impact at boundary.) As summarized in Kiessling & Baron-Szabo (2004): corals dominate reefs in Paleocene in contrast to Late Cretaceous (Kiessling et al. 1999); greater percentage of corals are reef associated in Paleocene; K/Pg mass extinction event is only mass extinction with a major drop in reefal carbonate at the stage level (Fluegel & Kiessling 2002); geography and timing of earliest Paleocene reefs indicates latest first appearance in Caribbean (although data is sparse) closer to impact	Fluegel & Kiessling 2002; Kiessling et al. 1999; Kiessling & Claeys 2001; Kiessling & Baron-Szabo 2004;	(*265-268*)

site (Kiessling & Claeys 2001); numerous survivor clade through early Danian (i.e., prolonged turnover).		
Increase in epifaunal echinoderm fecal pellet abundance in New Jersey and Turkey	Miller et al. 2010	(*242, 269*)
Mollusk ecological trait change suggestive of low-productivity driven extinction and uncoordinated recovery of functional diversity (Western Argentina)	Aberhan et al. 2007	(*270*)
Dwarfing in Danian echinoderms (sister taxa comparison)	Smith and Jeffery 1998	(*271*)
Persistent shift in molluscan community functional ecology across the K/Pg: increase in deposit feeding & increase in predators and predator-resistance post-K/Pg (Aberhan & Kiessling 2015); basic patterns of functional turnover reflected in high southern latitudes as well (Stilwell 2003)	Aberhan & Kiessling 2015; Stilwell 2003	(*272, 273*)
No change in the proportion of the two main clades of incrusting bryozoans in US and Danish sections suggesting no long-term crash in productivity or inadequate understanding of the inter-clade differences; also no dwarfing in zooids or colonies	Sogot et al. 2013; Sogot et al. 2014	(*274, 275*)
Regional benthic 'dead zones' with low abundance and/or benthic impoverished faunas. Known from Danish and Caribbean sections.	Hakansson and Thomsen 1999; Hansen et al. 2004	(*276, 277*)
Calcareous red algae in Pyrenean Basin show prolonged/delayed recovery of species richness extending until the early Thanetian; shallow water (tropical affinity) species had greatest extinction rates and the clades dominating immediately post-K/Pg in reef assemblages typically occur in deep water/cryptic habitats today. Depth selectivity of extinctions observed across sites (i.e., Aguirre et al. 2000).	Aguirre et al. 2007; Aguirre et al. 2000	(*278, 279*)
Changed pelagic community structure (relative abundance amongst microfossil taxa)	Hull et al. 2011; Sibert et al. 2014	(*22, 25*)
Blooms of aberrant planktonic foramnifera in Tunsia in early Danian	Arenillas et al. 2018	(*280*)
Low richness, short-lived successive communities in planktonic foraminifera and nannoplankton (global, early Danian)	Gerstel & Thunell 1986; Gerstel et al. 1987; Jiang et al. 2010; Fuqua et al. 2008, Pospichal 1996	(*16, 17, 32, 40, 224*)
Dominance of 'disaster' or 'opportunistic' taxa in the earliest Paleocene (global)	Jiang et al. 2010	(*17*)
Turnover in benthic community structure suggesting regional heterogeneity in detrital flux to the benthos (increased in some regions, declined in others)	Alegret & Thomas 2005, 2007, 2009; Alegret 2007	(*24, 190, 281, 282*)
Siliceous plankton bloom (New Zealand)	Hollis et al. 1995	(*283*)

	Low latitude incursions of high latitude dinoflagellates; dinoflagellate community turnover	Brinkhuis & Zachariasse 1988; Vellekoop et al. 2015	(*114, 284*)
	Short (~1,000-10,000 years) reduction in primary productivity (Sepulveda et al. 2009, 2019), with longer term (>1 myr) changes to the biological pump (D'Hondt et al. 1998, Zachos et al. 1989, Hull et al. 2011; Esmerary-Senlet et al. 2015; Birch et al. 2016	Sepulveda et al. 2009, 2019; Zachos et al. 1989; D'Hondt et al. 1998; Hull et al. 2011; Esmeray-Senlet et al. 2015; Birch et al. 2016	(*26, 37, 38, 76, 86, 89, 285*)
Chicxulub Impact: Elevated extinction	Review: dinosaur extinction coincident with impact (no support for Cretaceous decline in diversity)	Brusatte et al 2015	(*219*)
	Dinosaur extinction coincident with KPg impact	Sheehan et al. 1991; Sheehan et al. 2000	(*286, 287*)
	Mass bird extinction at KPg boundary (western N. America)	Longrich et al. 2011	(*288*)
	Mass snake & lizard extinction at the KPg (N. America)	Longrich et al. 2012	(*289*)
	75% Mammalian extinction in Hell Creek Formations across the KPg (Montana)	Wilson 2014	(*142*)
	22% species-level extinction in salamander & salamander-like species across the KPg, Hell Creek Formations (Montana)	Wilson et al. 2014	(*141*)
	30% (palynological) to 57% (megafloral types) floral extinction across the KPg (North Dakota)	Wilf & Johnson 2004; Johnson 1992	(*106, 290*)
	Elevated extinction of specialized and moderately insect trace fossils across the KPg boundary	Labandeira et al. 2002	(*291*)
	~75% species extinction in shelly marine invertebrates	Jablonski 1991; Barnosky et al. 2011	(*292, 293*)
	45% extinction in scleractinian corals, with particularly high extinction levels in photosymbiotic, colonial (particularly with high corallites), and narrow ranged taxa	Kiessling & Baron-Szabo 2004	(*265*)
	36% generic-level extinction in sea urchins, with selectivity by clade, feeding strategy, and endemic regionality (in narrow-ranging clades)	Smith and Jeffery 1998	(*271*)
	63% generic-level bivalve extinction; with molluscan extinction intensity declines with latitude if rudists are considered (high latitudes have less extinction)	Raup & Jablonski 1993; Vilhena et al. 2013	(*294, 295*)
	Rudist bivalve extinction (100%) consistent with catastrophic extinction coincident with K/Pg boundary in stratigraphically complete sections.	Steuber et al. 2002; Schlüter et al. 2008;	(*220-222*)

	Steuber & Schlüter 2012	
34% generic/45% species-level extinction in Neoselachian sharks with greater losses in shallow water species. Greater extinction amongst skates and rays.	Kriwet & Benton 2004	(*117*)
Mass extinction (100%) of all ammonites at, or just above, the K/Pg impact layer (global)	Ward and Kennedy 1993*;*Landman et al.; Miller et al. 2010	(*242, 296*)
~90% extinction in calcareous nannoplankton coincident with impact ejecta at the K/Pg boundary (global), with reworking (evidence by borrow counts and coeval iridium spread) spreading extinct taxa up-section	Bramlette & Martini 1964; Bown et al. 2004; Bown 2005; Pospichal 1990, 1994, 1996, Hull et al. 2011	(*20, 134, 145, 146, 224, 297, 298*)
~90% extinction in planktonic foraminifera coincident with impact ejecta at the K/Pg boundary (global)	Smit & Hertogen 1980; D'Hondt et al. 1996; Arenillas et al. 2000	(*147, 226, 299*)
Estimated 45% extinction of coral species; greater extinction amongst photosymbiotic species & colonial species; large number of failed survivors	Kiessling & Baron-Szabo 2004	(*265*)
70% species-level extinction in red calcareous algae	Aguirre et al. 2000	(*300*)
No elevation in extinction rates of fish teeth in open ocean sediments (Sibert et al. 2014), but major turnover in fish community structure (Sibert & Norris 2015; and morphological radiation amongst spiny finned teleosts (Friedman 2010) following ecomorphologically selective neritic extinctions (Friedman 2009)	Friedman 2009, 2010; Sibert et al. 2014; Sibert & Norris 2015;	(*25, 116, 301, 302*)
No elevation in extinction rates in benthic foraminifera	Culver 2003; Thomas 2007; Alegret & Thomas 2009	(*24, 303, 304*)
No elevation in extinction rates in ostracods	Elwa 2002	(*305*)
No elevation in extinction rates in radiolarians	Hollis et al. 2003	(*306*)
No elevation in extinction rates in dinoflagellates	Brinkhuis & Zachariasse 1988; Brinkhuis et al. 1998	(*284, 307*)

Table S2.
Details of age models used for foraminiferal data in global compilation (Fig. 1) from deep-sea drill cores.

Site	Reference for data	Type of data	Age Model Details
ODP 1209, Shatsky Rise	(*13*), this study	Planktonic and benthic $\delta^{18}O$	In the Danian, ages are interpolated between positions of short eccentricity cycles from ref. (*12*). In the Maastrichtian, we use the age model of Westerhold et al. (*13*), Age option 3, adjusted by -0.028 Ma to fit Dinarès-Turell et al.*(12)* K-Pg boundary of 66.022 Ma.
ODP 1210, Shatsky Rise	This study	Benthic $\delta^{18}O$	In the Danian, ages are interpolated between positions of short eccentricity cycles from ref. (*12*). In the Maastrichtian, beyond the age model of ref. (*12*), ages are tuned to long Westerhold et al. (*13*)'s Age Option 3 at Site 1209. These were then transposed to 1210 using tie points from ref. (*8*), and adjusted by -0.0028 Ma to fit Dinarès-Turell et al.*(12)* K-Pg boundary of 66.022 Ma.
DSDP 577	(*33*)	Benthic $\delta^{18}O$	Uses linear interpolation between magnetochrons from ref. (*308*), noting the updated composite splice of ref. (*309*).
DSDP 465, Hess Rise	This study	Benthic $\delta^{18}O$	Interpolation between foraminiferal and nannofossil biostratigraphic markers from (*310, 311*), with absolute ages for datums taken from (*81*).
DSDP 528, Walvis Ridge	(*81*)	Benthic $\delta^{18}O$	Sedimentation rate based on thickness of Cretaceous portion of magnetochron C29r, reported by refs. (*312, 313*), and length of time in Cretaceous C29r from (*60*).
ODP 1262, Walvis Ridge	This study, (*42, 89*)	Planktonic and benthic $\delta^{18}O$	Age model is take from Dinarès-Turell et al. (12), with the Cretaceous extension of Woelders et al. (*44*).
ODP 1267, Walvis Ridge	This study	Benthic $\delta^{18}O$	Age model is take from Dinarès-Turell et al. (12).
DSDP 525, Walvis Ridge	(*82*)	Planktonic and benthic $\delta^{18}O$	Sedimentation rate based on thickness of Cretaceous portion of magnetochron C29r, reported by ref. (*312*), and length of time in Cretaceous C29r from (*60*).
ODP 690, Maud Rise	(*83, 90, 91*)	Planktonic and benthic $\delta^{18}O$	Linearly interpolated between published magnetochron boundaries (*314*), nannofossil biozones (*146*), and the K-Pg Ir spike (*315*) using updated ages for each event from GTS2012 (*60*).
ODP 1049, Blake Nose	(*84*)	Benthic $\delta^{18}O$	Linearly interpolated between magnetochrons and planktonic foraminiferal biozones from (*316*). C30n/C29r boundary from ref. (*316*), with C29r/C29n boundary placed at Dan-C2 event by analogy with other Dan-C2 sections elsewhere (*84*).
DSDP 384, J-Anomaly Ridge	(*85*)	Benthic $\delta^{18}O$	Uses integrated magneto-biostratigraphy of ref. (*317*), updating age tie points to GTS2012 (*60*).
ODP 174AX, Bass River	(*86, 101*)	Planktonic and benthic $\delta^{18}O$ and Mg/Ca	Uses age model from Esmeray-Senlet et al. (*86*).

Tables S3-S30 are found in a separate file

Table S3.
Age tie points and dates used to create new age models (via linear interpolation) for already published deep sea isotope data for global compilation. Five deep sea sites are tuned in (or to) the latest astronomical age model of Dinarès-Turell et al. (2014): Sites U1403, 1209, 1210, 1262, and 1267, which has a K/Pg boundary age of 66.022 Ma. Age models for all other sites (deep sea and otherwise) were generated using bio- and magnetostratigraphic tie points with ages from the Geological Timescale 2012, with a K/Pg boundary age of 66.04 Ma. To plot these data together, we use ages relative to the K/Pg boundary when plotting all data together.

Table S4.
Global compilation of temperatures across the K/Pg boundary, with updated age models and ΔTemperatures for comparisons across realms and latitudes. Six major data types were mined to compile the first global temperature compilation spanning magnetochron C29r, and the events of the K/Pg boundary. These data types are listed adjacent to one another as slightly different column headers are needed to describe the data. They are, from left to right: Foraminiferal δ^{18}O data, TEX$_{86}$ data, Paleosol δ^{18}O data, Leaf margin data, Clumped isotope data, δ^{18}O shell data, Bulk Carbonate δ^{18}O, Mg/Ca, and δ^{18}O teeth data. Although some of this temperature data is freely available from the primary sources listed, we provide the data here on updated age models (with tie points relative to GTS 2012, or, where possible, D-T et al. 2014) and as ΔTemperature (see Methods), in order to examine the change in temperature across the late Cretaceous warming event and the K/Pg boundary. Also note that in 'Foraminiferal data: Sample Type', 'benthic' refers to benthic foraminifera and 'Planktonic' refers to planktonic foraminifera. For the 'Leaf margin data', note that the relative temperatures are calculated relative to the mean of 66.03 & 66.09 Ma data points. Since not all stratigraphic tie points lend themselves to conversion to Dinares-Turrel et al. (2014)'s age model, age is also given relative to the K-Pg, and temperatures calculated using Erez and Luz (1983) and a +0.35‰ vital effect for *N. truempyi*. Biostratigraphic markers for TEX$_{86}$ data come from the original papers. In calculating global average temperature we excluded data from bulk carbonate δ^{18}O and the δ^{18}O of fish apatite because these values did not appear to track temperature in the extinction aftermath, likely due to the biotic discussion (see supplementary text). We have included them here for completeness.

Table S5.
Stable oxygen isotopes from ODP Site 1210 analyzed by L.A. and E.T. at the University of California Santa Cruz, Yale University and the University of Michigan. Matching carbon isotope data published in Alegret et al. (2012).

Table S6.
Stable oxygen isotopes from ODP Site 1262 analyzed by L.A. and E.T. at the University of California Santa Cruz, Yale University and the University of Michigan. Matching carbon isotope data published in Alegret et al. (2012).

Table S7.
Stable oxygen isotopes from DSDP Site 465 analyzed by L.A. and E.T. at the University of California Santa Cruz, Yale University and the University of Michigan. Matching carbon isotope data published in Alegret et al. (2012).

Table S8.
Stable oxygen isotopes from ODP Site 1267 analyzed by L.A. and E.T. at the University of California Santa Cruz.

Table S9.
Stable carbon and oxygen isotopes from bulk carbonate at ODP Site 1267 analyzed E.T. at the University of California Santa Cruz.

Table S10.
Stable carbon and oxygen isotopes from benthic foraminifera and bulk carbonate at ODP Site 1262 generated by Kroon et al (2007) and previously figured in part in Kroon et al. 2007, Barnet et al. 2017, 2019, and Birch et al. 2016, and published in part by Woelders et al. 2017.

Table S11.
Stable carbon and oxygen isotopes from ODP Site 1209 analyzed across three laboratories (Bremen=MARUM, Universitaet Bremen; SIO=Scripps Institution of Oceanography; UCSC=University of California, Santa Cruz). Four types of sample material were processed: bulk foraminifera (i.e., homogenized 38-125mm sieve size fraction), bulk (i.e., homogenized bulk sediment sample), genus-level (i.e., *Woodringina*), and species-level (species include *Pramurica taurica*, *P. pseudoinconstans*, *P. inconstans*, *P. uncinata*, and *Morozovella angulata*). Bulk and species-level data was originally collected by P.M.H. under the supervision of R.D.N. during her PhD (with UCSC samples run in the lab of J.C.Z.) and additional bulk foraminifera and *Woodringina* samples were added in collaboration with B.D., U.R., and T.W. to investigate the bulk carbonate dynamics. Source indicates the lead during these two phases of sample collection. Note that sample rmcd and rmcd adj is from Westerhold and Röhl 2006 and the age model is from Dinarès-Turell et al. (2014).

Table S12.
Bulk carbonate stable carbon and oxygen isotope analyses from Site U1403 collected by A.B. at Friedrich-Alexander Universität Erlangen-Nürnberg (AB), P.M.H. at Yale University (PMH), O.F. at the Goethe-University Frankfurt (OF), and K.M. at Kanazawa-University. Carbon and oxygen stable isotopes are reported relative to the Vienna Peedee belemnite standard (VPDB). Depths at Site U1403 are reported relative to one (or more) of three scales: the primary sample ID, the meters below seafloor of the sample (historically called msbf; but known as CSF-A at Site U1403), or the revised meter composite depth scale (historically called rmcd, but known as rCCSF at Site U1403) from Batenburg et al. 2017. The column 'A/W' denotes samples from the archive (A) versus working (W) half of the core. Samples listed with an age of 'NA' fell outside the applicable range of the age model, and of the figures, but are provided here without an age model for others to use in future work.

Table S13.
Weight percent coarse fraction (>38mm sieve size fraction) of ODP Site 1267 samples prepared at Wesleyan University by E. T.

Table S14.
Weight percent coarse fraction (>63mm sieve size fraction) of ODP Site 1262 samples generated by Kroon et al (2007) and previously figured therein.

Table S15.
Weight percent coarse fraction (>38mm sieve size fraction) of Site U1403 samples prepared at Yale University. Depths at Site U1403 are reported relative to one (or more) of three scales: the primary sample ID, the meters below seafloor of the sample (historically called msbf; but known as CSF-A at Site U1403), or the revised meter composite depth scale (historically called rmcd, but known as rCCSF at Site U1403) from Batenburg et al. 2017 as described in the methods section.

Table S16.
Osmium isotope data from Site U1403 generated by G.E.R. at the University of Hawaii at Manoa. Depths at Site U1403 are reported relative to one (or more) of three scales: the primary sample ID, the meters below seafloor of the sample (historically called msbf; but known as CSF-A at Site U1403), or the revised meter composite depth scale (historically called rmcd, but known as rCCSF at Site U1403) from Batenburg et al. 2017. The column 'A/W' denotes samples from the archive (A) versus working (W) half of the core.

Table S17.
Resolved nannoplankton assemblage counts at IODP Site U1403, carried out by HK and PB at the University College London.

Table S18.
Resolved nannoplankton assemblage counts at ODP Site 1209, carried out by J.S. and T.B. at Penn State.

Table S19.
Weight % carbonate as calculated from mass spectrometer voltage intensity for the Site U1403 bulk carbonate samples measured at Yale University. In house standards were used to calibrate the relationship between the absolute mass of calcium carbonate and the intensity of the signal measured in mV. For a pure carbonate, intensity scaled as the mass (mg) * 22.683. With the relationship, we predicted the intensity for each sample ('Predicted Intensity (mV) as equal to the 'Weight (ug)' * 22.683). The difference between the actual intensity measured by the mass spectrometer ('Measured Intensity (mV')) and the predicted intensity was used to calculate the weight % carbonate of the bulk sediment. Depths at Site U1403 are reported relative to one (or more) of three scales: the primary sample ID, the meters below seafloor of the sample (historically called msbf; but known as CSF-A at Site U1403), or the revised meter composite depth scale (historically called rmcd, but known as rCCSF at Site U1403) from Batenburg et al. 2017.

Table S20.
XRF-based weight % carbonate (calc. wt % $CaCO_3$) and $CaCO_3$ mass accumulation rates for IODP Site U1403. XRF counts of Ca were linearly correlated to mass spectrometry inferred measurements of weight % carbonate (from Table S12) and discrete shipboard measurements (Norris et al. 2014). This correlation was used to calculate the 'calc. wt % $CaCO_3$' shown below for all XRF measurements of Ca. This calculated wt % carbonate was used in combination with linear sedimentation rates and linearly interpolated dry bulk density measurements (interpolated from shipboard measurements in Norris et al. 2014) to calculate the carbonate mass accumulation rates below.

Table S21.
XRF data for Danian of IODP Site U1403 collected by O.F., A.B., S.J., and I.M. at the IODP Bremen Core Repository. Depths at Site U1403 are reported relative to one (or more) of three scales: the primary sample ID, the meters below seafloor of the sample (historically called msbf; but known as CSF-A at Site U1403), or the revised meter composite depth scale (historically called rmcd, but known as rCCSF at Site U1403) from Batenburg et al. 2017.

Table S22.
Visualization of the adjustment to the off-splice boundary core (Core U1403B-28) relative to the CCSF used to calculate an appropriate relative depth for the sample sets collected off-splice in this section (coarse fraction, fish teeth and iridium records).

Table S23.
Cyclostratigraphic age model for Danian to Maastrichtian of Site U1403 generated by S.B. Age model combines new tie-points in the Danian with the Maastrichtian tie-points of Batenburg et al. 2017. Depths at Site U1403 are reported relative to one (or more) of three scales: the primary sample ID, the meters below seafloor of the sample (historically called msbf; but known as CSF-A at Site U1403), or the revised meter composite depth scale (historically called rmcd, but known as rCCSF at Site U1403) from Batenburg et al. 2017.

Table S24.
Updated nannofossil biostratigraphy from Hole U1403A of Paleocene species, revised by P.B. In 'Nanno event' B=bottom and T=top; in 'Preservation' G=good, M=moderate,P=poor (after Norris et al. 2014); in 'Nannofossil abundance' A=abundant, C=common, R=rare, F=frequent, SA=somewhat abundant, and numbers indicate absolute numbers observed (after Norris et al. 2014); in species counts '?' indicates uncertainty in an absence (-) or abundance (A,C,F,R, SA). Depths at Site U1403 are reported relative to one (or more) of three scales: the primary sample ID, the meters below seafloor of the sample (historically called msbf; but known as CSF-A at Site U1403), or the revised meter composite depth scale (historically called rmcd, but known as rCCSF at Site U1403) from Batenburg et al. 2017.

Table S25.
Updated nannofossil biostratigraphic tiepoints from Hole U1403A, revised by P.B. Depths at Site U1403 are reported relative to one (or more) of three scales: the primary sample ID, the meters below seafloor of the sample (historically called msbf; but known as CSF-A at Site

U1403), or the revised meter composite depth scale (historically called rmcd, but known as rCCSF at Site U1403) from Batenburg et al. 2017.

Table S26.
Samples from Site U1403 checked for organic-walled fossils by K.K.S. Samples were barren with the exception of a single dinocyst and two questionable palynomorphs. Depths at Site U1403 are reported relative to one (or more) of three scales: the primary sample ID, the meters below seafloor of the sample (historically called msbf; but known as CSF-A at Site U1403), or the revised meter composite depth scale (historically called rmcd, but known as rCCSF at Site U1403) from Batenburg et al. 2017.

Table S27.
Paleomagnetic data used for the final interpretation of the magnetozones at site U1403. Sample ID, rCCSF(m), mean declination, mean inclination of the ChRM and its corresponding 95% confidence angle are given. Samples collected by C.C. and P.L. and analyzed by C.C. at CEREGE (Aix-en-Provence, France) using a SQUID cryogenic magnetometer (2G Enterprises, model 755R, with noise level of $10{-}11 Am2$) with an attached automatic alternating field 3-axis degausser system (maximum peak field 170 mT) placed in a magnetically shielded room (field of ~nT).

Table S28.
IODP Site U1403 samples selected for organic geochemistry analysis via GC-MRM-MS by J.W., J.S. and R.S. Thermal maturity indices (expressed as %) based on the stereochemistry of algal steranes and bacterial hopanes compared to a laboratory blank. 1: ratio of C_{27} diasteranes and regular desmethyl cholestanes; 2: ratio of C_{27} $\alpha\beta\beta$ and $\alpha\alpha\alpha$ desmethyl cholestanes; 3: ratio of C_{27} $\alpha\alpha\alpha$ S and R desmethyl cholestanes; 4: ratio of C_{31} S and R hopanes.

Table S29.
Ichthyolith mass accumulation rates at Site U1403 collected by E.S. at the Scripps Institution of Oceanography (University of California San Diego).

Table S30.
LOSCAR model output for all Deccan and extinction simulations. Each scenario for the timing of Deccan outgassing was run with both low (3200 GtS, 4090 GtC) and high (8500 GtS, 9545 GtC) emission volumes, and across a range of climate sensitivities of 2, 3, and 4 degrees C per doubling of CO_2. For each run, timesteps are expressed both in model time (beginning at t=0, 390kyr before the K/Pg boundary) and as years relative to the K/Pg boundary. Surface temperature refers to the low-latitude surface Pacific Ocean, but does not differ significantly between oceans.

References

1. R. D. Norris, P. A. Wilson, P. Blum, a. t. E. Scientists, in *Proc. IODP, 342,* R. D. Norris, Wilson, P.A., Blum, P., and the Expedition 342 Scientists, Ed. (Integrated Ocean Drilling Program, College Station, TX, 2014).

2. R. D. Norris *et al.*, in *Proc. IODP 342,* R. D. Norris, P. A. Wilson, P. Blum, a. t. E. Scientists, Eds. (College Station, TX (Integrated Ocean Drilling Program), 2014).

3. T. Bralower, I. Premoli Silva, M. J. Malone, e. al., Site 1209. *Site 1209, Proc. ODP, Initial Reports* **198**, 1-102 (2002).

4. T. Bralower, I. Premoli Silva, M. J. Malone, e. al., Leg 198 Summary. *Leg 198 Summary, Proc. ODP, Initial Reports* **198**, 1-148 (2002).

5. G. R. Heath, L. H. Burckle, e. al., in *Init. Repts. DSDP, 86,* G. R. Heath, L. H. Burckle, e. al., Eds. (U.S. Govt. Printing Office, Washington, 1985), vol. 86, pp. 91-137.

6. S. S. Party, in *Proc. ODP, Init. Repts., 208,* J. C. Zachos, D. Kroon, P. Blum, Eds. (Ocean Drilling Program, College Station, TX, 2004), pp. 1-92.

7. S. S. Party, in *Proc. ODP, Init. Repts., 208,* J. C. Zachos, D. Kroon, P. Blum, Eds. (Ocean Drilling Program, College Station, TX, 2004).

8. T. Westerhold *et al.*, Astronomical calibration of the Paleocene time. *Palaeogeography Palaeoclimatology Palaeoecology* **257**, 377-403 (2008).

9. S. J. Batenburg *et al.*, Cyclostratigraphy and astronomical tuning of the Late Maastrichtian at Zumaia (Basque country, Northern Spain). *Earth and Planetary Science Letters* **359-360**, 264-278 (2012).

10. F. J. Hilgen, K. F. Kuiper, L. J. Lourens, Evaluation of the astronomical time scale for the Paleocene and earliest Eocene. *Earth and Planetary Science Letters* **300**, 139-151 (2010).

11. T. Westerhold, U. Rohl, J. Laskar, Time scale controversy: Accurate orbital calibration of the early Paleogene. *Geochemistry Geophysics Geosystems* **13**, (2012).

12. J. Dinarès-Turell, T. Westerhold, V. Pujalte, U. Röhl, D. Kroon, Astronomical calibration of the Danian stage (Early Paleocene) revisited: Settling chronologies of sedimentary records across the Atlantic and Pacific Oceans. *Earth and Planetary Science Letters* **405**, 119-131 (2014).

13. T. Westerhold, U. Röhl, B. Donner, H. K. McCarren, J. C. Zachos, A complete high-resolution Paleocene benthic stable isotope record for the central Pacific (ODP Site 1209). *Paleoceanography*, (2011).

14. C. Jung, S. Voigt, O. Friedrich, M. C. Koch, M. Frank, Campanian-Maastrichtian ocean circulation in the tropical Pacific. *Paleoceanography* **28**, 562-573 (2013).

15. C. Jung, S. Voigt, O. Friedrich, High-resolution carbon-isotope stratigraphy across the Campanian-Maastrichtian boundary at Shatsky Rise (tropical Pacific). *Cretaceous Research* **37**, 177-185 (2012).

16. L. M. Fuqua, T. J. Bralower, M. A. Arthur, M. E. Patzkowsky, Evolution of calcareous nannoplankton and the recovery of marine food webs after the cretaceous-paleocene mass extinction. *Palaios* **23**, 185-194 (2008).

17. S. J. Jiang, T. J. Bralower, M. E. Patzkowsky, L. R. Kump, J. D. Schueth, Geographic controls on nannoplankton extinction across the Cretaceous/Palaeogene boundary. *Nature Geoscience* **3**, 280-285 (2010).

18.   J. D. Schueth, K. Keller, T. J. Bralower, M. E. Patzkowsky, The Probable Datum Method (PDM): a technique for estimating the age of origination or extinction of nannoplankton. *Paleobiology* **40**, 541-559 (2014).

19.   J. D. Schueth, T. J. Bralower, S. Jiang, M. E. Patzkowsky, The role of regional survivor incumbency in the evolutionary recovery of calcareous nannoplankton from the Cretaceous/Paleogene (K/Pg) mass extinction. *Paleobiology*, 1-19 (2015).

20.   P. Bown, Selective calcareous nannoplankton survivorship at the Cretaceous-Tertiary boundary. *Geology* **33**, 653-656 (2005).

21.   T. J. Bralower, in *Proc. ODP, Sci. Results 146 (Pt. 2),* T. J. Bralower, I. Premoli Silva, M. J. Malone, Eds. (2005), pp. 1-15.

22.   P. M. Hull, R. D. Norris, T. J. Bralower, J. D. Schueth, A role for chance in marine recovery from the end-Cretaceous extinction. *Nature Geoscience*, (2011).

23.   I. Premoli Silva, M. R. Petrizzo, D. Melloni, in *Proc. ODP, Sci. Results, 198,* T. Bralower, I. Premoli Silva, M. J. Malone, Eds. (2005), vol. 198, pp. 1-16.

24.   L. Alegret, E. Thomas, Food supply to the seafloor in the Pacific Ocean after the Cretaceous/Paleogene boundary event. *Marine Micropaleontology* **73**, 105-116 (2009).

25.   E. C. Sibert, P. M. Hull, R. D. Norris, Resilience of Pacific pelagic fish across the Cretaceous/Palaeogene mass extinction. *Nature Geoscience* **7**, 667-670 (2014).

26.   P. M. Hull, R. D. Norris, Diverse patterns of ocean export productivity change across the Cretaceous-Paleogene boundary: New insights from biogenic barium. *Paleoceanography* **26**, 1-10 (2011).

27.   A. Dutton, K. C. Lohmann, R. M. Leckie, Insights from the Paleogene tropical Pacific: Foraminiferal stable isotope and elemental results from Site 1209, Shatsky Rise. *Paleoceanography* **20**, - (2005).

28.   T. D. Frank *et al.*, The Maastrichtian record from Shatsky Rise (northwest Pacific): A tropical perspective on global ecological and oceanographic changes. *Paleoceanography* **20**, (2005).

29.   L. Alegret, E. Thomas, K. C. Lohmann, End-Cretaceous marine mass extinction not caused by productivity collapse. *Proceedings of the National Academy of Sciences of the United States of America* **109**, 728-732 (2012).

30.   P. Schulte *et al.*, The Chicxulub Asteroid Impact and Mass Extinction at the Cretaceous-Paleogene Boundary. *Science* **327**, 1214-1218 (2010).

31.   H. V. Michel, F. Asaro, W. Alvarez, L. W. Alvarez, in *Init. Repts. DSDP, 86,* G. R. Heath, L. H. Burckle, e. al., Eds. (U. S. Govt. Printing Office, Washington, 1985), vol. 86, pp. 533-538.

32.   J. Gerstel, R. C. Thunell, The Cretaceous/Tertiary boundary event in the North Pacific: planktonic foraminiferal results from Deep Sea Drilling Project Site 577, Shatsky Rise. *Paleoceanography* **1**, 97-117 (1986).

33.   J. C. Zachos, M. A. Arthur, R. Thunell, D. F. Williams, E. J. Tappa, in *Init. Repts. DSDPP, 86,* G. R. Heath, L. H. Burckle, e. al., Eds. (U.S. Govt. Printing Office, Washington, 1985), pp. 513 - 532.

34.   A. A. Wright *et al.*, in *Init. Repts. DSDPP, 86,* G. R. Heath, L. H. Burckle, e. al., Eds. (U. S. Govt. Printing Office, Washington, 1985), pp. 799-804.

35.   B. R. T. Simoneit, H. R. Beller, in *Init. Repts. DSDP, 86,* G. R. Heath, L. H. Burckle, e. al., Eds. (U.S. Govt. Printing Office, Washington, 1985), pp. 671-674.

36. S. D'Hondt, G. Keller, Some patterns of planktic foraminiferal assemblage turnover at the Cretaceous Tertiary boundary. *Marine Micropaleontology* **17**, 77-118 (1991).

37. S. D'Hondt, P. Donaghay, J. C. Zachos, D. Luttenberg, M. Lindinger, Organic carbon fluxes and ecological recovery from the Cretaceous-Tertiary mass extinction. *Science* **282**, 276-279 (1998).

38. J. C. Zachos, M. A. Arthur, W. E. Dean, Geochemical evidence for suppression of pelagic marine productivity at the Cretaceous/Tertiary boundary. *Nature* **337**, 61-64 (1989).

39. H. K. Coxall, S. D'Hondt, J. C. Zachos, Pelagic evolution and environmental recovery after the Cretaceous-Paleogene mass extinction. *Geology* **34**, 297-300 (2006).

40. J. Gerstel, R. Thunell, R. Ehrlich, Danian Faunal Succession - Planktonic Foraminiferal Response to a Changing Marine-Environment. *Geology* **15**, 665-668 (1987).

41. D. Kroon, J. C. Zachos, L. S. Party, in *Proc. ODP, Sci. Results 208,* D. Kroon, J. C. Zachos, C. Richter, Eds. (Ocean Drilling Program, College Station, TX, 2007), pp. 1-55.

42. J. S. K. Barnet *et al.*, A new high-resolution chronology for the late Maastrichtian warming event: Establishing robust temporal links with the onset of Deccan volcanism. *Geology* **46**, 147-150 (2018).

43. J. S. K. Barnet *et al.*, A high-fidelity benthic stable isotope record of Late Cretaceous-Early Eocene climate change and carbon-cycling. *Paleoceanography and Paleoclimatology* **34**, 672-691 (2019).

44. L. Woelders *et al.*, Latest Cretaceous climatic and environmental change in the South Atlantic region. *Paleoceanography* **32**, 466-483 (2017).

45. S. Voigt, A. S. Gale, C. Jung, H. C. Jenkyns, Global correlation of Upper Campanian - Maastrichtian successions using carbon-isotope stratigraphy: development of a new Maastrichtian timescale. *Newsletters on Stratigraphy* **45**, 25-53 (2012).

46. S. J. Batenburg *et al.*, Late Maastrichtian carbon isotope stratigraphy and cyclostratigraphy of the Newfoundland Margin (Site U1403, IODP Leg 342). *Newsletters on Stratigraphy*, (2017).

47. T. J. Bralower, C. K. Paull, R. M. Leckie, The Cretaceous-Tertiary boundary cocktail: Chicxulub impact triggers margin collapse and extensive sediment gravity flows. *Geology* **26**, 331-334 (1998).

48. A. Klaus, R. D. Norris, D. Kroon, J. Smit, Impact-induced mass wasting at the K-T boundary: Blake Nose, western North Atlantic. *Geology* **28**, 319-322 (2000).

49. R. D. Norris, J. Firth, J. S. Blusztajn, G. Ravizza, Mass failure of the North Atlantic margin triggered by the Cretaceous-Paleogene bolide impact. *Geology* **28**, 1119-1122 (2000).

50. R. Tada *et al.*, in *Catastrophic events and mass extinctions: impacts and beyond: Geological Society of America Special Paper 356,* C. Koeberl, K. G. MacLeod, Eds. (2002), vol. 356, pp. 109-123.

51. J. Smit *et al.*, in *The Cretaceous-Tertiary event and other catastrophes in earth history,* G. Ryder, D. Fastovsky, S. Gartner, Eds. (1996), vol. 307, pp. 151-182.

52. J. Bourgeois, T. A. Hansen, P. L. Wiberg, E. G. Kauffman, A tsunami deposit at the Cretaceous-Tertiary boundary in Texas. *Science* **241**, 567-570 (1988).

53. J. Smit, The global stratigraphy of the Cretaceous-Tertiary boundary impact ejecta. *Annual Review of Earth and Planetary Sciences* **27**, 75-113 (1999).

54. G. Keller, W. Stinnesbeck, T. Adatte, D. Stuben, Multiple impacts across the Cretaceous-Tertiary boundary. *Earth-Science Reviews* **62**, 327-363 (2003).

55. G. Keller *et al.*, More evidence that the Chicxulub impact predates the K/T mass extinction. *Meteoritics & Planetary Science* **39**, 1127-1144 (2004).

56. G. Keller *et al.*, Chicxulub impact predates K-T boundary: new evidence from Brazos, Texas. *Earth and Planetary Science Letters* **255**, 339-356 (2007).

57. S. J. Batenburg *et al.*, Late Maastrichtian carbon isotope stratigraphy and cyclostratigraphy of the Newfoundland Margin (Site U1403, IODP Leg 342). *Newsletters on Stratigraphy*, (2017).

58. B. Schoene *et al.*, U-Pb constraints on pulsed eruption of the Deccan Traps across the end-Cretaceous mass extinction. *Science* **363**, 862-866 (2019).

59. C. J. Sprain, P. R. Renne, W. A. Clemens, G. P. Wilson, Calibration of chron C29r: New high-precision geochronologic and paleomagnetic constraints from the Hell Creek region, Montana. *Geological Society of America Bulletin* **130**, 1615-1644 (2018).

60. F. M. Gradstein, J. G. Ogg, M. D. Schmitz, G. M. Ogg, *The Geologic Time Scale 2012*. (Elsevier B.V., Amsterdam, 2012).

61. F. J. Hilgen, H. A. Abeis, K. F. Kuiper, L. J. Lourens, M. Wolthers, Towards a stable astronomical time scale for the Paleocene: Aligning Shatsky Rise with the Zumaia - Walvis Ridge ODP Site 1262 composite. *Newsletters on Stratigraphy* **48**, 91-110 (2015).

62. S. Expedition, Paleogene Newfoundland sediment drifts. *IODP Prel. Rept. 342*, (2012).

63. D. Paillard, L. Labeyrie, P. Yiou, Macintosh program performs time-series analysis. *EOS Trans. AGU* **77**, 379 (1996).

64. J. Laskar, M. Gastineau, J. B. Delisle, A. Farres, A. Fienga, Strong chaos induced by close encounters with Ceres and Vesta. *Astron Astrophys* **532**, (2011).

65. J. P. Cogn, PaleoMac: A Macintosh (TM) application for treating paleomagnetic data and making plate reconstructions. *Geochemistry Geophysics Geosystems* **4**, (2003).

66. B. Schoene *et al.*, U-Pb geochronology of the Deccan Traps and relation to the end-Cretaceous mass extinction. *Science* **347**, 182-184 (2015).

67. P. R. Renne *et al.*, State shift in Deccan volcanism at the Cretaceous-Paleogene boundary, possibly induced by impact. *Science* **350**, 76-78 (2015).

68. G. Ravizza, B. Peucker-Ehrenbrink, Chemostratigraphic evidence of Deccan volcanism from the marine osmium isotope record. *Science* **302**, 1392-1395 (2003).

69. N. Robinson, G. Ravizza, R. Coccioni, B. Peucker-Ehrenbrink, R. Norris, A high-resolution marine Os-187/Os-188 record for the late Maastrichtian: distinguishing the chemical fingerprints of Deccan volcanism and the KP impact event. *Earth and Planetary Science Letters* **281**, 159-168 (2009).

70. G. Ravizza, D. VonderHaar, A geochemical clock in earliest Paleogene pelagic carbonates based on the impact-induced Os isotope excursion at the Cretaceous-Paleogene boundary. *Paleoceanography* **27**, PA3219 (2012).

71. F. S. Paquay, G. E. Ravizza, T. K. Dalai, B. Peucker-Ehrenbrink, Determining chondritic impactor size from the marine osmium isotope record. *Science* **320**, 214-218 (2008).

72. G. Ravizza, Reconstructing the marine Os-187/Os-188 record and the particulate flux of meteoritic osmium during the late Cretaceous. *Geochimica Et Cosmochimica Acta* **71**, 1355-1369 (2007).

73.	D. Loroch, A. Deutsch, J. Berndt, A. Bornemann, The Cretaceous/Paleogene (K-Pg) boundary at the J Anomaly Ridge, Newfoundland (IODP Expedition 342, Hole U1403B). *Meteoritics & Planetary Science* **51**, 1370-1385 (2016).

74.	K. Moriya, A. S. Goto, T. Hasegawa, Stable carbon and oxygen isotope analyses of carbonate using a continuous flow isotope ratio mass spectrometry. *The science reports of the Kanazawa University* **56**, 45-58 (2012).

75.	F. Minoletti, M. de Rafelis, M. Renard, S. Gardin, J. Young, Changes in the pelagic fine fraction carbonate sedimentation during the Cretaceous-Paleocene transition: contribution of the separation technique to the study of Bidart section. *Palaeogeography Palaeoclimatology Palaeoecology* **216**, 119-137 (2005).

76.	J. Sepulveda, J. E. Wendler, R. E. Summons, K. U. Hinrichs, Rapid resurgence of marine productivity after the Cretaceous-Paleogene mass extinction. *Science* **326**, 129-132 (2009).

77.	H. Rashid, E. Grosjean, Detecting the source of Heinrich layers: An organic geochemical study. *Paleoceanography* **21**, (2006).

78.	A. H. Kasprak *et al.*, Episodic photic zone euxinia in the northeastern Panthalassic Ocean during the end-Triassic extinction. *Geology*, (2014).

79.	J. C. Zachos *et al.*, in *Proc. ODP, Sci. Results, 120,* S. W. Wise, Jr. , R. Schlich, Eds. (Ocean Drilling Program, College Station, TX, 1992), pp. 961–977.

80.	K. R. Johnson, M. L. Reynolds, K. W. Werth, J. R. Thomasson, Overview of the Late Cretaceous, early Paleocene, and early Eocene megafloras of the Denver Basin, Colorado. *Rockt Mountain Geology* **38**, 101-120 (2003).

81.	S. D'Hondt, M. Lindinger, A stable isotopic record of the Maastrichtian ocean-climate system: South Atlantic DSDP Site 528. *Palaeogeography Palaeoclimatology Palaeoecology* **112**, 363-378 (1994).

82.	L. Q. Li, G. Keller, Abrupt deep-sea warming at the end of the Cretaceous. *Geology* **26**, 995-998 (1998).

83.	L. Alegret, E. Thomas, Benthic foraminifera across the Cretaceous/Paleogene boundary in the Southern Ocean (ODP Site 690): Diversity, food and carbonate saturation. *Marine Micropaleontology* **105**, 40-51 (2013).

84.	F. Quillevere, R. D. Norris, D. Kroon, P. A. Wilson, Transient ocean warming and shifts in carbon reservoirs during the early Danian. *Earth and Planetary Science Letters* **265**, 600-615 (2008).

85.	W. A. Berggren, R. D. Norris, Biostratigraphy, phylogeny and systematics of Paleocene trochospiral planktic foraminifera. *Micropaleontology* **43**, 1-116 (1997).

86.	S. Esmeray-Senlet *et al.*, Evidence for reduced export productivity following the Cretaceous/Paleogene mass extinction. *Paleoceanography* **30**, (2015).

87.	J. Erez, B. Luz, Experimental Paleotemperature Equation for Planktonic-Foraminifera. *Geochimica Et Cosmochimica Acta* **47**, 1025-1031 (1983).

88.	N. J. Shackleton, M. A. Hall, A. Boersma, Oxygen and carbon isotope data from Leg 74 foraminifers. *Initial Rep. Deep Sea Drill. Proj. 74: Washington (U.S. Govt. Printing Office)*, 599–612 (1984).

89.	H. S. Birch, H. K. Coxall , P. N. Pearson, D. Kroon, D. N. Schmidt, Partial collapse of the marine carbon pump after the Cretaceous-Paleogene boundary. *Geology*, (2016).

90.	L. D. Stott, J. P. Kennett, in *Proc. ODP, Sci. Repts., 113,* P. F. Barker, J. P. Kennett, e. al., Eds. (Ocean Drilling Program, College Station, TX, 1990), pp. 829-848.

91. P. Wilf, K. R. Johnson, B. T. Huber, Correlated terrestrial and marine evidence for global climate chanaes before mass extinction at the Cretaceous-Paleogene boundary. *Proceedings of the National Academy of Sciences of the United States of America* **100**, 599-604 (2003).

92. L. Nordt, S. Atchley, I. Dworkin, Terrestrial evidence for two greenhouse events in the latest Cretaceous. *GSA Today* **13**, 4-9 (2003).

93. S. I. Dworkin, L. Nordt, S. Atchley, Determining terrestrial paleotemperatures using the oxygen isotopic composition of pedogenic carbonate. *Earth and Planetary Science Letters* **237**, 56-68 (2005).

94. C. E. Leslie et al., Revised Age Constraints for Late Cretaceous to Early Palaeocene Strata from the Dawson Creek Section, Big Bend National Park, West Texas. *GSA Bulletin*, (in review).

95. T. S. Tobin *et al.*, Extinction patterns, delta(18) O trends, and magnetostratigraphy from a southern high-latitude Cretaceous-Paleogene section: Links with Deccan volcanism. *Palaeogeography Palaeoclimatology Palaeoecology* **350**, 180-188 (2012).

96. T. S. Tobin, G. P. Wilson, J. M. Eiler, J. H. Hartman, Environmental change across a terrestrial Cretaceous-Paleogene boundary section in eastern Montana, USA, constrained by carbonate clumped isotope paleothermometry. *Geology*, (2014).

97. S. V. Petersen, A. Dutton, K. C. Lohmann, End-Cretaceous extinction in Antarctica linked to both Deccan volcanism and meteorite impact via climate change. *Nat Commun* **7**, (2016).

98. R. LeCain, W. C. Clyde, G. P. Wilson, J. Riedel, in *Through the End of the Cretaceous in the Type Locality of the Hell Creek Formation in Mon- tana and Adjacent Areas: Geological Society of America Special Paper 503,* G. P. Wilson, W. A. Clemens, J. R. Horner, J. H. Hartman, Eds. (2014), pp. 137-147.

99. J. Vellekoop *et al.*, Evidence for Cretaceous-Paleogene boundary bolide "impact winter" conditions from New Jersey, USA. *Geology* **44**, 619-622 (2016).

100. J. Vellekoop *et al.*, Rapid short-term cooling following the Chicxulub impact at the Cretaceous-Paleogene boundary. *Proceedings of the National Academy of Sciences of the United States of America* **111**, 7537-7541 (2014).

101. L. Woelders *et al.*, Robust multi-proxy data integration, using late Cretaceous paleotemperature records as a case study. *Earth and Planetary Science Letters* **500**, 215-224 (2018).

102. E. E. McIver, J. F. Basinger, Flora of the Ravenscrag Formation (Paleocene), southwestern Saskatchewan, Canada. *Palaeontographica Canadiana*, (1993).

103. K. S. Davies-Vollum, Early Palaeocene palaeoclimatic inferences from fossil floras of the western interior, USA. *Palaeogeography Palaeoclimatology Palaeoecology* **136**, 145-164 (1997).

104. D. J. Peppe, Megafloral change in the early and middle Paleocene in the Williston Basin, North Dakota, USA. *Palaeogeography Palaeoclimatology Palaeoecology* **298**, 224-234 (2010).

105. D. J. Peppe *et al.*, Sensitivity of leaf size and shape to climate: global patterns and paleoclimatic applications. *New Phytol.* **190**, 724-739 (2011).

106. P. Wilf, K. R. Johnson, Land plant extinction at the end of the Cretaceous: a quantitative analysis of the North Dakota megafloral record. *Paleobiology* **30**, 347-368 (2004).

107. I. M. Miller, M. T. Brandon, L. J. Hickey, Using leaf margin analysis to estimate the mid-Cretaceous (Albian) paleolatitude of the Baja BC block. *Earth and Planetary Science Letters* **245**, 95-114 (2006).

108. D. J. Peppe, D. A. D. Evans, A. V. Smirnov, Magnetostratigraphy of the Ludlow Member of the Fort Union Formation (Lower Paleocene) in the Williston Basin, North Dakota. *Geological Society of America Bulletin* **121**, 65-79 (2009).

109. R. K. Olsson, K. G. Miller, J. V. Browning, D. Habib, P. J. Sugarman, Ejecta layer at the Cretaceous-Tertiary boundary, Bass River, New Jersey (Ocean Drilling Program Leg 174AX). *Geology* **25**, 759-762 (1997).

110. R. K. Olsson, K. G. Miller, J. V. Browning, J. D. Wright, B. S. Cramer, Sequence stratigraphy and sea-level change across the Cretaceous-Tertiary boundary on the New Jersey passive margin. *Geol Soc Am Spec Pap* **356**, 97-108 (2002).

111. K. G. Miller *et al.*, in *Proc. ODP, Init. Repts., 174AX (Suppl.),* K. G. Miller, P. J. Sugarman, J. V. Browning, et al., Eds. (Ocean Drilling Program, College Station, TX 1999), pp. 1-65.

112. M. J. Henehan, P. M. Hull, D. E. Penman, J. W. B. Rae, D. N. Schmidt, Biogeochemical significance of pelagic ecosystem function: an end-Cretaceous case study. *Philosophical Transactions of the Royal Society B-Biological Sciences* **371**, 20150510 (2016).

113. T. Dunkley Jones *et al.*, Climate model and proxy data constraints on ocean warming across the Paleocene-Eocene Thermal Maximum. *Earth-Science Reviews* **125**, 123-145 (2013).

114. J. Vellekoop *et al.*, Palynological evidence for prolonged cooling along the Tunisian continental shelf following the K-Pg boundary impact. *Palaeogeography Palaeoclimatology Palaeoecology* **426**, 216-228 (2015).

115. E. C. Sibert, M. Friedman, P. M. Hull, G. Hunt, R. D. Norris, Two pulses of origination in Pacific pelagic fish following the Cretaceous-Paleogene Mass Extinction. *Proceedings of the Royal Society B-Biological Sciences*, (in review).

116. M. Friedman, Explosive morphological diversification of spiny-finned teleost fishes in the aftermath of the end-Cretaceous extinction. *Proceedings of the Royal Society B-Biological Sciences* **277**, 1675-1683 (2010).

117. J. Kriwet, M. J. Benton, Neoselachian (Chondrichthyes, Elasmobranchii) diversity across the Cretaceous-Tertiary boundary. *Palaeogeography Palaeoclimatology Palaeoecology* **214**, 181-194 (2004).

118. R. E. Zeebe, LOSCAR: Long-term Ocean-atmosphere-Sediment CArbon cycle Reservoir Model v2.0.4. *Geoscientific Model Development* **5**, 149-166 (2012).

119. M. P. Hain, D. M. Sigman, J. A. Higgins, G. H. Haug, The effects of secular calcium and magnesium concentration changes on the thermodynamics of seawater acid/base chemistry: Implications for Eocene and Cretaceous ocean carbon chemistry and buffering. *Global Biogeochemical Cycles* **29**, 517-533 (2015).

120. J. C. G. Walker, J. F. Kasting, Effects of fuel and forest conservation on future levels of atmospheric carbon dioxide. *Palaeogeography Palaeoclimatology Palaeoecology* **97**, 151-189 (1992).

121. J. Uchikawa, R. E. Zeebe, Influence of terrestrial weathering on ocean acidification and the next glacial inception. *Geophysical Research Letters* **35**, (2008).

122. A. Schmidt *et al.*, Selective environmental stress from sulphur emitted by continental flood basalt eruptions. *Nature Geoscience* **9**, 77-82 (2016).

123.   T. Tyrrell, A. Merico, D. I. A. McKay, Severity of ocean acidification following the end-Cretaceous asteroid impact. *Proceedings of the National Academy of Sciences of the United States of America*, 6556-6561 (2015).

124.   S. D'Hondt, Consequences of the Cretaceous/Paleogene mass extinction for marine ecosystems. *Annu. Rev. Ecol. Evol. Syst.* **36**, 295-317 (2005).

125.   E. Anagnostou *et al.*, Changing atmospheric CO2 concentration was the primary driver of early Cenozoic climate. *Nature* **533**, 380-+ (2016).

126.   N. Artemieva, J. Morgan, E. S. Party, Quantifying the Release of Climate-Active Gases by Large Meteorite Impacts With a Case Study of Chicxulub. *Geophysical Research Letters* **44**, 10180-10188 (2017).

127.   D. J. Beerling, B. H. Lomax, D. L. Royer, G. R. Upchurch, L. R. Kump, An atmospheric pCO(2) reconstruction across the Cretaceous-Tertiary boundary from leaf megafossils. *Proceedings of the National Academy of Sciences of the United States of America* **99**, 7836-7840 (2002).

128.   N. C. Arens, A. H. Jahren, Carbon isotope excursion in atmospheric CO2 at the Cretaceous-Tertiary boundary: evidence from terrestrial sediments. *Palaios* **15**, 314-322 (2000).

129.   T. Arinobu, R. Ishiwatari, K. Kaiho, M. A. Lamolda, Spike of pyrosynthetic polycyclic aromatic hydrocarbons associated with an abrupt decrease in delta C-13 of a terrestrial biomarker at the Cretaceous-Tertiary boundary at Caravaca, Spain. *Geology* **27**, 723-726 (1999).

130.   S. J. Day, M. Maslin, in *Large metorite impacts III: Geological Society of America Special Paper 384,* T. Kenkmann, F. Hörz, A. Deutsch, Eds. (2005), pp. 239-258.

131.   M. D. Max, W. P. Dillon, C. Nishimura, B. G. Hurdle, Sea-floor methane blow-out and global firestorm at the K-T boundary. *Geo-Marine Letters* **18**, 285-291 (1999).

132.   A. L. Chenet *et al.*, Determination of rapid Deccan eruptions across the Cretaceous-Tertiary boundary using paleomagnetic secular variation: 2. Constraints from analysis of eight new sections and synthesis for a 3500-m-thick composite section. *Journal of Geophysical Research-Solid Earth* **114**, B06103 (2009).

133.   Materials and methods are available as supplementary materials at the Science website.

134.   P. M. Hull, P. J. S. Franks, R. D. Norris, Mechanisms and models of iridium anomaly shape across the Cretaceous-Paleogene boundary. *Earth and Planetary Science Letters* **301**, 98-106 (2011).

135.   T. Yamaguchi, A. Bornemann, H. Matsui, H. Nishi, Latest Cretaceous/Paleocene deep-sea ostracode fauna at IODP Site U1407 (western North Atlantic) and their response to environmental changes at the Cretaceous/Paleogene boundary and the Latest Danian Event. *Marine Micropaleontology*, (in review).

136.   E. Sibert, R. Norris, J. Cuevas, L. Graves, Eighty-five million years of Pacific Ocean gyre ecosystem structure: long-term stability marked by punctuated change. *Proceedings of the Royal Society B-Biological Sciences* **283**, 20160189 (2016).

137.   M. Kucera, B. A. Malmgren, Terminal Cretaceous warming event in the mid-latitude South Atlantic Ocean: evidence from poleward migration of Contusotruncana contusa (planktonic foraminifera) morphotypes. *Palaeogeography Palaeoclimatology Palaeoecology* **138**, 1-15 (1998).

138. N. Thibault, S. Gardin, The calcareous nannofossil response to the end-Cretaceous warm event in the Tropical Pacific. *Palaeogeography Palaeoclimatology Palaeoecology* **291**, 239-252 (2010).

139. J. D. Witts *et al.*, Macrofossil evidence for a rapid and severe Cretaceous-Paleogene mass extinction in Antarctica. *Nat Commun* **7**, (2016).

140. J. Punekar, P. Mateo, G. Keller, Effects of Deccan volcanism on paleoenvironment and planktic foraminifera: A global survey. *Volcanism, Impacts, and Mass Extinctions: Causes and Effects* **505**, 91-116 (2014).

141. G. P. Wilson, D. G. DeMar Jr., G. Carter, in *Through the End of the Cretaceous in the Type Locality of the Hell Creek Formation in Montana and Adjacent Areas: Geological Society of America Special Paper 503,* W. G. P., W. A. Clemens, J. H. Horner, J. H. Hartman, Eds. (2014), pp. 271-297.

142. G. P. Wilson, Mammalian extinction, survival, and recovery dynamics across the Cretaceous-Paleogene boundary in northeastern Montana, USA. *GSA Spec. Paper* **503**, 365-392 (2014).

143. N. H. Landman *et al.*, Ammonite extinction and nautilid survival at the end of the Cretaceous. *Geology* **42**, (2014).

144. N. P. Kelley, N. D. Pyenson, Evolutionary innovation and ecology in marine tetrapods from the Triassic to the Anthropocene. *Science* **348**, 301-+ (2015).

145. J. J. Pospichal, Calcareous nannofossils at the K-T Boundary, El Kef - no evidence for stepwise, gradual, or sequential extinctions. *Geology* **22**, 99-102 (1994).

146. J. J. Pospichal, S. W. Wise Jr., F. Asaro, N. Hamilton, in *Global catastrophes in earth history: an interdisciplinary conference on impacts, volcanism, and mass mortality: Geological Society of America Special Paper 247,* V. L. Sharpton, P. D. Ward, Eds. (1990), vol. 247, pp. 497-507.

147. S. L. D'Hondt, T. D. Herbert, J. King, C. Gibson, in *The Cretaceous-Tertiary event and other catastrophes in Earth history: Geological Society of America Special Paper 307,* G. Ryder, D. Fastovsky, S. Gartner, Eds. (1996), pp. 303–317.

148. R. M. Corfield, N. J. Shackleton, J. Gerstel, R. Thunell, Danian Faunal Succession - Planktonic Foraminiferal Response to a Changing Marine-Environment - Comment and Reply. *Geology* **16**, 378-380 (1988).

149. K. J. Hsü *et al.*, Mass Mortality and Its Environmental and Evolutionary Consequences. *Science* **216**, 249-256 (1982).

150. L. R. Kump, Interpreting carbon-isotope excursions : Strangelove Oceans. *Geology* **19**, 299-302 (1991).

151. J. Brugger, G. Feulner, S. Petri, Baby, it's cold outside: Climate model simulations of the effects of the asteroid impact at the end of the Cretaceous. *Geophysical Research Letters* **44**, 419-427 (2017).

152. C. G. Bardeen, R. R. Garcia, O. B. Toon, A. J. Conley, On transient climate change at the Cretaceous-Paleogene boundary due to atmospheric soot injections. *Proceedings of the National Academy of Sciences of the United States of America* **114**, E7415-E7424 (2017).

153. J. Vellekoop *et al.*, Shelf hypoxia in response to global warming after the Cretaceous-Paleogene boundary impact. *Geology* **46**, 683-686 (2018).

154. R. W. Smith, T. S. Bianchi, X. X. Li, A re-evaluation of the use of branched GDGTs as terrestrial biomarkers: Implications for the BIT Index. *Geochimica Et Cosmochimica Acta* **80**, 14-29 (2012).

155. S. Fietz, A. Martinez-Garcia, C. Huguet, G. Rueda, A. Rosell-Mele, Constraints in the application of the Branched and Isoprenoid Tetraether index as a terrestrial input proxy. *Journal of Geophysical Research-Oceans* **116**, (2011).

156. W. Qin *et al.*, Confounding effects of oxygen and temperature on the TEX86 signature of marine Thaumarchaeota. *Proceedings of the National Academy of Sciences of the United States of America* **112**, 10979-10984 (2015).

157. S. J. Hurley *et al.*, Influence of ammonia oxidation rate on thaumarchaeal lipid composition and the TEX86 temperature proxy. *Proceedings of the National Academy of Sciences of the United States of America* **113**, 7762-7767 (2016).

158. R. Coccioni *et al.*, The Dan-C2 hyperthermal event at Gubbio (Italy): Global implications, environmental effects, and cause(s). *Earth and Planetary Science Letters* **297**, 298-305 (2010).

159. M. A. Richards *et al.*, Triggering of the largest Deccan eruptions by the Chicxulub impact. *Geological Society of America Bulletin* **127**, 1507-1520 (2015).

160. M. Gutjahr *et al.*, Very large release of mostly volcanic carbon during the Palaeocene–Eocene Thermal Maximum. *Nature* **548**, 573-577 (2017).

161. L. D. Stott, J. P. Kennett, New constraints on early Tertiary paleoproductivity from carbon isotopes in foraminifera. *Nature* **342**, 526-529 (1989).

162. S. V. Petersen *et al.*, Temperature and salinity of the Late Cretaceous Western Interior Seaway. *Geology* **44**, 903-906 (2016).

163. K. G. MacLeod, P. C. Quinton, J. Sepulveda, M. H. Negra, Postimpact earliest Paleogene warming shown by fish debris oxygen isotopes (El Kef, Tunisia). *Science* **360**, 1467-+ (2018).

164. R. A. Duncan, D. G. Pyle, Rapid Eruption of the Deccan Flood Basalts at the Cretaceous Tertiary Boundary. *Nature* **333**, 841-843 (1988).

165. V. Courtillot *et al.*, Deccan Flood Basalts and the Cretaceous Tertiary Boundary. *Nature* **333**, 843-846 (1988).

166. V. Courtillot *et al.*, Deccan flood basalts at the Cretaceous-Tertiary boundary. *Earth and Planetary Science Letters* **80**, 361-374 (1986).

167. A. L. Chenet, X. Quidelleur, F. Fluteau, V. Courtillot, S. Bajpai, K-40-Ar-40 dating of the Main Deccan large igneous province: Further evidence of KTB age and short duration. *Earth and Planetary Science Letters* **263**, 1-15 (2007).

168. C. J. Sprain *et al.*, The eruptive tempo of Deccan volcanism in relation to the Cretaceous-Paleogene boundary. *Science* **363**, 866-+ (2019).

169. C. J. Sprain, P. R. Renne, G. P. Wilson, W. A. Clemens, High-resolution chronostratigraphy of the terrestrial Cretaceous-Paleogene transition and recovery interval in the Hell Creek region, Montana. *GSA Bulletin*, (2014).

170. A. L. Chenet, F. Fluteau, V. Courtillot, M. Gerard, K. V. Subbarao, Determination of rapid Deccan eruptions across the Cretaceous-Tertiary boundary using paleomagnetic secular variation: Results from a 1200-m-thick section in the Mahabaleshwar escarpment. *Journal of Geophysical Research-Solid Earth* **113**, B04101 (2008).

171. S. Self, M. Widdowson, T. Thordarson, A. E. Jay, Volatile fluxes during flood basalt eruptions and potential effects on the global environment: A Deccan perspective. *Earth and Planetary Science Letters* **248**, 518-532 (2006).

172. S. Self, S. Blake, K. Sharma, M. Widdowson, S. Sephton, Sulfur and chlorine in Late Cretaceous Deccan magmas and eruptive gas release. *Science* **319**, 1654-1657 (2008).

173. H. B. Vonhof, J. Smit, High-resolution late Maastrichtian early Danian oceanic Sr-87/Sr-86 record: Implications for Cretaceous-Tertiary boundary events. *Geology* **25**, 347-350 (1997).

174. M. Widdowson, K. G. Cox, Uplift and erosional history of the Deccan Traps, India: Evidence from laterites and drainage patterns of the Western Ghats and Konkan Coast. *Earth and Planetary Science Letters* **137**, 57-69 (1996).

175. E. Font *et al.*, Mercury anomaly, Deccan volcanism, and the end-Cretaceous mass extinction. *Geology* **44**, 171-174 (2016).

176. E. Font *et al.*, Mercury anomaly, Deccan volcanism and the end-Cretaceous Mass Extinction. *Geology* **44**, (2016).

177. J. Smit, C. Koeberl, P. Claeys, A. Montanari, Mercury anomaly, Deccan volcanism and the end-Cretaceous mass extinction. *Geology*, (2016).

178. D. Stuben *et al.*, Late Maastrichtian paleoclimatic and paleoceanographic changes inferred from Sr/Ca ratio and stable isotopes. *Palaeogeography Palaeoclimatology Palaeoecology* **199**, 107-127 (2003).

179. B. Samant, D. M. Mohabey, P. Srivastava, D. Thakre, Palynology and clay mineralogy of the Deccan volcanic associated sediments of Saurashtra, Gujarat: Age and paleoenvironments. *J Earth Syst Sci* **123**, 219-232 (2014).

180. A. S. Khadkikar, D. A. Sant, V. Gogte, R. V. Karanth, The influence of Deccan volcanism on climate: insights from lacustrine intertrappean deposits, Anjar, western India. *Palaeogeography Palaeoclimatology Palaeoecology* **147**, 141-149 (1999).

181. P. Ghosh, M. R. G. Sayeed, R. Islam, S. M. Hundekari, Inter-basaltic clay (bole bed) horizons from Deccan traps of India: Implications for palaeo-weathering and palaeo-climate during Deccan volcanism. *Palaeogeography Palaeoclimatology Palaeoecology* **242**, 90-109 (2006).

182. V. C. Bowman, J. E. Francis, R. A. Askin, J. B. Riding, G. T. Swindles, Latest Cretaceous-earliest Paleogene vegetation and climate change at the high southern latitudes: palynological evidence from Seymour Island, Antarctic Peninsula. *Palaeogeography Palaeoclimatology Palaeoecology* **408**, 26-47 (2014).

183. D. B. Kemp *et al.*, A cool temperate climate on the Antarctic Peninsula through the latest Cretaceous to early Paleogene. *Geology* **42**, 583-586 (2014).

184. V. C. Bowman, J. E. Francis, J. B. Riding, Late Cretaceous winter sea ice in Antarctica? *Geology*, (2013).

185. A. O'Dea, E. Hakansson, P. D. Taylor, B. Okamura, Environmental change prior to the K-T boundary inferred from temporal variation in the morphology of cheilostome bryozoans. *Palaeogeography Palaeoclimatology Palaeoecology* **308**, 502-512 (2011).

186. E. Barrera, G. Keller, Productivity across the Cretaceous/Tertiary boundary in high latitudes. *Geological Society of America Bulletin* **106**, 1254-1266 (1994).

187. T. Mizukami, K. Kaiho, M. Oba, Significant changes in land vegetation and oceanic redox across the Cretaceous/Paleogene boundary. *Palaeogeography Palaeoclimatology Palaeoecology* **369**, 41-47 (2013).

188. Y. Kajiwara, K. Kaiho, Oceanic Anoxia at the Cretaceous Tertiary Boundary Supported by the Sulfur Isotopic Record. *Palaeogeography Palaeoclimatology Palaeoecology* **99**, 151-162 (1992).

189. K. Kaiho *et al.*, Oceanic primary productivity and dissolved oxygen levels at the Cretaceous/Tertiary boundary: Their decrease, subsequent warming, and recovery. *Paleoceanography* **14**, 511-524 (1999).

190. L. Alegret, E. Thomas, Cretaceous/Paleogene boundary bathyal paleo-environments in the central North Pacific (DSDP Site 465), the Northwestern Atlantic (ODP Site 1049), the Gulf of Mexico and the Tethys: the benthic foraminiferal record. *Palaeogeography Palaeoclimatology Palaeoecology* **224**, 53-82 (2005).

191. J. Punekar *et al.*, A multi-proxy approach to decode the end-Cretaceous mass extinction. *Palaeogeography Palaeoclimatology Palaeoecology* **441**, 116-136 (2016).

192. E. Font *et al.*, Atmospheric halogen and acid rains during the main phase of Deccan eruptions: Magnetic and mineral evidence. *Volcanism, Impacts, and Mass Extinctions: Causes and Effects* **505**, 353-368 (2014).

193. G. P. Wilson, Mammalian Faunal Dynamics During the Last 1.8 Million Years of the Cretaceous in Garfield County, Montana. *Journal of Mammalian Evolution* **12**, 53-76 (2005).

194. B. Samant, D. M. Mohabey, Palynoflora from Deccan volcano-sedimentary sequence (Cretaceous-Palaeogene transition) of central India: implications for spatio-temporal correlation. *Journal of Biosciences* **34**, 811-823 (2009).

195. B. Samant, S. Bajpai, Palynoflora from the Lakshmipur intertrappean deposits of Kutch, Gujarat: age implications. *Journal of the Palaeonotological Society of India* **Golden Jubilee Volume 50**, 169-176 (2005).

196. C. R. Marshall, P. D. Ward, Sudden and gradual molluscan extinctions in the latest Cretaceous of western European Tethys. *Science* **274**, 1360-1363 (1996).

197. W. J. Zinsmeister, R. M. Feldmann, M. O. Woodburne, D. H. Elliot, Latest Cretaceous Earliest Tertiary Transition on Seymour-Island, Antarctica. *Journal of Paleontology* **63**, 731-738 (1989).

198. T. S. Tobin, Recognition of a likely two phased extinction at the K-Pg boundary in Antarctica. *Sci Rep-Uk* **7**, (2017).

199. R. K. Olsson, J. D. Wright, K. G. Miller, Paleobiogeography of Pseudotextularia elegans during the latest Maastrichtian global warming event. *Journal of Foraminiferal Research* **31**, 275-282 (2001).

200. J. S. Adolfssen, D. J. Ward, Crossing the Boundary: An Elasmobranch Fauna from Stevns Klint, Denmark. *Palaeontology* **57**, 591-629 (2014).

201. N. Thibault, D. Husson, Climatic fluctuations and sea-surface water circulation patterns at the end of the Cretaceous era: Calcareous nannofossil evidence. *Palaeogeography Palaeoclimatology Palaeoecology* **441**, 152-164 (2016).

202. S. Abramovich, S. Yovel-Corem, A. Almogi-Labin, C. Benjamini, Global climate change and planktic foraminiferal response in the Maastrichtian. *Paleoceanography* **25**, (2010).

203. S. Abramovich, G. Keller, Planktonic foraminiferal response to the latest Maastrichtian abrupt warm event: a case study from South Atlantic DSDP Site 525A. *Marine Micropaleontology* **48**, 225-249 (2003).

204. G. Keller, S. Abramovich, Lilliput effect in late Maastrichtian planktic foraminifera: Response to environmental stress. *Palaeogeography Palaeoclimatology Palaeoecology* **284**, 47-62 (2009).

205. S. Abramovich, G. Keller, High stress late Maastrichtian paleoenvironment: inference from planktonic foraminifera in Tunisia. *Palaeogeography Palaeoclimatology Palaeoecology* **178**, 145-164 (2002).

206. G. Keller, Guembelitria-dominated late Maastrichtian planktic foraminiferal assemblages mimic early Danian in central Egypt. *Marine Micropaleontology* **47**, 71-99 (2003).

207. G. Keller, A. Pardo, Disaster opportunists Guembelitrinidae: index for environmental catastrophes. *Marine Micropaleontology* **53**, 83-116 (2004).

208. A. Pardo, G. Keller, Biotic effects of environmental catastrophes at the end of the Cretaceous and early Tertiary: Guembelitria and Heterohelix blooms. *Cretaceous Research* **29**, 1058-1073 (2008).

209. G. Keller, Low-diversity, late Maastrichtian and early Danian planktic foraminiferal assemblages of the eastern Tethys. *Journal of Foraminiferal Research* **34**, 49-73 (2004).

210. P. M. Hull, Life in the aftermath of mass extinctions. *Curr. Biol.* **25**, R941–R952 (2015).

211. P. A. Holroyd, G. P. Wilson, H. J. Hutchison, Temporal changes within the latest Cretaceous and early Paleogene turtle faunas of northeastern Montana. *Geological Society of America Special Papers*, 299-312 (2014).

212. D. A. Pearson, T. Schaefer, K. R. Johnson, D. J. Nichols, J. P. Hunter, in *The Hell Creek Formation and the Cretaceous-Tertiary Boundary in the Northern Great Plains,* J. H. Hartman, K. R. Johnson, D. J. Nichols, Eds. (Geological Society of America, Special Paper 361, 2002), pp. 145–167.

213. D. E. Fastovsky *et al.*, Shape of Mesozoic dinosaur richness. *Geology* **32**, 877-880 (2004).

214. S. C. Wang, P. Dodson, Estimating the diversity of dinosaurs. *Proceedings of the National Academy of Sciences of the United States of America* **103**, 13601-13605 (2006).

215. P. M. Sheehan, D. E. Fastovsky, C. Barreto, R. G. Hoffmann, Dinosaur abundance was not declining in a "3 m gap" at the top of the Hell Creek Formation, Montana and North Dakota: Reply. *Geology* **28**, 1151-1151 (2000).

216. P. M. Sheehan, D. E. Fastovsky, R. G. Hoffmann, C. B. Barreto, No statistical support for sudden (or gradual) extinction of dinosaurs: Comment. *Geology* **24**, 957-958 (1996).

217. J. D. Archibald, in *The Complete Dinosaur,* M. K. Brett-Surman, T. R. Holtz, J. O. Farlow, B. Walter, Eds. (Indiana Press, Bloomington, 2012), pp. 1027-1038.

218. P. M. Barrett, A. J. McGowan, V. Page, Dinosaur diversity and the rock record. *Proceedings of the Royal Society B-Biological Sciences* **276**, 2667-2674 (2009).

219. S. L. Brusatte *et al.*, The extinction of the dinosaurs. *Biological Reviews* **90**, 628-642 (2015).

220. M. Schlüter, T. Steuber, M. Parente, J. Mutterlose, Evolution of a Maastrichtian-Paleocene tropical shallow-water carbonate platform (Qalhat, NE Oman). *Facies* **54**, 513-527 (2008).

221. T. Steuber, M. Schlueter, Strontium-isotope stratigraphy of Upper Cretaceous rudist bivalves: Biozones, evolutionary patterns and sea-level change calibrated to numerical ages. *Earth-Science Reviews* **114**, 42-60 (2012).

222. T. Steuber, S. F. Mitchell, D. Buhl, G. Gunter, H. U. Kasper, Catastrophic extinction of Caribbean rudist bivalves at the Cretaceous-Tertiary boundary. *Geology* **30**, 999-1002 (2002).

223. P. Bown, Calcareous nannoplankton evolution: a tale of two oceans. *Micropaleontology* **51**, 299-308 (2005).

224. J. J. Pospichal, in *The Cretaceous-Tertiary event and other catastrophes in Earth history: Geological Society of America Special Paper 307,* G. Ryder, D. Fastovsky, S. Gartner, Eds. (1996), pp. 335-360.

225. I. Arenillas, J. A. Arz, E. Molina, Quantifying the evolutionary turnover across the K-T boundary catastrophic planktic foraminiferal extinction event at El Kef, Tunisia. *Gff* **124**, 121-126 (2002).

226. I. Arenillas, J. A. Arz, E. Molina, C. Dupuis, An independent test of planktic foraminiferal turnover across the Cretaceous/Paleogene (K/P) boundary at El Kef, Tunisia: Catastrophic mass extinction and possible survivorship. *Micropaleontology* **46**, 31-49 (2000).

227. I. Arenillas, J. A. Arz, E. Molina, Spanish and Tunisian Cretaceous/Tertiary boundary sections: A planktic foraminiferal biostratigraphic comparison and evolutionary events. *Gff* **122**, 11-12 (2000).

228. K. G. MacLeod, D. L. Whitney, B. T. Huber, C. Koeberl, Impact and extinction in remarkably complete K/T boundary sections from Demerara Rise, tropical western North Atlantic. *Geological Society of America Bulletin* **119**, 768-768 (2007).

229. B. T. Huber, K. G. MacLeod, R. D. Norris, Abrupt extinction and subsequent reworking of Cretaceous planktonic foraminifera across the Cretaceous-Tertiary boundary: Evidence from the subtropical North Atlantic. *Geol Soc Am Spec Pap* **356**, 277-289 (2002).

230. R. D. Norris, B. T. Huber, J. Self-Trail, Synchroneity of the K-T oceanic mass extinction and meteorite impact: Blake Nose, western North Atlantic. *Geology* **27**, 419-422 (1999).

231. G. Keller *et al.*, Environmental changes during the Cretaceous-Paleogene mass extinction and Paleocene-Eocene Thermal Maximum: Implications for the Anthropocene. *Gondwana Research* **56**, 69-89 (2018).

232. G. Keller, L. Li, N. MacLeod, The Cretaceous Tertiary boundary stratotype section at El Kef, Tunisia: How catastrophic was the mass extinction? *Palaeogeography Palaeoclimatology Palaeoecology* **119**, 221-254 (1996).

233. G. Keller, Extinction, Survivorship and Evolution of Planktic Foraminifera across the Cretaceous Tertiary Boundary at El-Kef, Tunisia. *Marine Micropaleontology* **13**, 239-263 (1988).

234. J. A. Arz, I. Arenillas, E. Molina, R. Sepulveda, Planktonic foraminiferal stability in the Upper Maastrichtian and the catastrophic mass extinction at the Cretaceous-Tertiary (K/T) boundary at Caravaca (Spain). *Rev Geol Chile* **27**, 27-47 (2000).

235. I. Arenillas, J. A. Arz, E. Molina, C. Dupuis, The Cretaceous/Paleogene (K/P) boundary at Ain Settara, Tunisia: Sudden catastrophic mass extinction in planktic foraminifera. *Journal of Foraminiferal Research* **30**, 202-218 (2000).

236. P. Claeys, W. Kiessling, W. Alvarez, in *Catastrophic events and mass extinctions: impacts and beyond: Geological Society of America Special Paper 356,* C. Koeberl, K. G. MacLeod, Eds. (2002), vol. 356, pp. 55 - 69.

237. K. R. Johnson, D. J. Nichols, M. Attrep, C. J. Orth, High-Resolution Leaf-Fossil Record Spanning the Cretaceous Tertiary Boundary. *Nature* **340**, 708-711 (1989).

238. J. R. Moore *et al.*, in *Through the End of the Cretaceous in the Type Locality of the Hell Creek Formation in Montana and Adjacent Areas: Geological Society of America Special Paper 503,* G. P. Wilson, W. A. Clemens, J. R. Horner, J. H. Hartman, Eds. (2014), pp. 123-135.

239. B. F. Bohor, E. E. Foord, P. J. Modreski, D. M. Triplehorn, Mineralogic Evidence for an Impact Event at the Cretaceous-Tertiary Boundary. *Science* **224**, 867-869 (1984).
240. J. F. Mchone, R. A. Nieman, C. F. Lewis, A. M. Yates, Stishovite at the Cretaceous-Tertiary Boundary, Raton, New-Mexico. *Science* **243**, 1182-1184 (1989).
241. S. R. Meyers, S. E. Peters, A 56 million year rhythm in North American sedimentation during the Phanerozoic. *Earth and Planetary Science Letters* **303**, 174-180 (2011).
242. K. G. Miller *et al.*, Relationshp between mass extinction and iridium across the Cretaceous-Paleogene boundary in New Jersey. *Geology* **38**, 867-870 (2010).
243. B. F. Bohor, P. J. Modreski, E. E. Foord, Shocked Quartz in the Cretaceous-Tertiary Boundary Clays - Evidence for a Global Distribution. *Science* **236**, 705-709 (1987).
244. R. A. Denne *et al.*, Massive Cretaceous-Paleogene boundary deposit, deep-water Gulf of Mexico: New evidence for widespread Chicxulub-induced slope failure. *Geology* **41**, 983-986 (2013).
245. H. Sigurdsson, R. M. Leckie, G. D. Acton, e. al., Caribbean volcanism, Cretaceous/Tertiary impact, and ocean-climate history: synthesis of Leg 165. *Proc. ODP, Initial Reports 165*, 377-400 (1997).
246. W. Alvarez, F. Asaro, A. Montanari, Iridium profile for 10-million years across the Cretaceous-Tertiary boundary at Gubbio (Italy). *Science* **250**, 1700-1702 (1990).
247. L. W. Alvarez, W. Alvarez, F. Asaro, H. V. Michel, Extraterrestrial cause for the Cretaceous-Tertiary extinction - experimental results and theoretical interpretation. *Science* **208**, 1095-1108 (1980).
248. H. V. Michel, F. Asaro, W. Alvarez, L. W. Alvarez, in *Init. Repts. DSDP, 62,* J. Thiede, T. L. Vallier, Eds. (U.S. Govt. Printing Office, Washington, 1981), vol. 62, pp. 847-849.
249. P. R. Renne *et al.*, Time Scales of Critical Events Around the Cretaceous-Paleogene Boundary. *Science* **339**, 684-687 (2013).
250. J. A. Wolfe, Paleobotanical Evidence for a June Impact Winter at the Cretaceous Tertiary Boundary. *Nature* **352**, 420-423 (1991).
251. E. E. McIver, Paleobotanical evidence for ecosystem disruption at the Cretaceous-Tertiary boundary from Wood Mountain, Saskatchewan, Canada. *Canadian Journal of Earth Sciences* **36**, 775-789 (1999).
252. R. H. Tschudy, C. L. Pillmore, C. J. Orth, J. S. Gilmore, J. D. Knight, Disruption of the terrestrial plant ecosystem at the Cretaceous-Tertiary boundary, western interior. *Science* **225**, 1030-1032 (1984).
253. D. J. Nichols, Geologic and Biostratigraphic Framework of the Nonmarine Cretaceous-Tertiary Boundary Interval in Western North-America. *Review of Palaeobotany and Palynology* **65**, 75-84 (1990).
254. A. R. Sweet, D. R. Braman, The K-T-Boundary and Contiguous Strata in Western Canada - Interactions between Paleoenvironments and Palynological Assemblages. *Cretaceous Research* **13**, 31-79 (1992).
255. R. Coccioni, S. Galeotti, K-T Boundary Extinction - Geologically Instantaneous or Gradual Event - Evidence from Deep-Sea Benthic Foraminifera. *Geology* **22**, 779-782 (1994).
256. G. P. Wilson, Mammals across the K/Pg boundary in northeastern Montana, USA: dental morphology and body-size patterns reveal extinction selectivity and immigrant-fueled ecospace filling. *Paleobiology* **39**, 429-469 (2013).

257. P. M. Sheehan, T. A. Hansen, Detritus Feeding as a Buffer to Extinction at the End of the Cretaceous. *Geology* **14**, 868-870 (1986).

258. D. S. Robertson, W. M. Lewis, P. M. Sheehan, O. B. Toon, K-Pg extinction patterns in marine and freshwater environments: The impact winter model. *J Geophys Res-Biogeo* **118**, 1006-1014 (2013).

259. R. F. Fleming, D. J. Nichols, in *Extinction Events in Earth History,* E. G. Kauffman, O. H. Walliser, Eds. (Springer-Verlag, Berlin, 1990), pp. 347–350.

260. B. Blonder, D. L. Royer, K. R. Johnson, I. Miller, B. J. Enquist, Plant Ecological Strategies Shift Across the Cretaceous-Paleogene Boundary. *Plos Biology* **12**, (2014).

261. M. P. Donovan, P. Wilf, C. C. Labandeira, K. R. Johnson, D. J. Peppe, Novel Insect Leaf-Mining after the End-Cretaceous Extinction and the Demise of Cretaceous Leaf Miners, Great Plains, USA. *PLoS One* **9**, (2014).

262. P. Wilf, C. C. Labandeira, K. R. Johnson, B. Ellis, Decoupled plant and insect diversity after the end-Cretaceous extinction. *Science* **313**, 1112-1115 (2006).

263. V. Vajda, A. Bercovici, The global vegetation pattern across the Cretaceous-Paleogene mass extinction interval: A template for other extinction events. *Global and Planetary Change* **122**, 29-49 (2014).

264. D. J. Nichols, K. R. Johnson, Plants and the K-T Boundary. *Plants and the K-T Boundary*, 1-280 (2008).

265. W. Kiessling, R. C. Baron-Szabo, Extinction and recovery patterns of scleractinian corals at the Cretaceous-Tertiary boundary. *Palaeogeography Palaeoclimatology Palaeoecology* **214**, 195-223 (2004).

266. W. Kiessling, E. Flugel, J. Golonka, Paleoreef maps: Evaluation of a comprehensive database on Phanerozoic reefs. *Aapg Bull* **83**, 1552-1587 (1999).

267. W. Kiessling, P. Claeys, in *Geological and biological effects of impact events,* E. Buffetaut, C. Koeberl, Eds. (Springer, Berlin, 2001), pp. 83-140.

268. E. Flügel, W. Kiessling, in *Phanerozoic Reef Patterns. SEPM Special Publication 72,* W. Kiessling, E. Flügel, J. Golonka, Eds. (2002), pp. 691-723.

269. S. Esmeray-Senlet, S. Ozkan-Altiner, D. Altiner, K. G. Miller, Planktonic Foraminiferal Biostratigraphy, Microfacies Analysis, Sequence Stratigraphy, and Sea-Level Changes across the Cretaceous-Paleogene Boundary in the Haymana Basin, Central Anatolia, Turkey. *Journal of Sedimentary Research* **85**, 489-508 (2015).

270. M. Aberhan, S. Weidemeyer, W. Kiessling, R. A. Scasso, F. A. Medina, Faunal evidence for reduced productivity and uncoordinated recovery in Southern Hemisphere Cretaceous-Paleogene boundary sections. *Geology* **35**, 227-230 (2007).

271. A. B. Smith, C. H. Jeffery, Selectivity of extinction among sea urchins at the end of the Cretaceous period. *Nature* **392**, 69-71 (1998).

272. M. Aberhan, W. Kiessling, Persistent ecological shifts in marine molluscan assemblages across the end-Cretaceous mass extinction. *Proceedings of the National Academy of Sciences of the United States of America* **112**, 7207-7212 (2015).

273. J. D. Stilwell, Patterns of biodiversity and faunal rebound following the K-T boundary extinction event in Austral Palaeocene molluscan faunas. *Palaeogeography Palaeoclimatology Palaeoecology* **195**, 319-356 (2003).

274. S. C. E., E. M. Harper, P. D. Taylor, Biogeographical and ecological patterns in bryozoans across the Cretaceous-Paleogene boundary: Implications for the phytoplankton collapse hypothesis. *Geology*, (2013).

275. C. E. Sogot, E. M. Harper, P. D. Taylor, The Lilliput Effect in Colonial Organisms: Cheilostome Bryozoans at the Cretaceous-Paleogene Mass Extinction. *PLoS One* **9**, (2014).

276. E. Hakansson, E. Thomsen, Benthic extinction and recovery patterns at the K/T boundary in shallow water carbonates, Denmark. *Palaeogeography Palaeoclimatology Palaeoecology* **154**, 67-85 (1999).

277. T. A. Hansen, P. H. Kelley, D. M. Haasl, Paleoecological patterns in molluscan extinctions and recoveries: comparison of the Cretaceous-Paleogene and Eocene-Oligocene extinctions in North America. *Palaeogeography Palaeoclimatology Palaeoecology* **214**, 233-242 (2004).

278. J. Aguirre, J. I. Baceta, J. C. Braga, Recovery of marine primary producers after the Cretaceous-Tertiary mass extinction: Paleocene calcareous red algae from the Iberian Peninsula. *Palaeogeography Palaeoclimatology Palaeoecology* **249**, 393-411 (2007).

279. J. Aguirre, R. Riding, J. C. Braga, Late Cretaceous incident light reduction: evidence from benthic algae. *Lethaia* **33**, 205-213 (2000).

280. I. Arenillas, J. A. Arz, V. Gilabert, Blooms of aberrant planktic foraminifera across the K/Pg boundary in the Western Tethys: causes and evolutionary implications. *Paleobiology* **44**, 460-489 (2018).

281. L. Alegret, E. Thomas, Deep-sea environments across the Cretaceous/Paleogene boundary in the eastern South Atlantic Ocean (ODP leg 208, Walvis ridge). *Marine Micropaleontology* **64**, 1-17 (2007).

282. L. Alegret, Recovery of the deep-sea floor after the Cretaceous-Paleogene boundary event: The benthic foraminiferal record in the Basque-Cantabrian basin and in South-eastern Spain. *Palaeogeography Palaeoclimatology Palaeoecology* **255**, 181-194 (2007).

283. C. J. Hollis, K. A. Rodgers, R. J. Parker, Siliceous plankton bloom in the earliest tertiary of Marlborough, New-Zealand. *Geology* **23**, 835-838 (1995).

284. H. Brinkhuis, W. J. Zachariasse, Dinoflagellate cysts, sea level changes and planktonic foraminifers across the Cretaceous-Tertiary boundary at El Haria, Northwest Tunisia. *Marine Micropaleontology* **13**, 153-191 (1988).

285. J. Sepulveda *et al.*, Stable isotope constraints on marine productivity across the Cretaceous-Paleogene mass extinction. *Paleoceanography and Paleoclimatology*, (2019).

286. P. M. Sheehan, D. E. Fastovsky, R. G. Hoffmann, C. B. Berghaus, D. L. Gabriel, Sudden Extinction of the Dinosaurs - Latest Cretaceous, Upper Great-Plains, USA. *Science* **254**, 835-839 (1991).

287. P. M. Sheehan, D. E. Fastovsky, C. Barreto, R. G. Hoffmann, Dinosaur abundance was not declining in a " 3 m gap " at the top of the Hell Creek Formation, Montana and North Dakota. *Geology* **28**, 523-526 (2000).

288. N. R. Longrich, T. Tokaryk, D. J. Field, Mass extinction of birds at the Cretaceous-Paleogene (K-Pg) boundary. *Proceedings of the National Academy of Sciences of the United States of America* **108**, 15253-15257 (2011).

289. N. R. Longrich, B. A. S. Bhullar, J. A. Gauthier, Mass extinction of lizards and snakes at the Cretaceous-Paleogene boundary. *Proceedings of the National Academy of Sciences of the United States of America* **109**, 21396-21401 (2012).

290. K. R. Johnson, Leaf-Fossil Evidence for Extensive Floral Extinction at the Cretaceous Tertiary Boundary, North-Dakota, USA. *Cretaceous Research* **13**, 91-117 (1992).

291.   C. C. Labandeira, K. R. Johnson, P. Wilf, Impact of the terminal Cretaceous event on plant-insect associations. *Proceedings of the National Academy of Sciences of the United States of America* **99**, 2061-2066 (2002).

292.   A. D. Barnosky *et al.*, Has the Earth's sixth mass extinction already arrived? *Nature* **471**, 51-57 (2011).

293.   D. Jablonski, Extinctions - a Paleontological Perspective. *Science* **253**, 754-757 (1991).

294.   D. A. Vilhena *et al.*, Bivalve network reveals latitudinal selectivity gradient at the end-Cretaceous mass extinction. *Sci Rep-Uk* **3**, (2013).

295.   D. M. Raup, D. Jablonski, Geography of End-Cretaceous marine bivalve extinctions. *Science* **260**, 971-973 (1993).

296.   P. D. Ward, W. J. Kennedy, Maastrichtian Ammonites from the Biscay Region (France, Spain). *Journal of Paleontology* **67**, 1-58 (1993).

297.   P. R. Bown, J. A. Lees, J. R. Young, in *Coccolithophores: from molecular processes to global impact,* H. R. Thierstein, J. R. Young, Eds. (Springer, Berlin, 2004), pp. 481- 508.

298.   M. N. Bramlette, E. Martini, The great change in calcareous nannoplankton fossils between the Maestrichtian and Danian. *Micropaleontology* **10**, 291-322 (1964).

299.   J. Smit, J. Hertogen, An extraterrestrial event at the Cretaceous-Tertiary boundary. *Nature* **285**, 198-200 (1980).

300.   J. Aguirre, R. Riding, J. C. Braga, Diversity of coralline red algae: origination and extinction patterns from the Early Cretaceous to the Pleistocene. *Paleobiology* **26**, 651-667 (2000).

301.   M. Friedman, Ecomorphological selectivity among marine teleost fishes during the end-Cretaceous extinction. *Proceedings of the National Academy of Sciences of the United States of America* **106**, 5218-5223 (2009).

302.   E. C. Sibert, R. D. Norris, New Age of the Fishes initiated by the Cretaceous-Paleogene mass extinction. *Proceedings of the National Academy of Sciences of the United States of America* **PNAS Early Edition**, 1-6 (2015).

303.   E. Thomas, in *Large ecosystem perturbations: causes and consequences: Geological Society of America Special Paper 424,* S. Monechi, R. Coccioni, M. R. Rampino, Eds. (2007), pp. 1–23.

304.   S. J. Culver, Benthic foraminifera across the Cretaceous-Tertiary (K-T) boundary: a review. *Marine Micropaleontology* **47**, 177-226 (2003).

305.   A. M. T. Elewa, Paleobiogeography of Maastrichtian to early Eocene Ostracoda of North and West Africa and the Middle East. *Micropaleontology* **48**, 391-398 (2002).

306.   C. J. Hollis, C. P. Strong, K. A. Rodgers, K. M. Rogers, Paleoenvironmental changes across the Cretaceous/Tertiary boundary at Flaxbourne River and Woodside Creek, eastern Marlborough, New Zealand. *New Zealand Journal of Geology and Geophysics* **46**, 177-197 (2003).

307.   H. Brinkhuis, J. P. Bujak, J. Smit, G. J. M. Versteegh, H. Visscher, Dinoflagellate-based sea surface temperature reconstructions across the Cretaceous-Tertiary boundary. *Palaeogeography Palaeoclimatology Palaeoecology* **141**, 67-83 (1998).

308.   U. Bleil, in *Init. Repts. DSDP, 86,* G. R. Heath, L. H. Burckle, e. al., Eds. (U.S. Govt. Printing Office, Washington, 1985), pp. 441-458.

309.   G. R. Dickens, J. Backman, Core alignment and composite depth scale for the lower Paleogene through uppermost Cretaceous interval at Deep Sea Drilling Project Site 577. *Newsletters on Stratigraphy* **46**, 47–68 (2013).

310. A. S. Henriksson, Biochronology of the Terminal Cretaceous Calcareous Nannofossil Zone of Micula-Prinsii. *Cretaceous Research* **14**, 59-68 (1993).
311. A. Boersma, in *Initial Rep. Deep Sea Drill. Proj. 62,* J. Thiede, T. L. Vallier, Eds. (U.S. Govt. Printing Office, Washington, D.C., 1981), pp. 377-396.
312. A. D. Chave, in *Initial Rep. Deep Sea Drill. Proj. 74,* J. H. Blakeslee, M. Lee, Eds. (U.S. Govt. Printing Office, Washington, D.C., 1984), pp. 525-531.
313. J. A. Alcalá-Herrera, E. L. Grossman, S. Gartner, Nannofossil Diversity and Equitability and Fine-Fraction Delta C-13 across the Cretaceous Tertiary Boundary at Walvis Ridge Leg-74, South-Atlantic. *Marine Micropaleontology* **20**, 77-88 (1992).
314. N. Hamilton, in *Proc. ODP, Sci. Repts., 113,* P. F. Barker, J. P. Kennett, e. al., Eds. (Ocean Drilling Program, College Station, TX, 1990).
315. H. V. Michel, F. Asaro, W. Alvarez, L. W. Alvarez, in *Proc. ODP, Sci. Results, 113,* P. F. Barker, J. P. Kennett, Eds. (Ocean Drilling Program, College, Station, TX, 1990), vol. 113, pp. 159-168.
316. B. T. Huber, K. G. Macleod, N. A. Tur, Chronostratigraphic framework for upper Campanian-Maastrichtian sediments on the blake nose (subtropical North Atlantic). *Journal of Foraminiferal Research* **38**, 162-182 (2008).
317. W. A. Berggren *et al.*, Integrated Paleocene calcareous plankton magnetobiochronology and stable isotope stratigraphy: DSDP Site 384 (NW Atlantic Ocean). *Palaeogeography Palaeoclimatology Palaeoecology* **159**, 1-51 (2000).